BAROTROPIC AND BAROCLINIC INSTABILITIES IN JUPITER'S ZONAL FLOW

Thesis by

David Pollard

In Partial Fulfillment of the Requirements

For the Degree of

Doctor of Philosophy

California Institute of Technology

Pasadena, California

1979

(Submitted November 28, 1978)

ACKNOWLEDGEMENTS

I would like to thank Dr. Andrew Ingersoll, who as my thesis advisor, originated this research project and provided invaluable guidance and ideas throughout. I have benefited greatly from his teaching and expert physical intuition of geophysical fluid dynamics, and am grateful for his patience and straightforward encouragement through the years.

For diligently typing and correcting the manuscript, I owe thanks to Kay Campbell, Hallee Kelso and Chris Seale.

To a few (magic) others:

If my words did glow with the gold of sunshine,
and my tunes were played on the harp unstrung,
would you hear my voice come through the music,
would you hold it near, as if it were your own?

It's a hand-me-down, the thoughts are broken,
perhaps they're better left unsung,
I don't know, don't really care,
let there be songs to fill the air.

by R. Hunter/ J. Garcia.

ABSTRACT

The barotropic and baroclinic stability of Jupiter's zonal jets is investigated using a two-layer quasi-geostrophic model. Each layer is of constant density, with the upper layer representing the cloudy levels of Jupiter's atmosphere above $p \sim 5$ bars containing the zonal jets $\bar{u}(y)$, and a much deeper lower layer in which $\bar{u} = 0$; [roughly consistent with Gierasch (Icarus, 29, 1976)]. Since Jupiter's vertical structure associated with the zonal jets is unknown at these levels, this model attempts to include the effects of baroclinicity and deep lower layer inertia with as few free vertical-structure parameters as possible (i.e., the upper layer Rossby radius of deformation L_r and the ratio of the upper layer to lower layer thickness δ).

Given that $\delta \ll 1$ for Jupiter, the linearized dynamical equations can be expanded in powers of δ and also of $\delta^{\frac{1}{2}}$. These expansions naturally categorize the possible disturbances into three types; barotropic (BTU) modes, almost entirely confined to the upper layer with potentially O(1) growth rates; baroclinic (BC) modes, which depend on interactions between the two layers and can only have $O(\delta^{\frac{1}{2}})$ growth rates; and barotropic (BTL) modes of the lower fluid with $O(\delta)$ growth rates. Some results for the BC modes are presented and compared to results of a continuously stratified model developed in the appendix, but mostly the faster growing BTU modes are investigated for two

analytically tractable velocity profiles [$\mathrm{sech}^2(y)$ and $\tanh(y)$, following Lipps (e.g., J. Fluid Mech., 21, 1965)]. The x-wavelengths, phase speeds, growth rates, horizontal morphologies and the latitudinal forms of the eddy transports $\overline{u'v'}(y)$ of the fastest growing disturbances depend on $\bar{u}(y)$ and on the model parameter L_r.

In mid 1979, two Voyager spacecraft may return images of cloud motions around the $p \sim 1$ bar level, yielding $\bar{u}(y)$ and eddy $u'(x,y,t)$ and $v'(x,y,t)$. Models of the present type are necessary to form a basis for interpreting such data, to initially identify and categorize the types of disturbances, at least until more is known of the vertical structure associated with the zonal jets. Best-fitting of the model's results to corresponding Voyager data may constrain L_r and δ, two basic vertical-structure parameters. In the last section, the theoretical results for BTU modes listed above are summarized and presented in forms most suitable for comparisons with the anticipated data.

TABLE OF CONTENTS

FIGURES

FIGURES (CONTINUED)

1. INTRODUCTION

A. Observations and Theoretical Concepts

Our present knowledge of Jupiter's meteorology has come from observations of cloud patterns and their relative motions. Ground-based observations (e.g., Peek, 1958) date back about 100 years, with spatial resolutions of a few 1000 kms; the Pioneer flyby spacecrafts in 1973 and 1974 returned images with spatial resolution down to ~200 kms (Gehrels, 1976), but provided little information on relative cloud motions. These observations, at visible and infrared wavelengths, refer to a layer about 100 km thick (pressures ~0.1 to ~5 bars) in which three major cloud decks are thought to form (Weidenschilling and Lewis, 1973; Ingersoll, 1976). The atmosphere below p~5 bars is thought to be adiabatic to depths greater than 10^4 km (e.g., Stevenson and Salpeter, 1976).

In equatorial and mid-latitudes, the overall pattern is highly axisymmetric, with the upper cloud deck organized into zonal (i.e., east-west) bands with latitudinal widths of ~3000 to ~10,000 km. There are zonal jets circling the planet, centered at particular latitudes which tend to be located at the edges of the cloud bands. Most of these jets are prograde (i.e. flow from west to east) relative to the planetary rotation of the deep interior as inferred from the magnetospheric radio rotation rate, but a few are retrograde, with typical velocities of ~30 m/s. The whole equatorial region from ~7°S to ~7°N forms

a prograde equatorial jet flowing at ~100 m/s relative to the radio rotation reference frame. Poleward of ~50° latitude, the banded structure disappears and the pattern is more mottled. No mean meridional (i.e., north-south) motion has been detected at any latitude. The overall pattern is extremely long-lived and stable, with the detailed positions, relative strengths, etc., of individual cloud bands and zonal jets varying slightly on a time scale of several years.

Local disturbances are seen embedded in the zonal flow, with horizontal scales of 500 to 3000 km and lifetimes of several months. Some of these disturbances, especially at mid-latitudes, have spiral morphologies reminiscent of mid-latitude cyclones in the earth's jet streams. Many other disturbances are oval-shaped, and occasionally there are wave-like disturbances periodic in longitude. The purpose of this study is to adapt and apply to Jupiter some simple meteorological models that have been developed successfully to describe local dynamic instabilities of the earth's jet streams. There are some important differences between the basic states of the two atmospheres, e.g. the absence of a rigid lower boundary on Jupiter. However, if this body of theory can be applied successfully, we can then use the growth rates, horizontal scales, etc., of the Jovian disturbances as diagnostics of the basic state, e.g. to constrain parameters describing the vertical structure of the zonal jets, about which very little is known. In mid 1979, two Voyager spacecraft are expected to return high-resolution

images over periods of several months, which will probably form a suitable data set to test many of the theoretical results of this study.

For a model of dynamic instabilities of Jupiter's zonal flow, we must make some assumptions about the basic state. At least two distinct concepts have been proposed concerning the basic state vertical structure of zonal jets; these are reviewed by Stone (1976). The horizontal scale and speeds of the jets at the observed cloud levels indicate that the jets are geostrophic; i.e. latitudinal pressure gradients are balanced by coriolis forces (as measured in the radio rotation reference frame). If the jets extend down to depths that are small compared to their horizontal scale of ~5000 km, then they are approximately in hydrostatic equilibrium, which leads to the concept of an earth-like 'weather' layer containing zonal shear flows balanced by latitudinal temperature gradients according to the thermal wind relation. Below this layer, the planet is supposed to be quiescent (except for small-scale random convection cells driven by the internal heat flow). This view, which is supported by the spatial relation of the zonal wind field to zones of upwelling inferred from the banding of the upper cloud layer, has been developed by Hess and Panofsky (1951), Stone (1967), and Ingersoll and Cuzzi (1969). A different concept is that the zonal jets are surface manifestations of organized convective

rolls driven by the internal heat flow, either axisymmetric and confined inside a spherical shell (Williams and Robinson, 1973), or non-axisymmetric and extending through the deep interior oriented parallel to the planetary spin axis (Busse, 1976). Such non-axisymmetric convective systems do occur in laboratory simulations (e.g. Busse and Carrigan, 1976).

The present data and theory neither strongly support nor rule out either of the above two concepts; this study adopts the former, and investigates instabilities occurring in models that represent a thin hydrostatic earth-like 'weather' layer above a much deeper quiescent layer. Comparisons between the model predictions and Voyager data will be a test of the validity of this concept for Jupiter.

B. Summary of Models and Results.

In the 1940's, a self-consistent set of scaling approximations was developed to reduce the Navier-Stokes equations to a single equation that describes large scale, hydrostatic and nearly geostrophic flows in the earth's atmosphere [e.g., Charney (1947); Eady (1949)]. This 'quasi-geostrophic' system was found to predict correctly many of the observed features of mid-latitude cyclones occurring in the earth's jet streams. In this system, there are generally two energy sources in the basic state that can amplify unstable perturbations; available potential energy due to the latitudinal temperature gradients associated with vertical shear ($\partial\bar{u}/\partial z$) of the zonal flow $\bar{u}$, and available kinetic energy due to horizontal shear ($\partial\bar{u}/\partial y$) of the zonal flow. When the basic state contains both of these sources, the resulting partial differential equation is non-separable in the independent variables height and latitude, and for this reason many analytic investigations have used basic state zonal winds with either vertical shear only ('baroclinic' currents), or horizontal shear only ('barotropic' currents).

Because of the preliminary nature of our present knowledge of Jupiter's basic state, we will only use simple models with as few basic state vertical parameters as possible, that nevertheless would still adequately describe features of mid-latitude cyclones when applied to the earth. One suitable choice is Eady's (1949) baroclinic model, with a zonal flow linear in

height and no latitudinal gradients in the basic state. In the appendix, we investigate baroclinic instabilities using Eady's model for the upper 'weather' layer extending from the tropopause at p~0.1 bars down to the base of the cloud decks at p~5 bars. This is coupled to a much deeper quiescent lower layer extending down from p~5 bars. The results show that the presence of this deep lower layer significantly reduces the baroclinic growth rates relative to those of the original single-layer Eady problem with a rigid lower boundary.

This modified Eady model gives a relatively good description of the vertical structure; however, at present it would be more useful to model the effects of latitudinal variations of the basic state, since the horizontal structure is much more readily observable (at cloud levels) on Jupiter than the vertical. Phillips (1951, 1954) investigated both horizonal and vertical structure, avoiding the difficulty of non-separability of the perturbation equation by using a two-level quasi-geostrophic model, i.e., with only two degrees of freedom in the vertical. This two level model is simple yet retains many important physical processes, and is used instructively by Holton (1972). It is mathematically equivalent to a two layer model in which each layer is immiscible and of constant density (e.g., Pedlosky, 1964a, b). We use this model for the main part of this study, with the upper layer containing a latitudinally varying zonal

flow and representing the upper 'weather' layer of Jupiter above p~5 bars; the lower, quiescent layer is much deeper but still hydrostatic.

The formulation and development of general mathematical results for this two layer model are collected into section 2. We will see that all of the unstable disturbances investigated later are modifications of various types of neutrally stable disturbances of the upper layer, and in section 3 these neutral solutions are derived and discussed for two types of analytically tractable zonal flow profiles.

Gill et al. (1974) used the two layer model with a deep lower layer and zonal velocity in the upper layer independent of latitude, to investigate baroclinic instabilities in the earth's oceans. In section 4.A we see that their results are qualitatively the same as the baroclinic results of our modified Eady model, which indicates that the constant density two-layer model is adequately describing the vertical structure. In section 4.B we show that baroclinic instabilities analogous to those of Gill et al. still occur when the zonal velocity is a function of latitude, but we conclude that their growth time scales are so long (~1000 earth days) due to the presence of the deep lower layer that they would not contribute significantly to the observed eddy field on Jupiter.

However, for the same basic states in the two layer model with latitudinally varying zonal flows, another type of instability

is possible with much faster growth rates, with the perturbation almost entirely confined to the upper layer. This is essentially a barotropic instability, and has been studied, among others, by Kuo (1949) and Lipps (1962, 1963, 1965). In section 5 we follow the analysis of Lipps in estimating growth rates of these unstable waves close to the neutral curves by a variational method, for two analytically tractable ($sech^2$ and tanh) zonal velocity profiles. In section 6 we present explicit numerical solutions confirming the existence of these unstable waves for the $sech^2$ velocity profile. The fastest growing solutions have growth time scales of ~30 earth days and horizontal scales comparable to the latitudinal scale (~5000 km) of the zonal flow. We conclude that these 'divergent barotropic' upper layer disturbances are the ones most likely to be seen on Jupiter, and in section 7 various model results for the phase speeds, growth rates, horizontal streamline patterns, etc., of these disturbances are presented. Also the dependence of these results on various parameters of the basic state (e.g., the effective depth of the lower layer) is discussed. Comparisons of the model predictions in section 7 with Voyager images of local disturbances in mid and high latitudes in 1979 should form a practical observational test of the validity of the 'upper weather layer' concept for Jupiter, and may help to constrain otherwise unknown basic vertical structure parameters.

C. Problems Not Investigated.

(i) Although we have chosen particular basic-state vertical structures for our model zonal jets, we do not attempt to model the long-term energy sources, sinks and transfer mechanisms that cause these jets. Several mechanisms have been proposed to account for the latitudinal temperature differences associated with the zonal shears in the hydrostatic 'thermal wind' concept described above; these include latent heat release in the water ice cloud deck thought to exist at $p \sim 5$ bars (Barcilon and Gierasch, 1970; Gierasch, 1976), radiative cooling to space (Gierasch, Ingersoll and Williams, 1973), and equatorial solar heating (Stone, 1967, 1972; Williams, 1978; but see Ingersoll and Porco, 1978). These energy sources and sinks have associated time constants of several years, so they are negligible in the development of the local disturbances whose lifetimes are several months. (However, the eddy transports of energy due to many such disturbances accumulating over time scales of several years may play an important role in the energetics of the mean zonal flow; we will estimate some of these eddy transports in the models below.)

(ii) All of the analysis in this study uses linearized perturbation equations. Incorporating the non-linear advective terms in a weakly non-linear analysis, Maxworthy and others

(e.g., 1976) have found neutral solitary wave solutions occurring in latitudinally varying barotropic zonal flows that account for many features of some Jovian disturbances, especially the Great Red Spot. This non-linear theory gives more information than linear theory on the longitudinal morphology of neutral disturbances, but the present linear study gives more insight into the energy sources and growth rates of unstable waves. Hopefully both studies will be useful in analyzing the rich variety of Jovian disturbances expected in the Voyager images.

(iii) The scaling approximations implicit in the quasi-geostrophic system for baroclinic flows assume that a particular balance exists between the basic state thermal field (which vertically stretches fluid columns moving horizontally between isentropic surfaces) and the strength of the horizontal motion field (which vertically stretches fluid columns due to horizontal convergence). The relative strengths of these two effects depend on the horizontal scale of the motions and on the amount of basic state stable stratification; for mid-latitude cyclones on the earth, the two effects are approximately equal. Gierasch (1976) has pointed out that on Jupiter, the amount of stratification may be different at different levels between $p \sim 5$ bars and the tropopause, so that for motions on a particular horizontal scale, different dynamical equations may apply at the various levels. However, the actual amount of stratification at these levels on Jupiter is very uncertain. For this study, we

have adopted the quasi-geostrophic system representing a stable layer above p~5 bars. In the limits of very small or very large stratification in this layer, the results tend continuously to the results from using Gierasch's correctly scaled equations for this layer; however, we have implicitly excluded his possibility of having two or more distinct layers with different dynamical regimes between p~5 bars and the tropopause.

Another effect concerning the stratification which may be important on Jupiter has been suggested by Stone (1966, 1970, 1972), who has found that non-geostrophic 'inertial' (or 'symmetric') instabilities can occur, and have faster growth rates than quasi-geostrophic instabilities, in basic states whose stable stratification lies in a particular range of small values. However, he has used a single-layer model with a rigid lower boundary and no deep lower layer, which is unrealistic for Jupiter. Also these instabilities are independent of longitude and have very small latitudinal wavelengths, of which no evidence is seen in the Pioneer images.

(iv) The two-layer model is clearly a poor representation of basic states with complicated vertical structure of the stratification and zonal flow. Charney and Stern (1962) discussed the case of an 'internal jet' whose structure is sufficiently complicated, [i.e., when the potential vorticity gradient changes sign with altitude; in the modified Eady model of the appendix, this possibility is excluded because the potential vorticity gradient is taken to be zero throughout the upper layer], so as to allow baroclinic

instability even with upper and lower boundary conditions that would render simpler flows baroclinically stable. Depending on the details of the basic state vertical structure on Jupiter between p~5 bars and the tropopause, these 'internal jet' baroclinic instabilities may or may not occur; like the barotropic (BTU) modes of the present study, these baroclinic instabilities would be essentially independent of the deep fluid below p~5 bars. They can occur in a 'three-layer' model, in which the present upper layer is split into two layers with different zonal velocities and the pressure perturbation is required to be zero in the deep layer below p~5 bars. Using this model, we find that for some zonal flows independent of latitude, baroclinic instabilities can occur with growth time scales of ~1 week. Their theoretical structure should be investigated for latitudinally varying zonal flows [c.f. Stone(1969)], and both their results and those for the barotropic(BTU) instabilities of the present study should be compared with the Voyager data for a more thorough test of the 'upper weather layer' concept for Jupiter.

2. TWO LAYER MODEL DEVELOPMENT

A. Model Formulation.

The model is composed of two layers of incompressible, homogeneous fluid with the upper layer of density ρ_1 lying immiscibly above the lower layer of greater density ρ_2 (see fig. 1). The density contrast $\Delta\rho = \rho_2 - \rho_1$ is much smaller than ρ_1 and ρ_2. The bottom boundary of the lower layer is a flat rigid surface, which may not be realistic for Jupiter; this is discussed in the appendix. The top boundary of the upper layer, which corresponds to the Jovian tropopause, is taken as a free surface for the algebra below, but taking it as a flat rigid lid would cause only insignificant differences (of order $\Delta\rho/\rho$) in the results. Upper and lower layer variables are subscripted 1 and 2 respectively. For large scale hydrostatic motions with viscosity and diabatic effects neglected, the quasi-geostrophic potential vorticity equations for the upper and lower layers are (e.g. Pedlosky, 1964a)

$$\left(\frac{\partial}{\partial t} - \frac{\partial \psi_1}{\partial y}\frac{\partial}{\partial x} + \frac{\partial \psi_1}{\partial x}\frac{\partial}{\partial y}\right)\left[\nabla_h^2 \psi_1 - L_r^{-2}(\psi_1 - \psi_2)\right] + \beta_D \frac{\partial \psi_1}{\partial x} = 0 \quad , \tag{2.1}$$

$$\left(\frac{\partial}{\partial t} - \frac{\partial \psi_2}{\partial y}\frac{\partial}{\partial x} + \frac{\partial \psi_2}{\partial x}\frac{\partial}{\partial y}\right)\left[\nabla_h^2 \psi_2 - \delta L_r^{-2}(\psi_2 - \frac{\rho_1}{\rho_2}\psi_1)\right] + \beta_D \frac{\partial \psi_2}{\partial x} = 0 \quad , \tag{2.2}$$

FIGURE 1. Two layer model vertical section in the (y,z) plane.

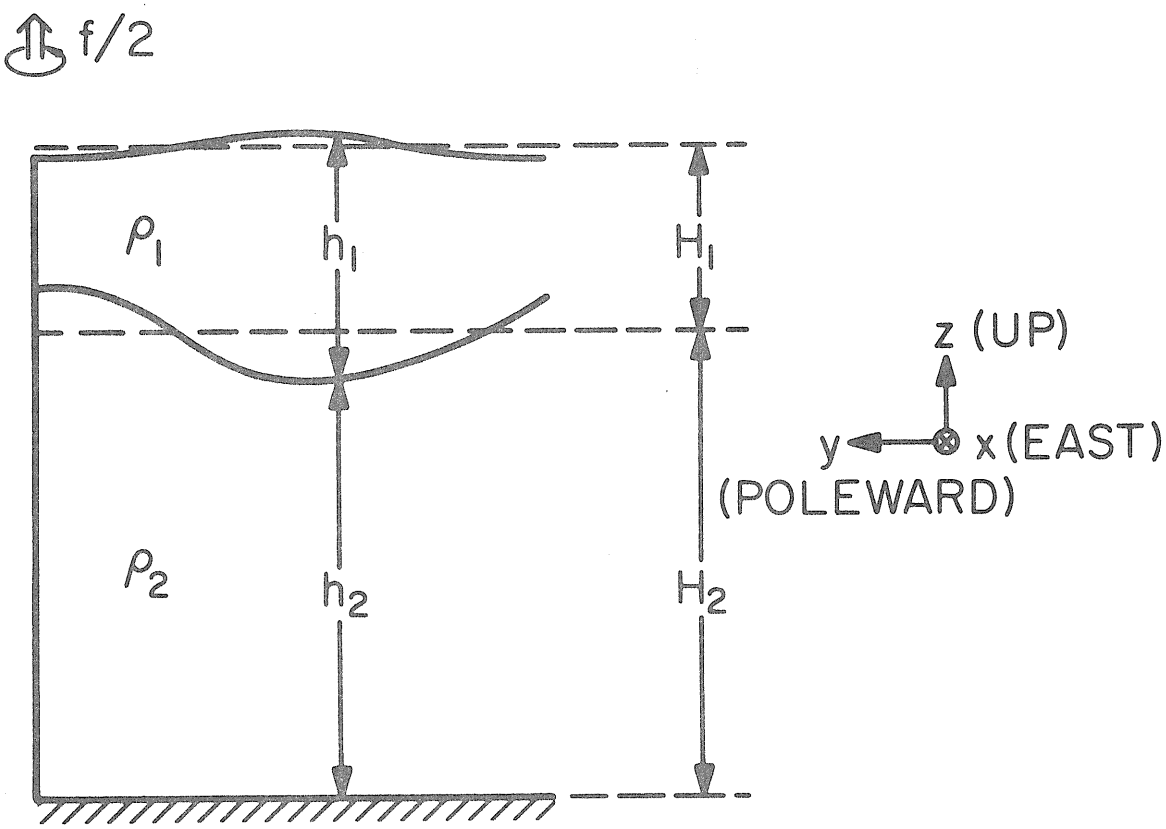

Figure 1

Here x and y are horizontal distance coordinates to the east and north respectively, and t is time. ∇_h^2 is the horizontal Laplacian operator. ψ (x, y, t) are streamfunctions for the geostrophic velocity field; the eastward and northward geostrophic velocities are $u_D = -\partial\psi/\partial y$ and $v_D = \partial\psi/\partial x$ respectively. (The subscript D is used to indicate a parameter is dimensional.) ψ_1 and ψ_2 are proportional to the hydrostatic pressure deviation from the horizontal mean, and are given by

$$\psi_1 = \frac{g}{fo}\left[(h_1 - H_1) + (h_2 - H_2)\right],$$

$$\psi_2 = \frac{g}{fo}\left[\frac{\rho_1}{\rho_2}(h_1 - H_1) + (h_2 - H_2)\right],$$

where h_1 and h_2 are the local thicknesses of the upper and lower layers respectively; the constant global mean thicknesses are H_1 and H_2. g is the gravitational acceleration, and fo is the value of $f = 2\Omega \sin$ (latitude) at the central latitude of the disturbance, where Ω is the planetary rotation rate; β_D is the value of df/dy at the central latitude.

L_r is the Rossby radius of deformation for the upper layer, given by

$$L_r = \left[\frac{\Delta\rho\ g\ H_1}{\rho_2\ f_o^2}\right]^{1/2}.$$

L_r is the horizontal length scale of motions for which the strengths of the dynamic and thermal stretching effects described

in section 1.C (iii) are approximately the same; in Eady-type models the x-wavelengths of the most unstable baroclinic waves have this scale, which for the earth corresponds to the observed scale of mid-latitude cyclones (e.g. Holton, 1972). In the appendix, L_r for Jupiter's upper weather layer is estimated to be between ~500 km and ~3000 km.

$\delta = H_1/H_2$ is the ratio of the mean thickness of the upper layer to that of the lower layer. The appropriate value of δ for Jupiter depends on the effective thickness of the deep fluid below p ~ 5 bars. The lower boundary of this region is taken to be a flat rigid surface for the two layer model, which represents simply some reflection mechanism for the disturbances deep in the Jovian interior, e.g. from a molecular-metallic phase transition at p~3 x 10^6 bars across which $\Delta\rho/\rho \sim .1$ (Stevenson and Salpeter, 1976, 1977) [compared to $\frac{\Delta\rho}{\rho} \sim 10^{-2}$ across the model interface at p~5 bars (Gierasch 1976)], or from non-hydrostatic effects at depths greater than the horizontal scales of the disturbances (see appendix). For compressible models the equivalent parameter to δ is the ratio of the upper layer pressure thickness to the pressure thickness of the disturbance in the lower layer, and for reflection due to the molecular-metallic phase transition, $\delta \sim 10^{-6}$.

We will investigate the stability of basic states with a quiescent lower layer ($\overline{u}_D = \overline{v}_D = 0$) and an upper layer containing a zonal velocity field $\overline{u}_D$ (y) (with $\overline{v}_D = 0$). For small perturbations ψ' (x, y, t) away from this basic state, the

coefficients in the perturbation forms of (2.1) and (2.2) depend only on y, so in the linearized equations (i.e., neglecting terms of order ψ'^2), we can look at the stability of individual Fourier-components of the form

$$\psi' = \mathrm{Re} \left\{ \varphi(y) \exp [ik_D (x - c_D t)] \right\} \quad .$$

Also it is convenient to non-dimensionalize (2.1) and (2.2) using a velocity U and length scale L (both positive) characteristic of the magnitude and latitudinal scale respectively of $\bar{u}_D(y)$. Defining

$$\hat{y} = y/L, \ \bar{u} = \bar{u}_D/U, \ \beta = \beta_D L^2/U, \ \lambda = L/L_r, \ c = c_D/U,$$

$$k = k_D L, \ \hat{\varphi} = \varphi/LU,$$

and subsequently dropping the $\wedge$ superscripts, φ_1 and φ_2 obey the linearized non-dimensional equations

$$\left[\frac{d^2}{dy^2} - k^2 - \lambda^2 + \frac{b}{\bar{u} - c} \right] \varphi_1 + \lambda^2 \varphi_2 = 0 \quad , \qquad (2.3)$$

$$\left[\frac{d^2}{dy^2} - k^2 - \delta \lambda^2 + \frac{\beta - \delta \lambda^2 \bar{u}}{-c} \right] \varphi_2 + \delta \lambda^2 \varphi_1 = 0 \quad . \qquad (2.4)$$

Here $b(y) \equiv \beta - \bar{u}_{yy} + \lambda^2 \bar{u}$ is the non-dimensional basic state potential vorticity gradient in the upper layer. The ρ_1/ρ_2 term appearing explicitly in (2.2) has been approximated to be 1 in (2.4) for clarity; this is equivalent to the Boussinesq approximation, and does not significantly affect any of the results below for $\Delta\rho/\rho \ll 1$. For Jupiter U is typically ~30m/s and L is ~5000 km. β is typically

$0(1)$ and λ^2 may be between 1 and 100. The time scale defined by L/U is ~2 earth days (~4 Jovian days). [The quasi-geostrophic scaling is strictly valid only for $\lambda^2 \sim 0(1)$, but (2.3) and (2.4) yield correct results for $\lambda^2 >> 1$ and $<< 1$; see section 1.C(iii).]

We will usually use horizontal boundary conditions requiring that the perturbation vanish as $y \to \pm \infty$, but in some cases the flow will be confined between rigid latitudinal walls at which $v_1' = y_2' = 0$, i.e., $\varphi_1 = \varphi_2 = 0$ for $k \neq 0$. Each of these boundary conditions can only be approximately correct for Jupiter; the former is accurate if the waves are evanescent in y and decay nearly to zero before being modified by basic state variations in neighboring latitudes, and the latter represents reflection in y (important for waves oscillatory in y) either by neighboring basic state variations or by the sphericity of the planet. For a particular real x-wavelength k (always taken positive without loss of generality), (2.3) and (2.4) present an eigenvalue problem to find c so that the solutions satisfy the horizontal boundary conditions. If $c_i \equiv \mathrm{Im}\,(c) > 0$, the wave is amplified; if $c_i < 0$, the wave is damped; and if $c_i = 0$, the wave is neutrally stable. Since all parameters in the coefficients of (2.3) and (2.4) are real except c, for any solution with $c = c_r + i\, c_i$ there is a complex conjugate solution with $c = c_r - i\, c_i$ (but see Lin, 1955, Ch. 8.4).

B. δ and $\delta^{1/2}$ Expansions (Deep Lower Layer).

Since $\delta = H_1/H_2 \ll 1$ and all other quantities are generally $\gg O(\delta)$ and $\ll O(\delta^{-1})$, we can expand (2.3) and (2.4) in powers of δ. This is useful because the expansion can be used to categorize the types of possible disturbances in this two layer system. Writing

$$a = \sum_{n=0}^{\infty} a^{(n)} \delta^n$$

where a represents any of φ_1, φ_2 or c, and defining the operators

$$G^{(0)} \equiv \frac{d^2}{dy^2} - k^2 - \lambda^2 + \frac{b}{\bar{u} - c^{(0)}}, \quad H^{(0)} \equiv \frac{d^2}{dy^2} - k^2 + \frac{\beta}{-c^{(0)}},$$

then substitution into (2.3) and (2.4) yields the zero order equations

$$\left[G^{(0)}\right] \varphi_1^{(0)} = -\lambda^2 \varphi_2^{(0)} \tag{2.5}$$

$$\left[H^{(0)}\right] \varphi_2^{(0)} = 0 \tag{2.6}$$

The first order [0 (δ)] equations are

$$\left[G^{(0)}\right] \varphi_1^{(1)} = -\lambda^2 \varphi_2^{(1)} - \frac{b\, c^{(1)}}{(\bar{u} - c^{(0)})^2} \varphi_1^{(0)}, \tag{2.7}$$

$$\left[H^{(0)}\right] \varphi_2^{(1)} = -\lambda^2 \varphi_1^{(0)} - \lambda^2 \left(\frac{\bar{u} - c^{(0)}}{c^{(0)}}\right) \varphi_2^{(0)} - \frac{\beta\, c^{(1)}}{c^{(0)2}} \varphi_2^{(0)}. \tag{2.8}$$

Assuming this δ expansion is uniformly valid over the whole latitudinal range, solutions fall into two categories. One type is basically a free barotropic disturbance of the upper layer, i.e., a solution $\varphi_1^{(0)}$ of the homogeneous equation (2.5)

with $\varphi_2^{(0)} = 0$, which forces an $0(\delta)$ disturbance $\varphi_2^{(1)}$ in the lower layer through (2.8). This is called a 'BTU' mode below. The other type is basically a free barotropic disturbance of the lower layer, i.e., a solution $\varphi_2^{(0)}$ of (2.6), which forces an 0(1) disturbance $\varphi_1^{(0)}$ in the upper layer through (2.5). This is called a 'BTL' mode below.

In both BTU and BTL modes, the interactions between the two layers only cause $0(\delta)$ modifications to the basically single-layer 0(1) free disturbances, and for the BTU mode we will see below that if the $\bar{u}$ (y) flow is barotropically stable at 0(1), the interaction with the lower fluid cannot destabilize the flow at $0(\delta)$. However, we now show that there is one other type of expansion of (2.3) and (2.4) in powers of $\delta^{1/2}$ with $\varphi_2^{(0)} = 0$, which permits an $0(\delta^{1/2})$ interaction between the layers that can destabilize at $0\ (\delta^{1/2})$ an otherwise stable $\bar{u}$ (y) flow. Writing $a = \sum_{n=0}^{\infty} a^{(n)}\ \delta^{n/2}$, where a represents any of φ_1, φ_2 or c, then substitution into (2.3) and (2.4) with $\varphi_2^{(0)} = 0$ yields just one zero order equation:

$$\left[G^{(0)}\right]\ \varphi_1^{(0)} = 0 \quad . \tag{2.9}$$

The first order $[0\ (\delta^{1/2})]$ equations are

$$\left[G^{(0)}\right]\ \varphi_1^{(1)} = -\lambda^2\ \varphi_2^{(1)} - \frac{b\ c^{(1)}}{(\bar{u} - c^{(0)})^2}\ \varphi_1^{(0)} \quad , \tag{2.10}$$

$$\left[H^{(0)}\right] \varphi_2^{(1)} = 0 \tag{2.11}$$

The second order [$0(\delta)$] equations are

$$\left[G^{(0)}\right] \varphi_1^{(2)} = -\lambda^2 \varphi_2^{(2)} - \frac{b}{(\bar{u} - c^{(0)})^2} \cdot \left(c^{(1)} \varphi_1^{(1)} + c^{(2)} \varphi_1(0) + \frac{c^{(1)^2} \varphi_1^{(0)}}{\bar{u} - c^{(0)}} \right), \tag{2.12}$$

$$\left[H^{(0)}\right] \varphi_2^{(2)} = -\lambda^2 \varphi_1^{(0)} - \frac{\beta c^{(1)}}{c^{(0)^2}} \varphi_2^{(1)} \quad . \tag{2.13}$$

In this system of equations, there can simultaneously be an $0(1)$ free disturbance $\varphi_1^{(0)}$ in the upper layer obeying (2.9) and an $0(\delta^{1/2})$ free disturbance $\varphi_2^{(1)}$ in the lower layer obeying (2.11). We will see that $c^{(1)}$ is determined by the higher order interactions in (2.10) and (2.13), and that these interactions can cause an essentially baroclinic instability. This is called a 'BC' mode below.

By inspection the three disturbance modes (BTU, BTL and BC) described by the δ and $\delta^{1/2}$ expansions above seem to be the only essentially unique modes contained in (2.3) and (2.4). Before considering specific solutions for particular basic state zonal wind profiles, we will first derive some general results for each type of mode that will put limits on the phase speeds, growth rates, and the types of modes and profiles for which instability is possible.

C. BTU Mode (Barotropic Upper Layer).

The governing zero order equation for this mode is (2.5) with $\varphi_2^{(0)} = 0$, i.e., the divergent barotropic vorticity equation for a single layer containing zonal flow $\bar{u}$ (y). This equation has been studied extensively [e.g. Kuo (1949), Lipps (1962, 1963, 1965)], and both stable and unstable solutions have been found with boundary conditions $\varphi = 0$ either at rigid walls or as $y \to \pm \infty$.

With these boundary conditions, we can show that if the flow is stable for the zero order BTU mode, it is still stable at $O(\delta)$. Forming the equation

$$\int \varphi_1^{(0)*} \cdot \text{eqn (2.7)} - \int \varphi_2^{(1)} \cdot \text{eqn (2.8)}^*$$

where * denotes complex conjugate and $\int$ denotes y-integration over the whole latitudinal range, we find

$$c^{(1)} \int \frac{b \left|\varphi_1^{(0)}\right|^2}{(\bar{u} - c^{(0)})^2} = -\int \left|\frac{d\,\varphi_2^{(1)}}{dy}\right|^2 - \int \left(k^2 + \frac{\beta}{c^{(0)}}\right) \left|\varphi_2^{(1)}\right|^2$$

If $c^{(0)}$ is real and outside the range of $\bar{u}$, this equation implies $c^{(1)}$ is real. For real $c^{(0)}$ within the range of $\bar{u}$, there would be singularities and corresponding imaginary contributions (Foote and Lin, 1950) from the left hand integral; however in this case we will see in section 5 that there must

be neighboring $\varphi_1^{(0)}$ solutions unstable at $0(1)$ with $|c_i^{(0)}| >> |\delta c^{(1)}|$. Therefore for BTU modes the presence of the lower layer cannot destabilize at $0(\delta)$ an otherwise barotropically stable $\bar{u}$ (y) flow in the upper layer.

Kuo (1949) and Pedlosky (1964b) have derived a necessary condition for the existence of neutral and marginally unstable ($c_i \ll c_r$) waves that have critical points where $\bar{u}$ (y) = c_r, in one and two layer models. We now rederive this result in a similar way, for a single barotropic layer. This result will be useful for the analysis of neutral upper layer solutions in section 3; furthermore, these neutral solutions form the starting points for investigations of unstable BTU modes in subsequent sections (see start of section 3). Writing

$$\varphi_1^{(0)} = A\ (y)\ \exp\ [i\ \theta\ (y)]$$

where A and θ are real, then substituting into (2.5) with $\varphi_2^{(0)} = 0$ and taking the imaginary part of this equation, we find

$$\frac{d}{dy}\left(A^2\ \frac{d\theta}{dy}\right) = -\ \mathrm{Im}\left(\frac{b\ A^2}{\bar{u} - c^{(0)}}\right) = -\ \frac{c_i^{(0)}\, b\ A^2}{\left|\bar{u} - c^{(0)}\right|^2} \qquad . \qquad (2.14)$$

In the limit as $c_i^{(0)} \to 0$, the right hand side tends to zero at all points where $\bar{u}$ (y) $\neq c_r^{(0)}$, so $A^2\ \frac{d\theta}{dy}$ becomes constant in latitude except across critical points where $\bar{u} = c_r^{(0)}$. In the vicinity of these critical points, viscosity becomes

important, but Foote and Lin (1950) show that the inviscid solutions on either side are joined correctly for $c_i^{(0)} \geq 0$ by taking the path of integration in the complex y-plane above the critical point if $\bar{u}_y \equiv \frac{d\bar{u}}{dy} < 0$, and below the critical point if $\bar{u}_y > 0$.

Integrating (2.14) with respect to y, the total change in $A^2 \frac{d\theta}{dy}$ over the whole latitudinal range in the limit $c_i^{(0)} \to 0^+$ is then

$$\Delta \left[A^2 \frac{d\theta}{dy}\right] = \sum_c \pi \frac{b\,(y_c)\, A^2\,(y_c)}{\bar{u}_y\,(y_c)} \quad , \tag{2.15}$$

where the sum is over all critical points $y = y_c$ where $\bar{u} = c_r^{(0)}$. However, $A^2 \frac{d\theta}{dy}$ must equal zero at both latitudinal boundaries (since $\varphi_1^{(0)} = 0$ there), so either the critical point jumps must cancel out or bA^2 must equal zero at every critical point. For velocity profiles that are monotonic, or symmetric and monotonic in each half range, the critical point jumps cannot cancel, so either b or A must vanish at every critical point. Furthermore, we can generalize Kuo's (1949) proof that A(y) cannot vanish at the critical points to cover divergent barotropic flows. Equation (2.5) with $\varphi^{2\,(0)} = 0$ can be written

$$\frac{d^2}{dy^2}\,\varphi_1^{(0)} = \left[k^2 + \left(\frac{\beta + \lambda^2 c^{(0)}}{c^{(0)} - \bar{u}}\right) + \frac{\bar{u}_{yy}}{\bar{u} - c^{(0)}}\right] \varphi_1^{(0)}$$

$$\equiv S\,\varphi_1^{(0)} \quad .$$

This is to be compared with the equation

$$\frac{d^2 F}{dy^2} = \left[\frac{\bar{u}_{yy}}{\bar{u} - c^{(0)}} \right] F \equiv S_F F$$

which has a solution $F = \bar{u} - c^{(0)}$ with $F = 0$ at critical points. For real $c^{(0)}$ and any velocity profile $\bar{u}$ (y) with critical points, $S > S_F$ at all points either between two adjacent critical points or between a critical point and the adjacent boundary. So for one or the other of these two ranges, Sturm's comparison theorem implies that $\varphi_1^{(0)}$ cannot be zero at both end points of the range, since F oscillates slower than $\varphi_1^{(0)}$ over the range and has a zero only at one end point. Hence $A = |\varphi_1^{(0)}|$ cannot be zero both at the boundaries and at all critical points. For velocity profiles that are monotonic, or symmetric and monotonic in each half range, the only remaining possibility satisfying $\Delta [A^2 \frac{d\theta}{dy}] = 0$ is that the basic state potential vorticity gradient b (y) vanishes at all critical points. Therefore, for all neutral or marginally unstable waves in the single upper layer, either $c_r^{(0)}$ lies outside the range of $\bar{u}$ or else the basic state potential vorticity gradient b (y) vanishes at all critical points where $\bar{u}$ (y) = $c_r^{(0)}$.

Charney and Stern (1962) derived a different condition which, applied to the present single layer, requires that b (y) must vanish at some latitude for any unstable waves to exist. Combining this with the condition derived above, we see that the

only $\bar{u}$ (y) flows that can be unstable to BTU modes must have b (y) vanish somewhere, and the only neutral disturbances for these flows either have $c^{(0)}$ outside the range of $\bar{u}$ or have $c^{(0)}$ equal to $\bar{u}$ (y_c) where b (y_c) = 0. These criteria will be useful for the analysis of the BTU modes in subsequent sections since they only allow situations in which the governing equation (2.5) is non-singular over the whole latitudinal range.

Pedlosky (1964 a, b) has derived several inequalities bounding the phase speed c_r and growth rate kc_i for a two-layer model. Some of these results (non-dimensionalized as in section 2.A) are listed below applied to a single divergent barotropic layer, which causes slight differences from Pedlosky's two layer versions; however the derivations are essentially the same. These results will be useful in section 6 in finding BTU solutions numerically, since they limit the areas in the (c_r, c_i) plane to be searched for eigenvalues.

For a single layer containing zonal flow $\bar{u}$ (y) with $\varphi = 0$ boundary conditions, the equivalent equation to (4.2.6) of Pedlosky (1964a) is

$$\bar{u}_{min} - \max\left\{0, \frac{\beta + \lambda^2 \bar{u}_{max}}{2(k^2 + \lambda^2)}\right\} \leq c_r \leq \bar{u}_{max} + \max\left\{0, -\left[\frac{\beta + \lambda^2 \bar{u}_{min}}{2(k^2 + \lambda^2)}\right]\right\} \tag{2.16}$$

where $\bar{u}_{min}$ and $\bar{u}_{max}$ are extrema for the whole latitudinal range. (2.16) applies only to unstable disturbances with

$c_i \neq 0$. For neutral disturbances, the single layer equivalent to (2.9) in Pedlosky (1964b) is

$$\bar{u}_{min} - p - \sqrt{p^2 + 2p\,(\bar{u}_{max} - \bar{u}_{min})} \leq c \leq \bar{u}_{max} + q + \sqrt{q^2 + 2q\,(\bar{u}_{max} - \bar{u}_{min})} \qquad (2.17)$$

where $p = \max\left\{0, \dfrac{\beta + \lambda^2 \bar{u}_{max}}{2(k^2 + \lambda^2)}\right\}$ and $q = \max\left\{0, -\left[\dfrac{\beta + \lambda^2 \bar{u}_{min}}{2(k^2 + \lambda^2)}\right]\right\}$.

By a straightforward adaption of Kuo's (1949) proof that $c \leq \bar{u}_{max}$ for non-divergent flows, we can also show that for neutral disturbances

$$\min\left\{-\frac{\beta}{\lambda^2}, \bar{u}_{min}\right\} \leq c \leq \max\left\{-\frac{\beta}{\lambda^2}, \bar{u}_{max}\right\} \qquad (2.18)$$

The one layer versions of (4.2.11) and (4.2.12) in Pedlosky (1964a) are

$$|kc_i| \leq \frac{k\,|\bar{u}_y|_{max}}{2(k^2+\lambda^2)^{1/2}} \qquad (2.19)$$

$$(kc_i)^2 \leq \frac{k^2\,(\bar{u}\,b)_{max}}{k^2 + \lambda^2} \qquad (2.20)$$

In both (2.19) and (2.20), the growth rate bounds decrease to zero as the non-dimensional Rossby radius of deformation λ^{-1} decreases to zero. This behavior is seen for explicit solutions in sections 5 and 7 .

D. BTL Mode (Barotropic Lower Layer)

The governing zero order equation for this mode is (2.6), the barotropic vorticity equation for a single quiescent layer. The only type of boundary conditions that solutions $\varphi_2^{(0)}$ can satisfy are $\varphi = 0$ at rigid latitudinal walls, which require that $c^{(0)}$ is real, so that these solutions are neutral (westward propagating) Rossby waves in the lower fluid.

With these boundary conditions, we can derive an expression for $c^{(1)}$. Forming the equation

$$\int \varphi_1^{(0)} \cdot \text{eqn (2.5)}^* - \int \varphi_2^{(0)*} \cdot \text{eqn (2.8)} \quad ,$$

we find

$$\frac{\beta c^{(1)}}{c^{(0)2}} \int \left|\varphi_2^{(0)}\right|^2 = -\frac{\lambda^2}{c^{(0)}} \int (\bar{u} - c^{(0)}) \left|\varphi_2^{(0)}\right|^2 - \int \left|\frac{d\varphi_1^{(0)}}{dy}\right|^2 - \int \left(k^2 + \lambda^2 - \frac{b}{\bar{u} - c^{(0)}}\right) \left|\varphi_1^{(0)}\right|^2 \quad .$$

For real $c^{(0)}$ outside the range of $\bar{u}$, this equation implies $c^{(1)}$ is real. For real $c^{(0)}$ within the range of $\bar{u}$, the last integral on the right hand side contains critical point singularities and corresponding inaginary contributions to $c^{(1)}$; (unlike the BTU mode above, there are not necessarily any neighboring BTU solutions unstable at O(1) since the upper layer equation (2.5) now contains the $\varphi_2^{(0)}$ forcing term and section 5 does not apply).

So for BTL modes, the kinetic and potential energies of the upper layer flow $\bar{u}$ are available to amplify 0(1) free Rossby waves in the lower layer, if $c^{(0)}$ is within the range of $\bar{u}$. However due to the inertia of the lower layer the instability can only occur at $0(\delta)$, compared to 0(1) for unstable BTU modes and $0(\delta^{1/2})$ for unstable BC modes (see below), and so we do not consider the BTL mode any further in this work.

E. BC Mode (Baroclinic).

The zero order equation for this mode is (2.9) for $\varphi_1^{(0)}$ in the upper layer, which is the same equation as for the zero order BTU mode. The lower layer $0(\delta^{1/2})$ solutions $\varphi_2^{(1)}$ are free Rossby waves obeying (2.11). With boundary conditions $\varphi_1 = \varphi_2 = 0$ either at rigid walls or as $y \to \pm \infty$, (2.11) requires that $c^{(0)}$ be real; the only distinction of the BC mode as compared to the BTU mode is the possibility of destabilizing at $0(\delta^{1/2})$ an otherwise barotropically stable flow in the upper layer.

With these boundary conditions and $c^{(0)}$ real, the same criterion applies for the existence of neutral solutions of (2.9) as for the zero order BTU mode above; i.e., if there are any critical points at which $\bar{u}(y_c) = c^{(0)}$, then $b(y_c)$ must vanish. Therefore the phases of $\varphi_1^{(0)}$ [from (2.15)] and of $\varphi_2^{(1)}$ are constant in latitude, even across critical points.

Having found free solutions $\varphi_1^{(0)}$ and $\varphi_2^{(1)}$ for a given real $c^{(0)}$, we can derive expressions giving $c^{(1)}$ and the relative amplitudes and phases of $\varphi_1^{(0)}$ and $\varphi_2^{(1)}$. Multiplying (2.10) by $\varphi_1^{(0)*}$ and (2.13)* by $\varphi_2^{(1)}$, and integrating over the whole latitudinal range, we find

$$c^{(1)} \int \frac{b \left|\varphi_1^{(0)}\right|^2}{\left(\bar{u} - c^{(0)}\right)^2} = c^{(1)*} \int \frac{\beta \left|\varphi_2^{(1)}\right|^2}{c^{(0)2}} = -\lambda^2 \int \varphi_1^{(0)*} \varphi_2^{(1)} \,. \tag{2.21}$$

If $c^{(1)} \neq 0$, taking the modulus of the left hand equality in (2.21) shows

$$\int \left|\varphi_2^{(1)}\right|^2 = \frac{c^{(0)2}}{\beta} \left| \int \frac{b \left|\varphi_1^{(0)}\right|^2}{(\bar{u} - c^{(0)})^2} \right| , \qquad (2.22)$$

which sets the magnitude of $\varphi_2^{(1)}$ relative to $\varphi_1^{(0)}$. Taking arguments in both equalities of (2.21) and eliminating arg $[c^{(1)}]$ shows

$$\arg\left[\int \varphi_1^{(0)*} \varphi_2^{(1)}\right] = \frac{1}{2} \arg\left[\int \frac{b \left|\varphi_1^{(0)}\right|^2}{(\bar{u} - c^{(0)})^2}\right] + n\pi . \qquad (2.23)$$

Finally the right hand equality in (2.21) implies

$$c^{(1)} = -\lambda^2 \int \varphi_1^{(0)} \varphi_2^{(1)*} \Bigg/ \int \frac{\beta \left|\varphi_2^{(1)}\right|^2}{c^{(0)2}} . \qquad (2.24)$$

In (2.23) n = 0 or 1, chosen to make Im $(c^{(1)}) \geq 0$. So if the upper layer integral on the right hand side of (2.23) is either real and negative or is complex due to critical point singularities (Foote and Lin, 1950), then $\varphi_1^{(0)}$ and $\varphi_2^{(1)}$ are out of phase (in the x direction) by an amount other than 180°, and $c^{(1)}$ is complex. The magnitude of $c^{(1)}$ depends on the 'interaction' integral $\int \varphi_1^{(0)} \varphi_2^{(1)*}$, which generally can be large when $\varphi_1^{(0)}$ and $\varphi_2^{(1)}$ have similar y-wavelengths (i.e. $G^{(0)} \approx H^{(0)}$) over a large latitudinal range.

The above shows for the BC mode that $c^{(0)}$ must be real, but $c^{(1)}$ may be complex. So the dynamics of the lower layer

can destabilize at $O(\delta^{1/2})$ an otherwise barotropically stable flow in the upper layer. We will see in section 4.A that this type of instability still occurs for $\bar{u}$ independent of latitude, so it is essentially baroclinic in nature.

F. Energy Equations.

As discussed in section 1. C(i), the baroclinic and barotropic disturbances have associated eddy fluxes that transfer energy between the zonally averaged flow and the disturbances. In later sections some of these fluxes are evaluated for various disturbance modes to see if their accumulated effect could be significant in the long-term energetics of the zonal flow. To derive energy equations describing these transfers, we can start from the two layer non-linear equations (2.1) and (2.2). The standard method [e.g. Holton (1972) Ch. 11] is to form the equations

$$\int \overline{\psi_1} \cdot \overline{(2.1)} \quad , \quad \int \overline{\psi_1' \cdot (2.1)'} \quad , \quad \int \overline{\psi_2} \cdot \overline{(2.2)} \quad ,$$

$$\int \overline{\psi_2' \cdot (2.2)'} \quad ,$$

where the overbar denotes zonal mean, the prime denotes departure from the zonal mean, and $\int$ denotes integration over y with $v_D = \partial\psi/\partial x = 0$ at latitudinal boundaries. After some manipulation, this yields (with all quantities dimensional including u and v)

$$\frac{\partial}{\partial t}\int \frac{1}{2}\rho_1 (\bar{u}_1^2 + \bar{v}_1^2) H_1 = \int \bar{p}_1 \bar{w}_1 \Big|_{I^+} - \int \rho_1 \bar{u}_1 \left(\overline{u_1' v_1'}\right)_y H_1 \quad , \quad (2.25)$$

$$\frac{\partial}{\partial t}\int \frac{1}{2}\ \rho_1 \left(\overline{u_1'^2 + v_1'^2}\right)\ H_1 = \int \overline{p_1'\ w_1'}\Big|_{I^+} + \int \rho_1\ \bar{u}_1 \left(\overline{u_1'\ v_1'}\right)_y\ H_1\ , \tag{2.26}$$

$$\frac{\partial}{\partial t}\int \frac{1}{2}\ g\ \Delta\rho\ \ \overline{h_2}^2 = -\int \overline{p_1}\ \overline{w_1}\Big|_{I^+} + \int \overline{p_2}\ \overline{w_2}\Big|_{I^-} - \int f_o\ \rho_1\ (\bar{u}_1 - \bar{u}_2)\ \ \overline{v_1'\ h_1'}\ , \tag{2.27}$$

$$\frac{\partial}{\partial t}\int \frac{1}{2}\ g\ \Delta\rho\ \ \overline{h_2'^2} = -\int \overline{p_1'\ w_1'}\Big|_{I^+} + \int \overline{p_2'\ w_2'}\Big|_{I^-} + f_o\ \rho_1\ (\bar{u}_1 - \bar{u}_2)\ \ \overline{v_1'\ h_1'}\ , \tag{2.28}$$

$$\frac{\partial}{\partial t}\int \frac{1}{2}\ \rho_2 \left(\bar{u}_2^{\,2} + \bar{v}_2^{\,2}\right) = -\int \overline{p_2}\ \overline{w_2}\Big|_{I^-} - \int \rho_2\ \overline{u_2} \left(\overline{u_2'\ v_2'}\right)_y\ H_2\ , \tag{2.29}$$

$$\frac{\partial}{\partial t}\int \frac{1}{2}\ \rho_2 \left(\overline{u_2'^2 + v_2'^2}\right) = -\int \overline{p_2'\ w_2'}\Big|_{I^-} + \int \rho_2\ \bar{u}_2 \left(\overline{u_2'\ v_2'}\right)_y\ H_2\ . \tag{2.30}$$

Here $p = f_o\ \rho\ \psi$ is the local hydrostatic pressure, and h is the local thickness of a layer, related to ψ_1 and ψ_2 as in section 2.A. I^+ and I^- denote values taken on horizontal surfaces just above and below the fluid interface, respectively. w is the vertical velocity upwards of fluid particles; for the two layer model, w is linear in height within each layer and is related to

ψ and h by the kinematic conditions at the fluid surfaces [e.g. Pedlosky (1964a)].

(2.25) and (2.26) are the zonal mean and eddy kinetic energy equations for the upper layer, and (2.29) and (2.30) are the same equations for the lower layer. (2.27) and (2.28) are the zonal mean and eddy equations for the available potential energy (a.p.e.) of the sloping fluid interface. [The a.p.e. of the free top surface of the upper layer has been omitted from this set of equations, since this a.p.e. is of order $\Delta\rho/\rho$ compared to the interface a.p.e. for flows with $O(|\psi_1|) \leq O(|\psi_1 - \psi_2|)$, e.g. for all BTU and BC disturbances.] These two layer equations (2.25) to (2.30) correspond term for term with the quasi-geostrophic energy equations with continuous vertical resolution [e.g. Holton (1972) Ch. 11], but here the available potential energy and vertical energy transfers are concentrated at the interface and not distributed over all depths. This provides further evidence that the two layer model contains all the important quasi-geostrophic processes of vertically continuous models.

Although these equations are derived from the non-linear equations (2.1) and (2.2), the corresponding eddy equations $(2.1)'$, $(2.2)'$ and also (2.26), (2.28) and (2.30) are obeyed exactly by the linear disturbances of this work, and in subsequent sections several of the energy transfer terms on the right hand sides

of the energy equations are interpreted and evaluated for some explicit linear solutions.

3. NEUTRAL WAVES

All of the unstable modes investigated in later sections will be either barotropically unstable waves in the upper layer (BTU modes), or barotropically stable waves in the upper layer that are destabilized baroclinically at $O(\delta^{1/2})$ by the perturbing effect of the lower layer (BC modes, in section 4). In section 5, the growth rates of unstable BTU modes are estimated analytically by a variational method for waves just slightly different from the neutrally stable waves, so for both these sections the starting points are the zero order upper layer neutral solutions to (2.5) with $\varphi_2^{(0)}$ set equal to zero and with $c^{(0)}$ real. These neutral waves are derived below for particular velocity profiles used in the subsequent sections.

For $\bar{u}$ independent of y, the only unstable modes are baroclinic (BC), with nearly free Rossby waves in each layer. In section 4 we investigate this case to compare with the continuously stratified model of the appendix. For $\bar{u}$ dependent on y, the criterion of section 2.C requires that for real $c^{(0)}$ within the range of $\bar{u}(y)$, the potential vorticity gradient b(y) be zero at the point where $\bar{u}(y) = c^{(0)}$. For this case we investigate the two analytically tractable sech^2 and tanh profiles used by Lipps (1962, 1963, 1965), both of which yield evanescent neutral disturbance solutions obeying $\varphi \to 0$ as $y \to \pm \infty$. In addition we find neutral solutions for the sech^2 profile that are oscillatory in y

outside the jet and can only obey the boundary conditions $\varphi = 0$ at rigid latitudinal walls. The remaining case of $c_r^{(0)}$ having general values outside the range of $\bar{u}(y)$ would be relatively complicated analytically; however the numerical searches in section 6 for the sech^2 profile found no solutions with this property.

A. Sech^2 Velocity Profile.

As in Lipps (1962, 1963) we consider profiles of the form (in dimensional quantities)

$$\overline{u_D}(y) = U_1 + U_0 \operatorname{sech}^2 (y/L)$$

where U_0 and U_1 can be positive or negative. This type of profile represents an isolated zonal jet centered at y = 0 embedded in a constant velocity field U_1. Many Jovian disturbances are observed at the centers of retrograde jets, corresponding to $U_o < 0$ and $U_1 + U_o < 0$. To find neutral solutions $\varphi_1^{(0)}$ of (2.5) with $\varphi_2^{(0)} = 0$, it is analytically convenient to non-dimensionalize in a slightly different way from that in section 2.A, to absorb the ambient velocity U_1. Defining

$$\hat{y} = y/L, \quad \bar{u} = (\bar{u}_D - U_1)/U_0, \quad B = (\beta_D + L_r^{-2} U_1)/(L_r^{-2} U_0),$$

$$c^{(0)} = (c_D^{(0)} - U_1)/U_0, \; k = k_D L, \quad \lambda = L/L_r, \quad \hat{\varphi}_1 = \varphi_1/L U_0,$$

then dropping the $\wedge$ and (0) superscripts, (2.5) with $\varphi_2^{(0)} = 0$ is replaced by the non-dimensional equation

$$\frac{d^2}{dy^2}\varphi - k^2\varphi - \lambda^2\varphi + \left[\frac{(B + \bar{u})\,\lambda^2 - \bar{u}_{yy}}{\bar{u} - c}\right]\varphi = 0 \quad , \qquad (3.1)$$

with $\bar{u} = \operatorname{sech}^2 y$. For this profile, the potential vorticity gradient $(B + \bar{u})\,\lambda^2 - \bar{u}_{yy}$ can be written as the quadratic $6\bar{u}^2 + (\lambda^2 - 4)\,\bar{u} + B\lambda^2$. For real c lying within the range of $\bar{u}$ (i.e., $0 < c < 1$), the condition of section 2.C requires

that the potential vorticity gradient vanish at $\bar{u} = c$, so that c must be a root of this quadratic. Therefore

$$c = -\left(\frac{\lambda^2 - 4}{12}\right) \pm \sqrt{\left(\frac{\lambda^2 - 4}{12}\right)^2 - \frac{B\lambda^2}{6}} \quad , \tag{3.2}$$

and (3.1) becomes

$$\frac{d^2}{dy^2}\varphi + (6\ \mathrm{sech}^2\ y - k^2 + 6c - 4)\ \varphi = 0 \quad .$$

Following Lipps, we change the independent variable to $z = \tanh y$, which implies

$$(1 - z^2)\ \frac{d^2\varphi}{dz^2} - 2z\ \frac{d\varphi}{dz} + \left[6 - \left(\frac{k^2 - 6c + 4}{1 - z^2}\right)\right]\varphi = 0 \quad . \tag{3.3}$$

(3.3) is a form of Legendre's equation (e.g. Abramowitz and Stegun, 1965, sec. 8.1). With boundary conditions $\varphi \to 0$ as $y \to \pm\infty$, i.e., as $z \to \pm 1$, there are only two (associated Legendre function) solutions; the symmetric solution (i.e., an even function of y)

$$\varphi = (1 - z)\ (1 + z) = \mathrm{sech}^2\ y \quad \text{for which } k^2 = 6c \quad , \tag{3.4a}$$

and the antisymmetric solution (i.e., an odd function of y)

$$\varphi = z\ (1 - z)^{1/2}\ (1 + z)^{1/2} = \mathrm{sech}\ (y)\ \tanh\ (y) \quad \text{for which } k^2 = 6c - 3 \quad . \tag{3.4b}$$

Since $k^2 \geq 0$, the latter wave is possible only if $c \geq 1/2$. These solutions are evanescent as $y \to \pm\infty$, decaying with the

same latitudinal length scale L as the jet. (Numerical solutions in section 6 indicate that these modes are modified insignificantly by imposing rigid wall boundaries at $y = \pm Y$ for $Y \geq 3$.)

There are other solutions to (3.3) that are oscillatory far from the jet, essentially becoming Rossby waves there. On Jupiter, such waves would be reflected and/or absorbed at large $|y|$ either by basic state variations of the neighboring belt-zone structure or by the sphericity of the planet. The form of the boundary conditions most appropriate for Jupiter is largely unknown; for simplicity below we consider purely reflective boundaries by imposing rigid walls at various $y = \pm Y$. The oscillatory solutions are (Abramowitz and Stegun, 1965, Ch. 15.4)

$$\varphi = \left(\frac{1+z}{1-z}\right)^{i\ell/2} (1 + \ell^2 + 3i\ell z - 3z^2) \text{ where } \ell = \pm (6c - 4 - k^2)^{1/2}$$

and $i^2 = -1$. This requires $6c - 4 - k^2 > 0$, so these waves are possible only if $c > 2/3$. Rearranging, this gives two independent symmetric and antisymmetric solutions

$$\varphi = (1 + \ell^2 - 3z^2) \cos\left[\ell \ln\left(\frac{1+z}{1-z}\right)^{1/2}\right] - (3\ell z) \sin\left[\ell \ln\left(\frac{1+z}{1-z}\right)^{1/2}\right], \tag{3.5a}$$

$$\varphi = (3\ell z) \cos\left[\ell \ln\left(\frac{1+z}{1-z}\right)^{1/2}\right] + (1 + \ell^2 - 3z^2) \sin\left[\ell \ln\left(\frac{1+z}{1-z}\right)^{1/2}\right]. \tag{3.5b}$$

As $y \to \pm \infty$, $\ell \ln \left(\frac{1 + z}{1 - z}\right)^{1/2} \to \ell y$ so these solutions become sinusoidal with y-wavenumber ℓ. For particular basic states and walls located symmetrically north and south of the jet center, there are generally several discrete values of ℓ that place $\varphi = 0$ nodes of these oscillatory waves at the walls where $z = \tanh(\pm Y)$.

The latitudinal forms of the neutral wave types (3.4a, b) and (3.5a, b) are shown in fig. 2. For the oscillatory waves, $\varphi(y)$ depends on the value of ℓ, but the qualitative shapes including the central structures are essentially independent of ℓ.

For basic state profiles observed on Jupiter, the theory above predicts that neutral waves travel with the velocity $\bar{u}_D$ at which the upper layer potential vorticity has an extremum. However this can not be tested directly by observations of cloud motions, since even if $\bar{u}_D(y)$ is measured perfectly, the potential vorticity still depends on the unknown upper layer radius of deformation L_r, (which enters in the non-dimensional parameters B and λ^2 above). The dependence of the locations of potential vorticity extrema on the values of L_r, U_o and U_1 is discussed in detail below for the sech^2 velocity profile, for general ranges of the equivalent non-dimensional parameters. Some particular examples for values of L_r, U_o and U_1 most likely to be useful for analysis of Jovian observations are presented in section 7.

FIGURE 2. Latitudinal shapes of $\bar{u}_D$ and the upper layer neutral solutions (3.4a,b) and (3.5a,b) for the velocity profile $\bar{u}_D = U_1 + U_0 \operatorname{sech}^2 (y/L)$. (Relative scales on the abscissae are arbitrary.)

(a): $\bar{u}_D$ vs. (poleward) latitudinal coordinate y/L, for retrograde jet with $U_0 < 0$.

(b) and (c): φ vs. y/L for evanescent solutions (3.4a) and (3.4b), respectively.

(d) and (e): φ vs. y/L for oscillatory solution (3.5a) with $\ell = .99$, and oscillatory solution (3.5b) with $\ell = 1.29$, respectively.

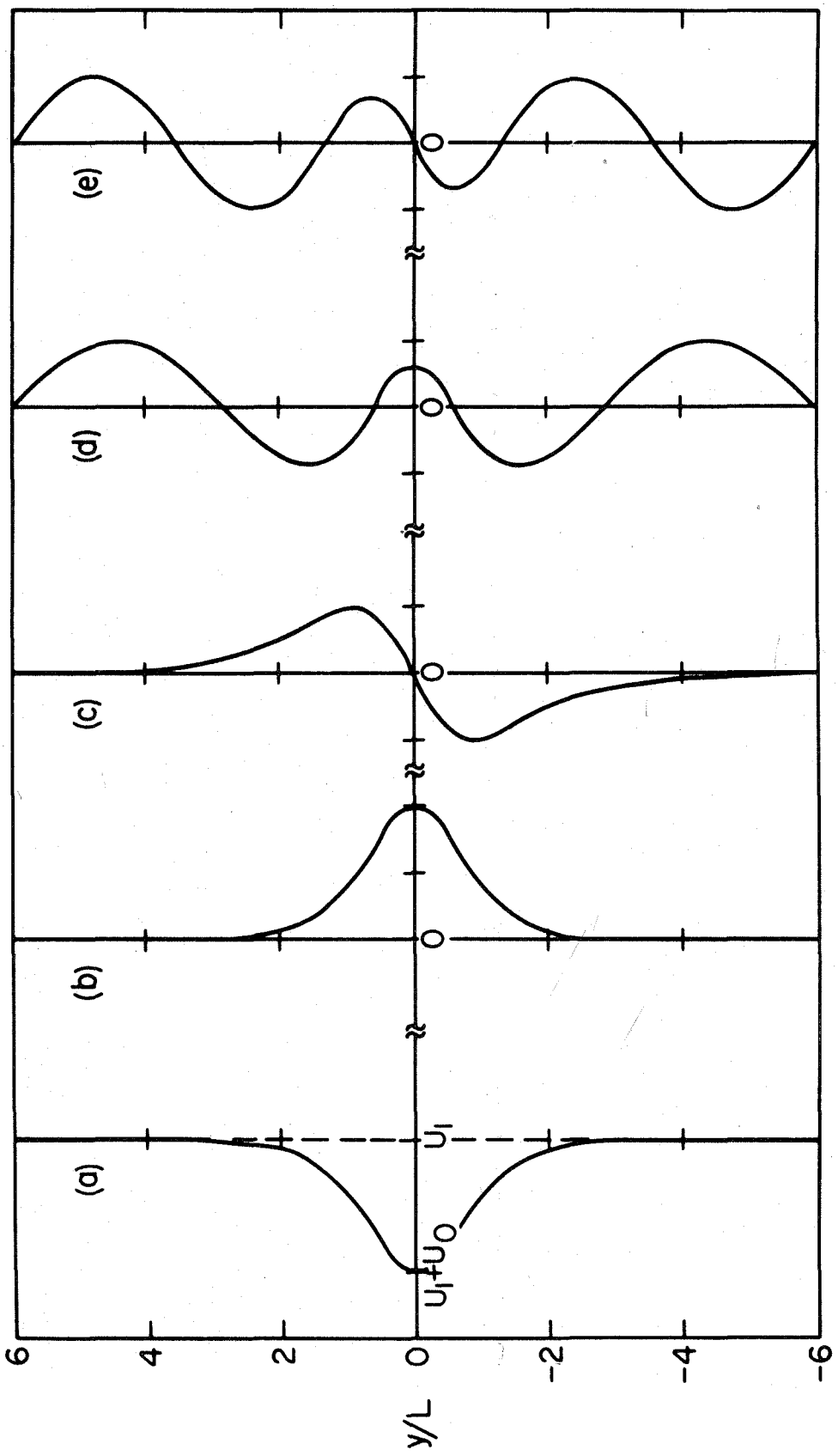

Figure 2

For given values of the non-dimensional basic state parameters B and λ^2, the phase speed c of all the neutral disturbance types on the sech^2 velocity profile is determined by (3.2), and is equal to the value of $\bar{u}$ at the potential vorticity extremum. Fig. 3 shows c as a function of B for various values of λ^2. This $c = (c_D - U_1)/U_0$ is non-dimensionalized relative to the jet so that c equals zero for waves with dimensional phase speed c_D equal to the flow U_1 outside the jet, and c equals 1 for waves with c_D equal to the velocity $U_0 + U_1$ at the jet center. If a given basic state has both c's as defined by (3.2) outside the range (0, 1), the neutral waves found above can still exist but then there is no potential vorticity extremum at any latitude, and the criterion of Charney and Stern (1962) shows no barotropically unstable disturbances can exist; for this reason these cases are not investigated in this work.

The parameter B is equal to $(\beta_D + L_r^{-2} U_1)/(L_r^{-2} U_0)$ where β_D is the dimensional planetary vorticity gradient and L_r is the upper layer radius of deformation. This parameter is the ratio of the contribution to the upper layer potential vorticity gradient (which dimensionally is $\beta_D - (\bar{u}_D)_{yy} + L_r^{-2} \bar{u}_D$) from β_D plus the slope of the fluid interface associated with the ambient U_1, compared to that from the interface slope associated with the sech^2 jet strength U_0. The parameter

FIGURE 3. Non-dimensional phase speeds $c = (c_D - U_1)/U_0$ of neutral disturbances on velocity profile $\bar{u}_D = U_1 + U_0 \operatorname{sech}^2 (y/L)$, as functions of the basic state parameter $B = (\beta_D + L_r^{-2} U_1)/(L_r^{-2} U_0)$, for various values of $\lambda^2 = L^2/L_r^2$.

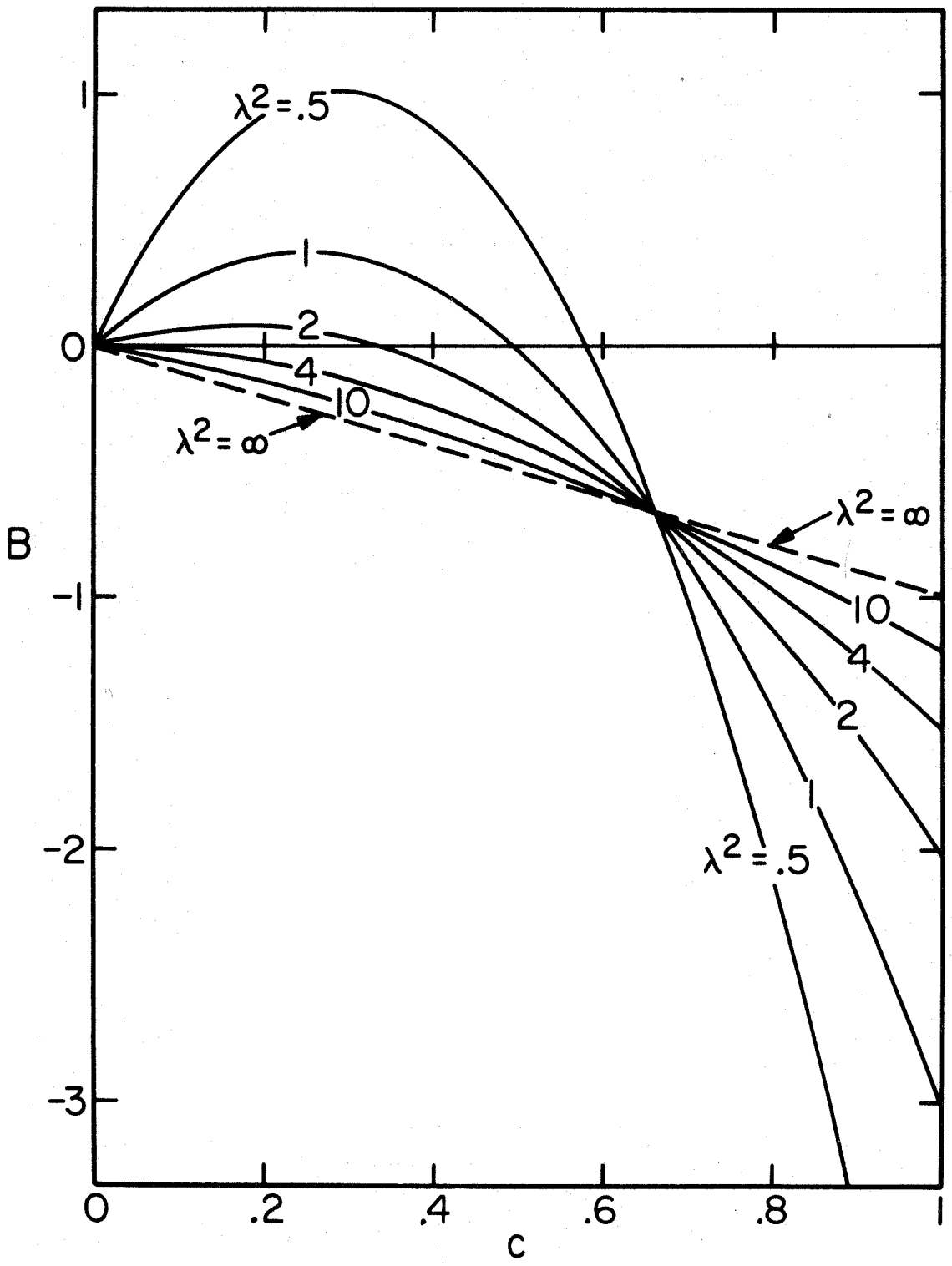

Figure 3

$\lambda^2 = L^2/L_r^2$ is a measure of the vorticity gradient $(\bar{u}_D)_{yy} \sim U_0/L^2$ due to the horizontal shear of the jet compared to that due to the sloping fluid interface of the jet $\sim U_0/L_r^2$. For large values of λ, L_r and $\Delta\rho$ are small so that the fluid interface slope is large for a given $\bar{u}_D$, and $(\bar{u}_D)_{yy}$ (and β_D) are relatively unimportant compared to $\bar{u}_D/L_r^2$; for $\lambda^2 \to 0$, the converse is true. (Fig. 3 cannot show the non-divergent case $\lambda^2 = 0$; this is shown in Lipps (1963), whose parameter B corresponds to the present $B\lambda^2$, and also in fig. 18.)

For Jupiter, λ^2 is probably ≥ 4 ($L_r \leq 2500$ km); for these values the potential vorticity gradient is controlled more by the interface slope $\sim \bar{u}_D/L_r^2$ than by β_D or $(\bar{u}_D)_{yy}$, so vorticity extrema can only occur close to points where $\bar{u}_D = 0$, so that $c_D \approx 0$ and $c \approx -U_1/U_0$. For large λ^2, $B \approx U_1/U_0$ and so in fig. 3 all curves with $\lambda^2 \geq 4$ cluster around the $\lambda^2 = \infty$ straight line with slope -1. Usually for Jupiter $U_1 \geq 0$ so that vorticity extrema are only possible in retrograde jets with $U_0 < -U_1$. For values of $\lambda^2 \leq 4$, β and the sech^2 curvature $(\bar{u}_D)_{yy}$ become more significant and the curves in fig. 3 have more complex behavior with possibly two values of c for given basic states [which may be prograde with U_0 and $U_1 \geq 0$; this case with $\lambda^2 \approx 1$ is more appropriate for the earth's jet stream and Gulf Stream (Lipps, 1963)]. Some implications of fig. 3 for Jovian observations are discussed in section 7.

The values of the x-wavenumber k of the various neutral

wave types in (3.4a, b) and (3.5a, b) are determined by $k^2 = 6c +$ constant; however as shown above this constant is different for each type of neutral wave, and the range of c for which a particular wave is possible may be restricted by the constraint $k^2 \geq 0$, which in turn may restrict B to certain ranges via fig. 3. For a particular basic state and for values of k smaller than the neutral value, the waves become unstable, and in section 5 growth rates are estimated using a variational method by considering departures from the neutral curves of fig. 3.

B. Tanh Velocity Profile.

Following Lipps (1965), another type of velocity profile that is still analytically tractable is (in dimensional quantities)

$$\bar{u}_D(y) = U_1 + U_0 \tanh (y/L) \quad .$$

This represents a shear zone between two constant velocity regions, and may be a better representation than the sech^2 profile of some regions of Jupiter, e.g. at the latitudes of the Great Red Spot.

Defining non-dimensional quantities using U_0, U_1 and L as above for the sech^2 profile, $\bar{u}$ is now tanh y and the potential vorticity gradient $(B + \bar{u})\ \lambda^2 - \bar{u}_{yy}$ can be written as the cubic $-2\ \bar{u}^3 + (\lambda^2 + 2)\ \bar{u} + B\lambda^2$. For real c lying within the range of $\bar{u}$ (i.e. $-1 < c < 1$), c must be a root of this cubic, and then the differential equation becomes

$$\frac{d^2\varphi}{dy^2} + (2\ \text{sech}^2\ y - k^2 - 2c\ \tanh\ y - 2\ c^2)\ \varphi = 0 \quad . \qquad (3.6)$$

Again changing the independent variable to z = tanh y, this becomes

$$(1 - z^2)\ \frac{d^2\varphi}{dz^2} - 2z\ \frac{d\varphi}{dz} + \left[2 - \left(\frac{2cz + 2c^2 + k^2}{1 - c^2}\right)\right]\ \varphi = 0 \quad . \qquad (3.7)$$

Following Lipps (1965), a solution obeying boundary conditions $\varphi = 0$ as $y \to \pm\ \infty$ $(z = \pm\ 1)$ is found by substituting $\varphi = (1 + z)^p\ (1 - z)^q\ z^r$ where p, q and r are real constants.

This gives

$$\varphi = (1 + z)^{(1 - c)/2} \quad (1 - z)^{(1 + c)/2} \text{ for which } k^2 = 1 - c^2 . \tag{3.8}$$

Since (3.7) is not a standard equation, it would be complicated to find other solutions; however, Lipps (1965) notes that for $\beta = \lambda^2 = 0$ (3.7) reduces to Legendre's equation and (3.8) is the only solution that vanishes at $z = \pm 1$.

The latitudinal forms of three neutral wave solutions (3.8) are shown in fig. 4. The shape depends on the value of c, becoming more skewed for larger values of $|c|$.

Fig. 5 is the equivalent diagram for the tanh profile to fig. 3 above, showing the neutral phase speed c (determined from the roots of the cubic in $\bar{u}$ above for the potential vorticity gradient) as a function of the basic state parameter $B = (\beta_D + L_r^{-2} U_1)/(L_r^{-2} U_0)$, for various values of $\lambda^2 = L^2/L_r^2$. The discussion of fig. 3 above also applies to fig. 5, except now the range of the non-dimensional $\bar{u}$ and c is extended to (- 1, 1). Due to the antisymmetry of $\bar{u}$ about y = 0, the solution $\varphi(y)$ for a particular value of U_0 is antisymmetric to the solution for U_0 of the opposite sign, and both solutions have the same dimensional phase speed c_D. This behavior is reflected in fig. 5, and implies for instance that all disturbances on profiles with $\beta_D + L_r^{-2} U_1 > 0$ have $c_D < U_1$ irrespective of the sign of U_0, and vice versa.

FIGURE 4. Latitudinal shapes of $\bar{u}_D$ and two upper layer neutral solutions (3.8) for the velocity profile $\bar{u}_D = U_1 + U_0 \tanh (y/L)$. (Relative scales on the abscissae are arbitrary.)

(a): $\bar{u}_D$ vs. poleward latitudinal coordinate y/L, with $U_0 > 0$ representing a region of anticyclonic shear.

(b): φ vs. y/L for solution (3.8) with $c = 0$ ($c_D = U_1$).

(c): φ vs. y/L for solution (3.8) with $c = -.4$ ($c_D = U_1 - .4\, U_0$).

(d): φ vs. y/L for solution (3.8) with $c = -.8$ ($c_D = U_1 - .8\, U_0$).

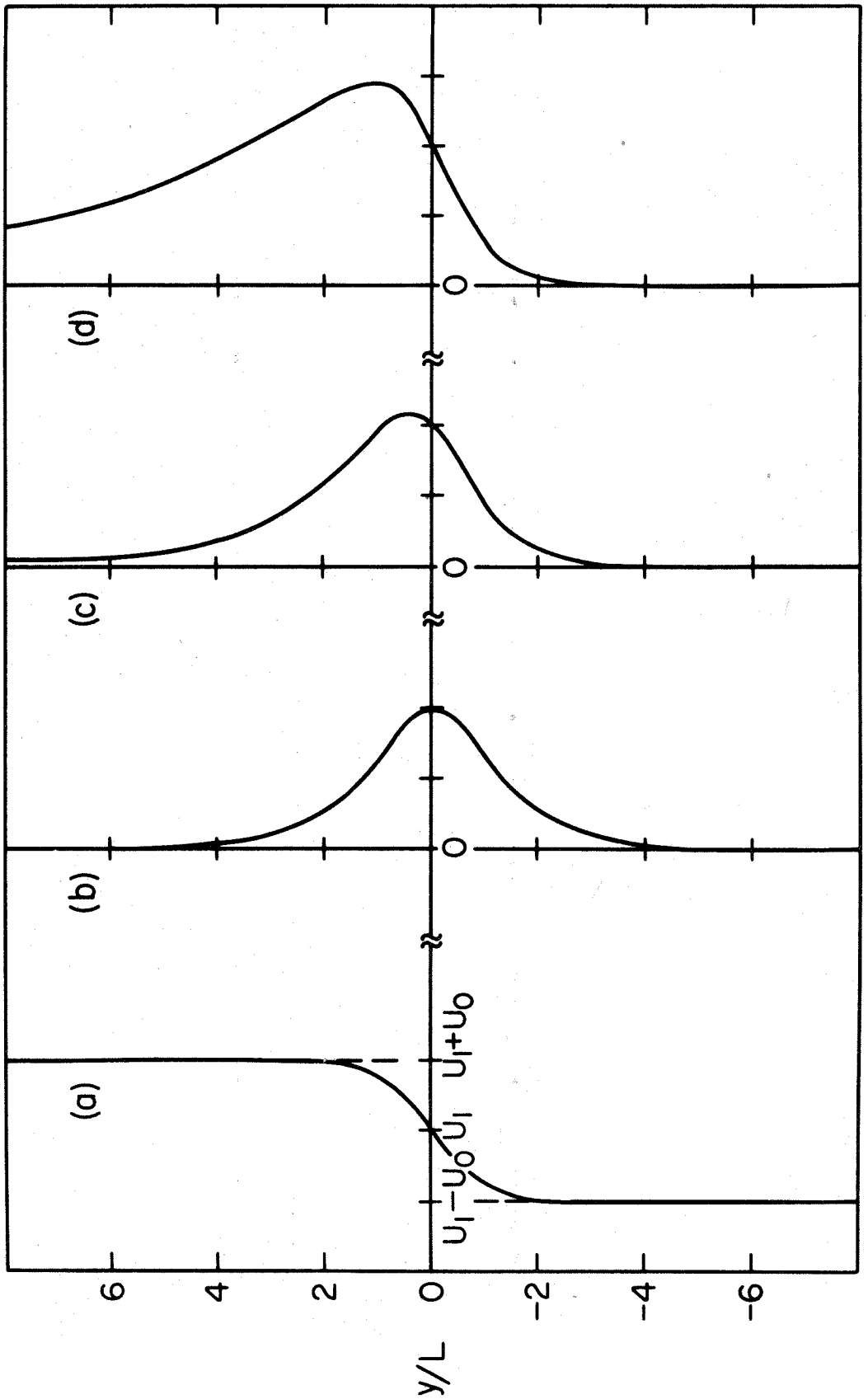

Figure 4

FIGURE 5. Non-dimensional phase speeds $c = (c_D - U_1)/U_0$ of neutral disturbances on velocity profile $\bar{u}_D = U_1 + U_0 \tanh(y/L)$, as functions of the basic state parameter $B = (\beta_D + L_r^{-2} U_1)/(L_r^{-2} U_0)$, for various values of $\lambda^2 = L^2/L_r^2$.

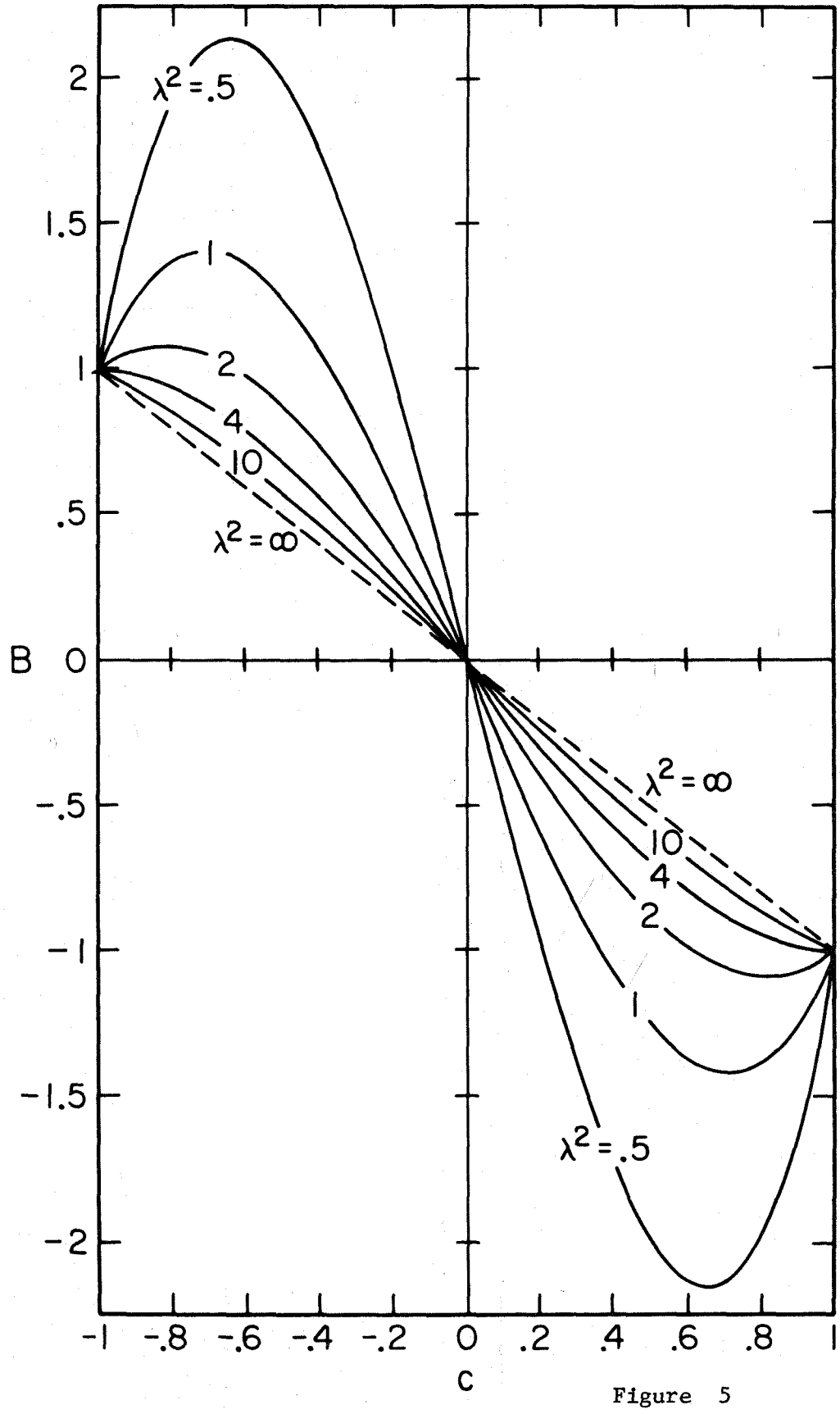

Figure 5

4. BAROCLINIC (BC) INSTABILITY.

The $\delta^{1/2}$ expansion in section 2 showed that baroclinic instabilities, which rely on the dynamics of the disturbance in the lower layer, can have non-dimensional growth rates only of order $\delta^{1/2}$. For Jupiter the appropriate value of δ may be $\sim 10^{-6}$ (see section 2.A) which would imply growth times of $\sim 10^{3}$ days, much longer than those of the barotropic upper layer (BTU) modes in sections 5 and 6. However a study of baroclinic instabilities in the two layer model enables comparisons to be made with the results of the continuously stratified model in the appendix; also the appropriate Jovian value of δ may be greater than $\sim 10^{-6}$.

A. $\bar{u}$ = constant Velocity Profile.

We consider the simplest possible upper layer velocity profile $\bar{u}_D$ independent of y, with rigid wall boundaries. The y-dependences of φ_1 and φ_2 must be sinusoidal, and as with the x and t dependences, the only non-zero linear interactions between φ_1 and φ_2 occur for individual fourier components with the same y-wavenumber. If the boundaries are sufficiently far apart, a nearly continuous spectrum of y-wavenumbers is allowed. The original perturbation equations (2.3) and (2.4) are simply algebraic and the general solution is given below, but some insight is gained by first considering the δ and $\delta^{1/2}$ expansions for this case.

It is convenient to non-dimensionalize using the constant

velocity $\bar{u}_D$ (which may be negative) and the upper layer radius of deformation L_r, by defining

$$\beta = \beta_D L_r^2/\bar{u}_D, \quad c = c_D/\bar{u}_D, \quad k = k_D L_r \quad .$$

This non-dimensionalization is essentially the same as that for equations (2.3) and (2.4), and all the equations of section 2 apply here with $\lambda = 1$, $\bar{u} = 1$ and $b = \beta + 1$. We also define $\kappa = \kappa_D L_r = \sqrt{k^2 + \ell^2}$ where ℓ is the non-dimensional y-wavenumber of the perturbation. For general k and $c^{(0)}$, the δ expansion is appropriate, with $c^{(0)}$ real and ℓ determined by (2.5) with $\varphi_2^{(0)} = 0$ and with the forced amplitude of $\varphi_2^{(1)}$ set by (2.8). Then as shown in section 2.C the flow is also stable at $O(\delta)$. However for the particular values of k and $c^{(0)}$ such that $G^{(0)} = H^{(0)}$, i.e.,

$$\ell^2 = -k^2 - 1 + \frac{\beta + 1}{1 - c^{(0)}} = -k^2 + \frac{\beta}{-c^{(0)}} \quad , \tag{4.1}$$

then (2.8) would resonate and $\varphi_2^{(1)}$ could not be zero at both boundaries. So in this case we are led to the $\delta^{1/2}$ expansion, in which the leading equations (2.9) and (2.11) require k, $c^{(0)}$ and ℓ to satisfy (4.1), which implies

$$\kappa = |\beta|^{1/4} \quad , \quad c^{(0)} = |\beta|^{1/2} \quad , \tag{4.2}$$

for which β must be negative, i.e. $\bar{u}_D$ must be retrograde. Then (2.22) to (2.24) imply

$$c^{(1)} = \pm \left[\frac{c^{(0)^2} \; (1 - c^{(0)})^2}{\beta \; (\beta + 1)} \right]^{1/2} = \pm \left(\frac{|\beta|^{1/2} - 1}{|\beta|^{1/2} + 1} \right)^{1/2} \qquad (4.3)$$

$c^{(1)}$ is imaginary and the mode is unstable at $O(\delta^{1/2})$ if $-1 < \beta < 0$, i.e., if the upper layer potential vorticity gradient $\beta_D + L_r^{-2} \bar{u}_D$ is negative [cf. Pedlosky, 1964a, (3.2.4)]. Also (2.24) implies

$$\frac{\varphi_2^{(1)}}{\varphi_1^{(0)}} = - \frac{c^{(0)^2}}{\beta \; c^{(1)}} = \pm \left(\frac{|\beta|^{1/2} + 1}{|\beta|^{1/2} - 1} \right)^{1/2} . \qquad (4.4)$$

So for unstable modes, $\varphi_1^{(0)}$ and $\varphi_2^{(1)}$ are 90° out of phase.

As κ departs from the particular value $\kappa_c = |\beta|^{1/4}$, we would expect a transition from unstable $\delta^{1/2}$ - solutions with $|\varphi_2/\varphi_1| \sim O(\delta^{1/2})$ valid for $|\kappa - \kappa_c| \leq O(\delta^{1/2})$, to stable δ-solutions with $|\varphi_2/\varphi_1| \sim O(\delta)$ valid for κ outside this range. This is more easily seen using the general results from (2.3) and (2.4). Defining $\nu = c \kappa$, elimination of φ_2/φ_1 between (2.3) and (2.4) yields the dispersion relation

$$\nu^2 [1 + \kappa^2 + \delta] + \nu [-\kappa^3 + \beta (2\kappa + \kappa^{-1}) + \delta (\beta\kappa^{-1} - 2\kappa)] + (\beta - \kappa^2) (\beta - \delta) = 0 . \qquad (4.5)$$

Gill et al. (1974) derived this equation [their eqn. (9.3)] for their two layer model of baroclinic instabilities in the earth's oceans, and used it directly to obtain the results (4.1) to (4.3) above. The exact solutions of (4.5) for unstable waves are shown in fig. 6, where the non-dimensional phase speeds $c_r = \mathrm{Re}\,[c_D/\bar{u}_D]$ and the growth rates

FIGURE 6. Baroclinic instability for $\bar{u}$ = constant, showing the unstable exact solutions of equation (4.5) with $\delta = .005$.

(a): Non-dimensional phase speeds $c_r = \mathrm{Re}[c_D/\bar{u}_D]$, and

(b): Growth rates $\nu_i = \mathrm{Im}[k_D\, c_D/(L_r^{-1}|\bar{u}_D|)]$ for $k = \kappa$, as functions of the horizontal wavenumber $\kappa = \kappa_D\, L_r = \sqrt{k^2 + \ell^2}$ for various values of $\beta = \beta_D\, L_r^2/\bar{u}_D$. For particular values of β and values of κ outside the ranges in fig. 6, [and also for all κ if β is outside the range $(-1, \delta^{\frac{1}{2}})$], both solutions of (4.5) are neutrally stable ($\nu_i = 0$) and correspond to the BTU and BTL modes of the δ-expansion in section 2.

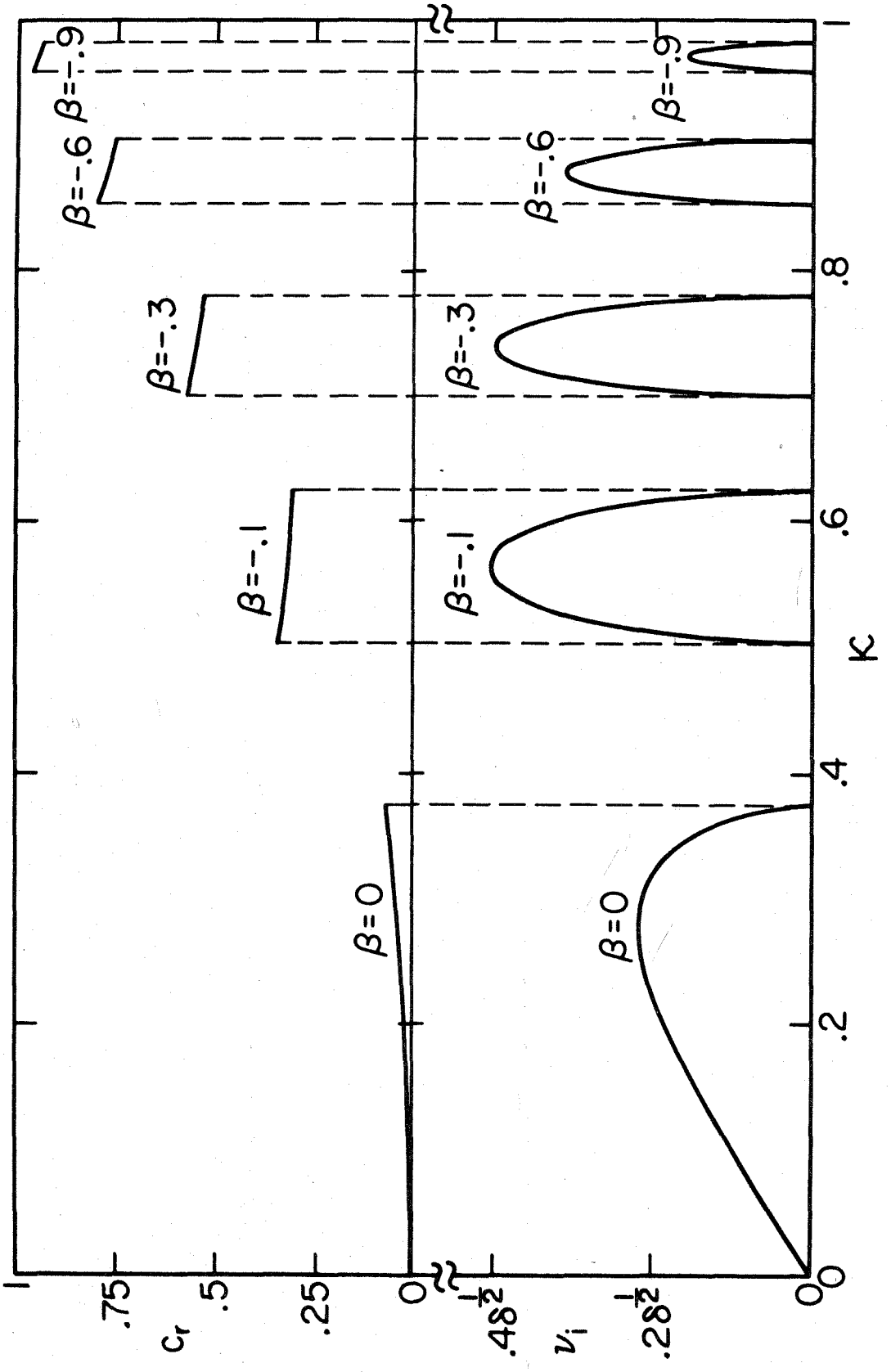
β=-.9
β=-.6
β=-.3
β=-.1
β=0
β=-.9
β=-.6
β=-.3
β=-.1
β=0
1
.75
.5
.25
0
c_r
$-\frac{1}{2}$
.48$\frac{1}{2}$
$-\frac{1}{2}$
.28$\frac{1}{2}$
ν_i
0
.2
.4
.6
.8
1
K

Figure 6

$\nu_i = \mathrm{Im}\,[k_D\, c_D/(L_r^{-1}\,\bar{u}_D)]$ are plotted (for $k = \kappa$) as functions of the horizontal wavenumber $\kappa = \kappa_D\, L_r$, for various values of $\beta = \beta_D\, L_r^2/\bar{u}_D$. (For a given κ, the fastest growth occurs for the largest value of k consistent with $k^2 + \ell^2 = \kappa^2$, so that the most unstable waves have perturbation velocities and wavenumbers oriented mainly north-south.) The growth rates are $O(\delta^{1/2})$ and are largest for values of β intermediate between 0 and -1, for which the upper layer potential vorticity gradient $\beta_D + L_r^{-2}\,\bar{u}_D$ is comparable to but has the opposite sign of the lower layer gradient β_D. For clarity, an arbitrary value of $\delta = .005$ is used for fig. 6. For a given intermediate value of β, fig. 6 shows the waves are only unstable for a range of κ-wavenumbers of width $\sim 0.1 \sim O(\delta^{1/2})$, in agreement with the $\delta^{1/2}$ expansion analysis above; (also the values of κ, $c^{(0)}$ and $c^{(1)}$ for unstable waves predicted by (4.2) and (4.3) agree with fig. 6). For Jupiter, $\delta^{1/2}$ may be $\sim 10^{-3}$ so only an extremely small range of κ would be unstable if $\bar{u}$ were constant; however we will see in section 4.B that this constraint no longer applies for $\bar{u}$ dependent on y.

As $\beta \to 0$ (i.e., for very small β_D or very large $|\bar{u}_D|$) the wavenumbers of unstable waves tend to zero [$\kappa \approx |\beta|^{1/4}$ from (4.2)]; however for $O(\kappa^2)$ or $O(|\beta|) \leqslant O(\delta^{1/2})$, the $\delta^{1/2}$ expansion [which implicitly requires all quantities except $\delta^{1/2}$ to be $\gg O(\delta^{1/2})$] becomes invalid, as do (4.1) to (4.4).

We discuss the case $\beta = 0$ below; although this case is instructive, in practice it is not a problem in applying the $\delta^{1/2}$ (and δ) expansions to Jupiter since the non-dimensional β's of this work are all $>> 0(\delta^{1/2})$ at mid and high latitudes.

For $\beta = 0$, the general equation (4.5) is still valid. We compare this below with equation (10) of the appendix, which is the equivalent equation for a similar two layer model with $\beta_D = 0$, but with continuous basic state stratification and vertical shear of $\bar{u}$ in the upper layer. For the present constant density model with $\beta = 0$, (4.5) can be written

$$\left[\nu^2 - \nu\left(\frac{\kappa^3}{1+\kappa^2}\right)\right] + \delta\left[\frac{1}{(1+\kappa^2)}\ (\nu - \kappa)^2\right] = 0\ , \qquad (4.6)$$

and in equivalent units for the continuously stratified model, equation (10) of the appendix becomes

$$[\nu^2 - \nu\ (\kappa - \tanh\kappa)] + \delta\left[\frac{\tanh\kappa}{\kappa}\ \left(\nu^2 - \nu\kappa + \frac{\kappa - \tanh\kappa}{\tanh\kappa}\right)\right] = 0. \qquad (4.7)$$

The forms of these two equations are evidently very similar, and their exact solutions (stable and unstable) are compared in fig. 7, with δ again arbitrarily chosen to be .005. The unstable parts of the curves for (4.6) labelled CD in fig. 7 correspond to the $\beta = 0$ curves in fig. 6, but here the ν_i axis is scaled relative to $\delta^{3/4}$, since approximate solutions of (4.6) and (4.7)

FIGURE 7. Baroclinically unstable and neutral solutions for $\bar{u}$ = constant with $\beta_D = 0$, showing non-dimensional phase speeds $c_r = \mathrm{Re}[c_D/\bar{u}_D]$, and growth rates $\nu_i = \mathrm{Im}[k_D\, c_D/(L_r^{-1}|\bar{u}_D|)]$ for $k = K$, as functions of the horizontal wavenumber $K = K_D\, L_r = \sqrt{k^2 + \ell^2}$. Curves labelled CD are exact solutions of (4.6) for the constant density model, and curves labelled S are exact solutions of (4.7) for the continuously stratified upper layer model, both using $\delta = .005$.

(a): Phase speeds c_r vs. K showing the neutral solution branches with $c_r \sim O(1)$ of the quadratics (4.6) and (4.7).

(b): Phase speeds c_r vs. K showing the $O(\delta^{3/4})$ unstable solutions ($K \leqslant .5$), and also the neutral solution branches with $c_r \sim O(\delta)$ ($K \geqslant .5$).

(c): Growth rates ν_i vs. K showing the $O(\delta^{3/4})$ unstable solutions.

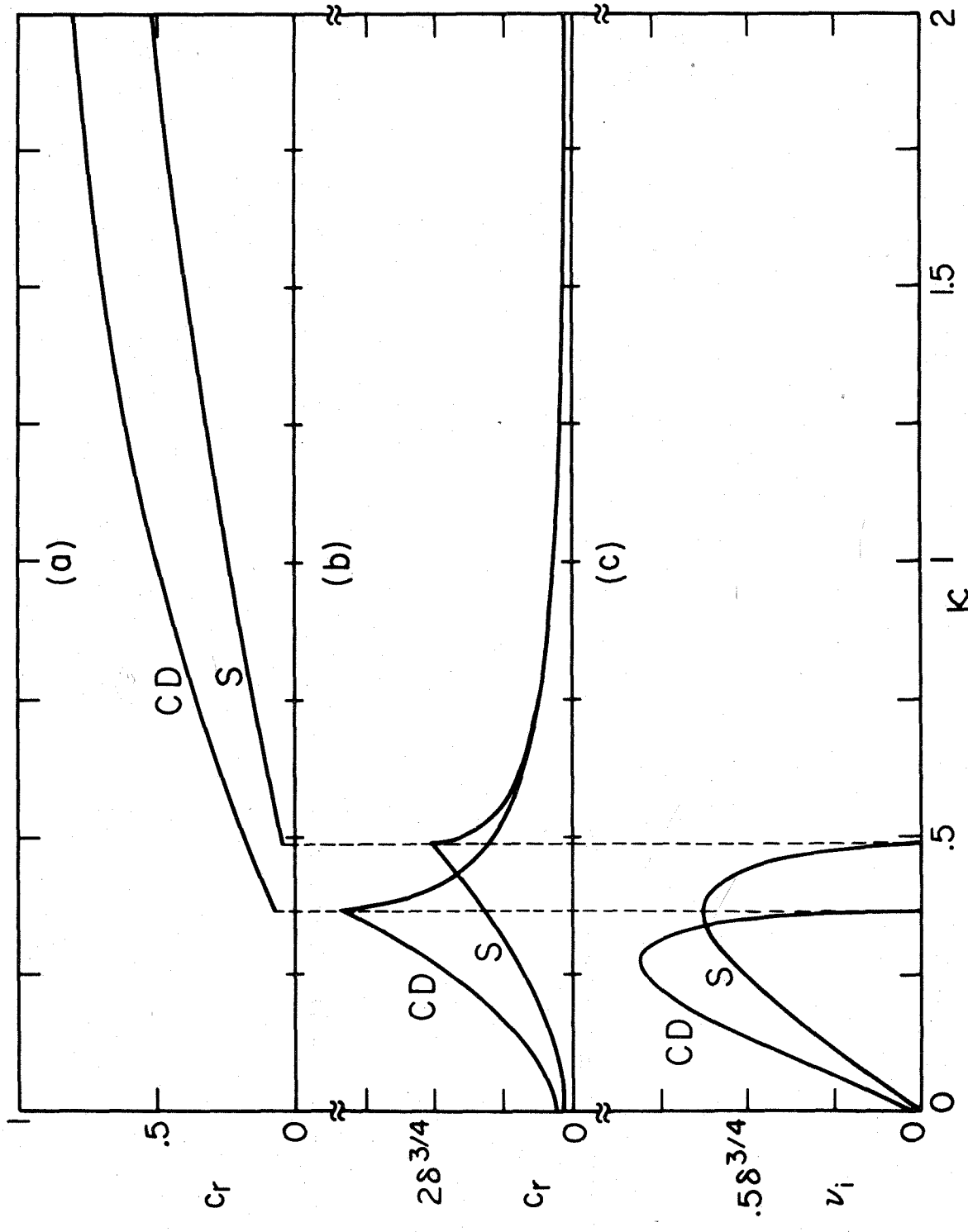

Figure 7

(see appendix) show that only long waves with $0 < \kappa \leqslant (12\delta)^{1/4}$ (= .5 for δ = .005) are unstable and have ν_i and $c_r \sim 0(\delta^{3/4})$. The similarity of the curves in fig. 7 suggests that the present constant density model is adequately representing the basic mechanisms of the more complex continuously stratified model, at least for $\beta = 0$. However, Gill et al. (1974) found more marked differences between their two model results (continuously stratified single layer vs. two layer constant density) for $\beta \neq 0$.

In practice $|\beta| \sim 0(1)$ for Jupiter, and a general result from this section is that for velocity profiles $\bar{u}$ = constant, the only baroclinically unstable flows with the full $0(\delta^{1/2})$ growth rates realizable in the BC mode are retrograde flows of moderate strength ($-\beta_D L_r^2 \leqslant \bar{u}_D < 0$). This result will echo through subsequent sections in analogous results both for baroclinic and barotropic (BTU) instabilities for $\bar{u} = \text{sech}^2 y$ profiles; in all cases the flows are most unstable when the planetary vorticity gradient β_D is approximately cancelled by the gradient associated with the flow $-(\bar{u}_D)_{yy} + \bar{u}_D/L_r^2$. This is also a reflection of the necessary criterion for instability of Charney and Stern (1962).

Finally for the $\bar{u}$ = constant profile with $\beta \neq 0$ we evaluate the zonal mean eddy fluxes due to growing baroclinic disturbances appearing in the energy equations in section (2.F). Although the upper layer flux of zonal momentum [i.e., the $\overline{u_1' v_1'}$ term

appearing in (2.25) and (2.26)] is dominated by unstable BTU disturbances (see section 6), the latitudinal transport of upper fluid [i.e., the $\overline{v_1' h_1'}$ team appearing in (2.27) and (2.28), which is the two layer model representation of latitudinal heat transport] occurs only at $0(\delta)$ for BTU modes, compared to $0(\delta^{1/2})$ for baroclinic modes. So for the latter transport, baroclinic instabilities may be important even with comparatively small magnitudes of φ_1. From the information in (4.1) to (4.4), we find for the present baroclinic instabilities that the conversion of mean a.p.e. to eddy a.p.e. appearing in (2.28) is (averaged over y)

$$f_o \rho_1 \bar{u}_D (\overline{v_1' h_1'}) = - \delta^{1/2} \bar{u}_D \frac{\rho_1 V_1^2}{2} \frac{k}{\kappa} \frac{H_1}{L_r} \frac{1}{|\beta|^{1/4}} \sqrt{\frac{1 + |\beta|^{1/2}}{1 - |\beta|^{1/2}}} \tag{4.8}$$

where $V_1 = \kappa_D |\varphi_1|$ is the (dimensional) magnitude of the disturbance velocity in the upper layer. $\overline{v_1' h_1'}$ is negative, so that 'heat', (i.e. positive h_1') is being transported equatorward from the 'warm' side ($\bar{h}_1 > 0$) of the retrograde mean flow to the 'cold' side ($\bar{h}_1 < 0$).

The vertical energy flux upwards from the interface into the upper layer appearing in (2.26) is (averaged over y)

$$\overline{p_1' w_1'}_{I^+} = - p_1' \frac{dh_1'}{dt} + f_o \rho_1 \bar{u}_D (\overline{v_1' h_1'})$$

$$= - \delta^{1/2} \bar{u}_D \frac{\rho_1 V_1^2}{2} \frac{k}{\kappa} \frac{H_1}{L_r} |\beta|^{1/4} \sqrt{\frac{1 - |\beta|^{1/2}}{1 + |\beta|^{1/2}}} \quad . \tag{4.9}$$

Since $\bar{u}_D$ is negative, this flux is positive and energizes the disturbance kinetic energy in the upper layer.

These eddy fluxes are proportional to V_1^2, and we can estimate how large V_1 would have to be to make the eddy fluxes comparable to other known planetary fluxes. For instance, the magnitude of observed latitudinal variations of I.R. emission on the belt-zone scale is typically $\sim 10^3$ ergs/cm^2/sec (Ingersoll (1976) fig. 10). In the present two layer model, this would be analogous to a diabatic forcing on the right hand side of the mean a.p.e. equation (2.27). For the baroclinic eddy conversion term (4.8) to be comparable to this forcing, (using $\bar{u}_D = - 30$ m/s, $\beta = - 0.2$, $H_1/L_r = 0.1$, $\delta = 10^{-6}$), V_1 would have to be ~ 30 m/s. This is perhaps unreasonably large for typical eddy velocities, but if δ were $\sim 10^{-4}$, the required V_1 would be ~ 3 m/s.

B. Sech^2 Velocity Profile.

The growth rate $k\,\delta^{1/2}\,c_i^{(1)}$ of unstable baroclinic (BC) modes given by (2.24) depends on the 'interaction' integral $\int \varphi_1^{(0)}\,\varphi_2^{(1)*}\,dy$. $\varphi_2^{(1)}$ is always purely sinusoidal for BC modes, and for the $\bar{u}_D$ = constant case above with $\varphi_1^{(0)}$ purely sinusoidal, this integral is non-zero only if $\varphi_1^{(0)}$ and $\varphi_2^{(1)}$ have the same y-wavenumber, constraining k and $c^{(0)}$ to particular values in (4.2). When $\bar{u}$ depends on y, this constraint is relaxed since the interaction integral is generally non-zero for non-sinusoidal $\varphi_1^{(0)}$. Below we investigate baroclinic instability for the isolated jet velocity profile (in dimensional quantities) $\bar{u}_D = U_1 + U_0\,\mathrm{sech}^2\,(y/L)$.

If the appropriate locations of rigid wall boundaries for Jupiter (see section 3.A) are far away from the sech^2 jet, i.e. at $y/L = \pm Y$ with $Y >> 1$, then the neutral oscillatory $\varphi_1^{(0)}$ solutions (3.5) would be essentially sinusoidal over most of the latitudinal range, so the interaction integral and whole baroclinic instability would be nearly the same as for the $\bar{u}_D$ = constant case above with $\bar{u}_D = U_1$. Also $\varphi_1^{(0)}$ of the evanescent solutions (3.4) is only significant in the vicinity of the jet ($|y/L| \leqslant 3$), so the interaction integral and $|c^{(1)}|$ from (2.22) and (2.24) would be proportional to $Y^{-1/2}$ for $Y >> 1$. However, if the appropriate rigid wall locations are just slightly outside the sech^2 jet, the dependence of $\bar{u}$ on y will have a significant new effect on baroclinic instabilities

and $c_i^{(1)}$ can be 0(1). We illustrate this case below for the symmetric evanescent upper layer solutions $\varphi_1^{(0)} = \text{sech}^2 y$ of (3.4), using the non-dimensional notation defined in section 3.A.

These $\varphi_1^{(0)}$ solutions are modified insignificantly by imposing rigid wall boundaries at $y = \pm Y$ for $Y \geq 3$ (see section 6). Then the zero order phase speed $c^{(0)}$ is determined by (3.2) and $k^2 = 6c^{(0)}$; [for other values of k, the upper layer $\varphi_1^{(0)}$ solutions would be barotropically unstable at 0(1) (see sections 5 and 6)]. The y-wavenumber ℓ_2 of the lower layer is set by (2.11), i.e.,

$$\ell_2^2 = -k^2 + \frac{\beta_D L^2}{-c_D^{(0)}} \quad . \tag{4.10}$$

$\varphi_2^{(1)}$ is proportional to cos $(\ell_2 y)$ for the symmetric mode; in reality the boundary conditions $\varphi_2 = 0$ at $y = \pm Y$ would only allow discrete values of ℓ_2, but for simplicity in fig. 8 below we adjust Y for each wave to $Y = \max(3, \ell_2 \pi/2)$, (so that for $\ell_2 > 6/\pi$ the lower fluid boundary conditions are actually not obeyed). Then the relative magnitude and x-phase of $\varphi_2^{(1)}$ are determined by (2.22) and (2.23), and $c^{(1)}$ is determined by (2.24).

Fig. 8(a) shows the non-dimensional phase speed $c^{(0)} = (c_D^{(0)} - U_1)/U_0$ and x-wavenumber $k = k_D L$ as functions of the basic state parameter $B = (\beta_D + L_r^{-2} U_1)/(L_r^{-2} U_0)$, for $\lambda^2 = L^2/L_r^2 = 4$. This value of λ^2 corresponds to an upper layer radius of deformation L_r of ~2500 km, which may be

FIGURE 8. Baroclinic instability for upper layer velocity profile $\bar{u}_D = U_1 + U_0 \operatorname{sech}^2 (y/L)$, and $\lambda^2 = L^2/L_r^2 = 4$.

(a): Non-dimensional phase speed $c^{(0)} = (c_D^{(0)} - U_1)/U_0$ and x-wavenumber $k = k_D L$ set by the symmetric upper layer neutral solution (3.4a), as functions of the basic state parameter $B = (\beta_D + L_r^{-2} U_1)/(L_r^{-2} U_o)$.

(b): Non-dimensional baroclinic growth rate $\nu_i = \delta^{1/2} \operatorname{Im}[k_D c^{(1)}/(L^{-1}|U_0|)]$ and y-wavenumber ℓ_2 of the lower layer solution, as functions of B for velocity profiles with $U_1/U_0 = -.5$.

(c): As for fig. 8 (b), but for velocity profiles with $U_0 = -\beta_D L^2 (\sim -50$ m/s).

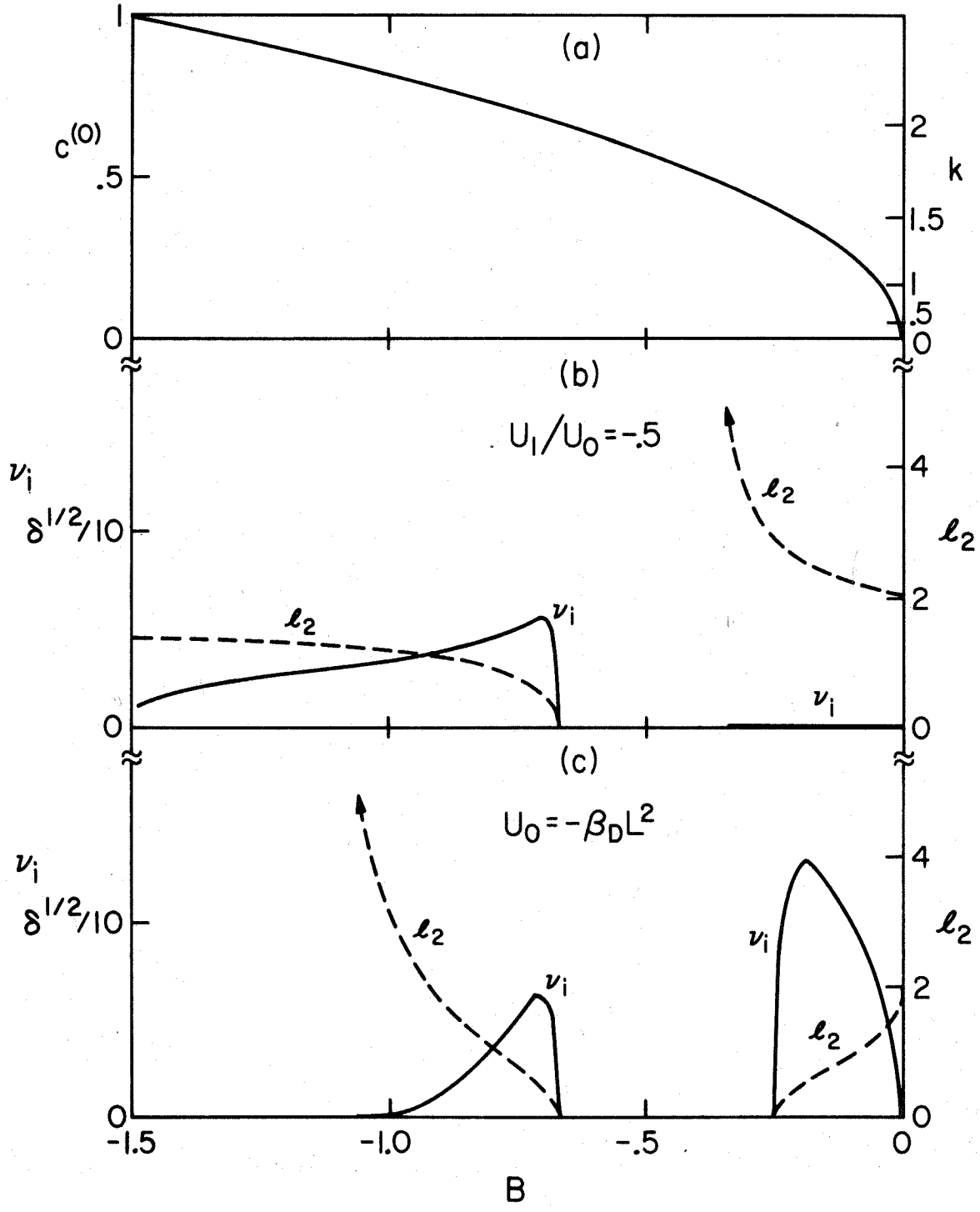

Figure 8

appropriate for Jupiter. Fig. 8(a) is determined by the upper layer neutral solution; the same curve appears in fig. 3 and is discussed in section 3A. For $U_1 > -\beta_D L_r^2$, only retrograde jets ($u_0 < 0$, $B < 0$) can have neutral $\varphi_1^{(0)}$ solutions.

For the non-dimensional quantities used in fig. 8(a), (4.10) becomes

$$\ell_2^2 = -k^2 - \lambda^2 \frac{(B - U_1/U_0)}{(c^{(0)} + U_1/U_0)} ,$$

So to specify ℓ_2 we must choose a particular (arbitrary) value for U_1/U_0. Fig. 8(b) shows the non-dimensional y-wavelength ℓ_2 of $\varphi_2^{(1)}$ and the baroclinic growth rate $\nu_i = \delta^{1/2}\ \mathrm{Im}\ [k_D\, c^{(1)}/(L^{-1}|U_0|)]$ of the disturbance as functions of B, for velocity profiles with $U_1/U_0 = -0.5$. Fig. 8(c) shows ℓ_2 and ν_i for profiles with U_0 equal to $-\beta_D L^2$ (so that $U_1/U_0 = B + \lambda^{-2}$). In these figures, the requirement $\ell_2^2 > 0$ restricts the baroclinic instability to certain limited ranges of B.

The maximum growth rates in figs. 8(b) and (c) are somewhat smaller than those for the $\bar{u}_D$ = constant profile in fig. 6, because now only the centers of the retrograde sech^2 jets are locally baroclinically unstable, and the energy extracted there from the mean flow must be distributed to amplify the disturbance over the whole latitudinal range.

The latitudinal forms of $\bar{u}_D$, $\varphi_1^{(0)}$ and $\varphi_2^{(1)}$ are shown in fig. 9 for the particular BC mode with $\lambda^2 = 4$, $B = -0.7$,

FIGURE 9. Latitudinal forms of a baroclinically unstable mode for upper layer velocity profile $\bar{u}_D = U_1 + U_0 \operatorname{sech}^2 (y/L)$, with $B = -.70$, $\lambda^2 = 4$, and $U_0 = -\beta_D L^2$ [cf. fig. 8 (c)].

(a): $\bar{u}_D$ vs. y/L, for retrograde jet with $U_0 < 0$.

(b): Upper layer symmetric evanescent solution $\varphi_1^{(0)} \propto \operatorname{sech}^2 (y/L)$.

(c): Lower layer symmetric solution $\delta^{1/2} \varphi_2^{(0)} \propto \cos(\ell_2 y)$, (scaled relative to $|\varphi_1^{(0)}(0)|$).

(d): y-dependence of energy transfer term $f_0 \rho_1 \bar{u}_D(\overline{v_1' h_1'})$, (scaled relative to $|U_0| \rho_1(|\varphi_1^{(0)}(0)|^2/2L^2) \lambda^2 H_1/L$).

(e): y-dependence of energy transfer term $\overline{p_1' w_1'} \,|_I+$, [scaled relative to same factor as in (d)].

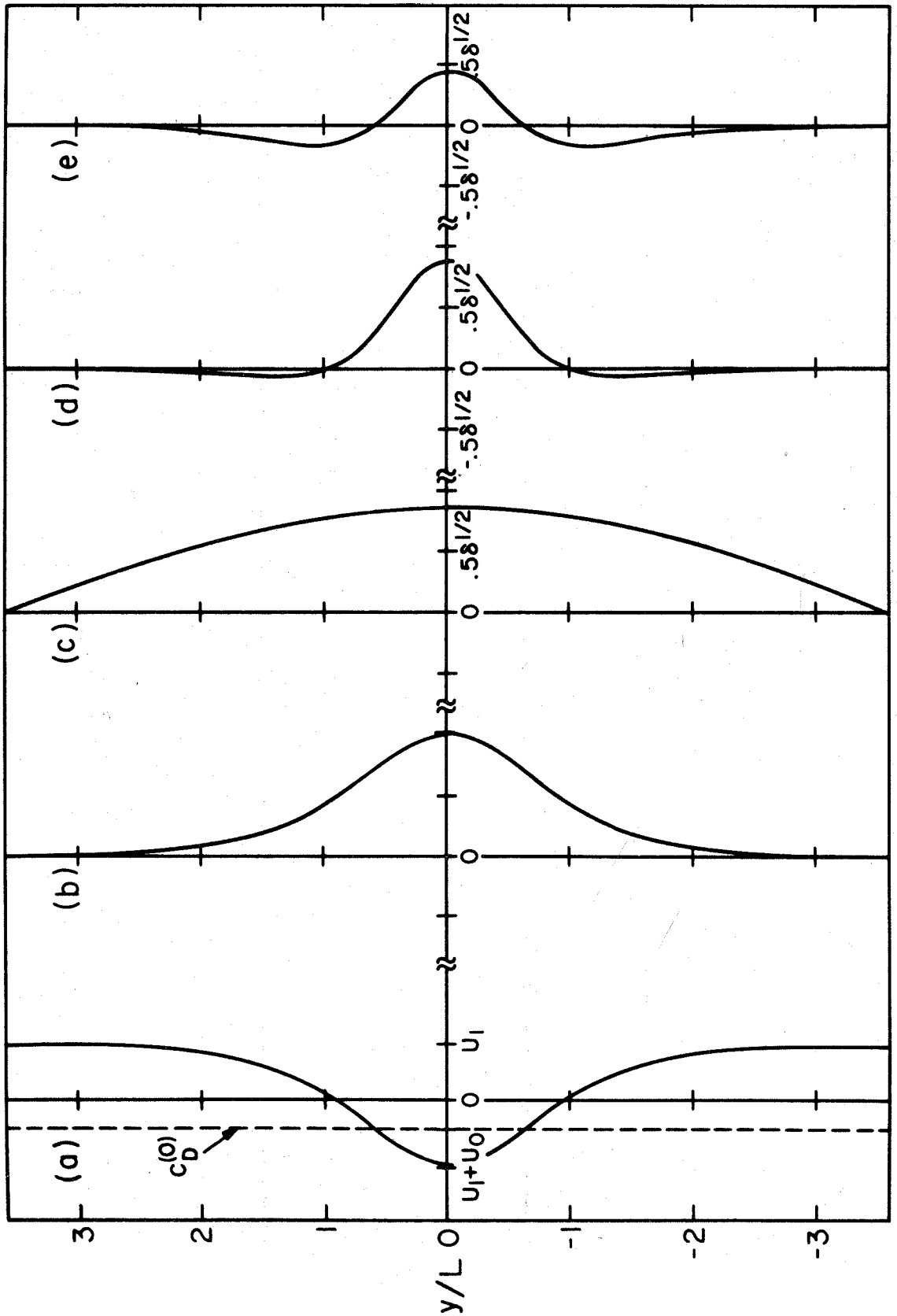

Figure 9

$U_0 = -\beta_D L^2$ [which has a relatively significant growth rate in fig. 8(c)]. Fig. 9 also shows the y-dependences of the $0(\delta^{1/2})$ energy transfer term $f_o \rho_1 \bar{u}_D \overline{v_1' h_1'}$ (associated with the horizontal transport of 'heat' h_1) and the vertical energy flux into the upper layer $\overline{p_1' w_1'}$; these were discussed for the $\bar{u}$ = constant profile in section 4A. In this case these fluxes are acting to amplify the disturbance baroclinically only in the central region where the jet is retrograde. The amplification in the outer regions must rely on the upper layer $\overline{u_1' v_1'}$ flux to redistribute upper layer kinetic energy; [however, this flux would be complicated to evaluate since it involves the $0(\delta^{1/2})$ forced $\varphi_1^{(1)}$ solution of (2.10)].

Since all baroclinic instabilities can potentially have growth rates only of order $\delta^{1/2}$, we expect that the upper layer eddy velocity field on Jupiter is dominated by the barotropic (BTU) instabilities of sections 5 and 6. For this reason we will not present any more general baroclinic results than the examples above; i.e., for other values of λ^2, for other $\varphi_1^{(0)}$ solutions, and for the tanh velocity profile. All of these other cases have baroclinic growth rates smaller than or comparable to those presented above. [For instance, as the value of λ^2 increases above ~4, maximum baroclinic growth rates for both sech^2 and tanh profiles decrease at rates comparable to λ^{-4} (not shown).]

5. BAROTROPIC (BTU) INSTABILITY: "VARIATIONAL" RESULTS.

In section 3, various types of neutrally stable upper layer solutions [(3.4), (3.5), (3.8)] were found for the sech^2 and tanh velocity profiles. For a given basic state, their phase speed c is determined uniquely by the velocity $\bar{u}_D$ at the basic state potential vorticity extremum (figs. 3 and 5), and the x-wavenumber $k = k_D L$ for each type of neutral wave is a particular function of c. For other values of k, the same wave type may still exist but with c complex to still satisfy the boundary conditions; i.e., the upper layer BTU solution to (3.1) may be barotropically unstable at O(1) [with only insignificant $O(\delta)$ interactions with the lower layer]. In this section, following Lipps (1962,1963,1965), we estimate growth rates for x-wavenumbers close to the neutral values over wide ranges of the basic state parameters. In section 6, explicit numerical solutions are found for a few particular basic states, and their growth rates confirm the variational estimates for the evanescent wave types (3.4), but differ considerably from variational estimates for oscillatory wave types (3.5). For this reason the general variational results of this section are shown only for the evanescent (i.e. $\varphi \to 0$ as $y \to \pm \infty$) wave types.

Below we use the non-dimensional notation defined in section 3.A, in which the basic state is specified by the parameters $B = (\beta_D + L_r^{-2} U_1)/(L_r^{-2} U_0)$ and $\lambda^2 = L^2/L_r^2$. Neutral curves in the (B,k^2) plane (with λ^2 fixed) are obtained

immediately from the neutral curves in the (B,c) plane of figs. 3 and 5 using the function k = k(c) appropriate for each wave type. Growth rates are estimated for waves close to these neutral curves by expanding c and φ in Taylor series of the form

$$c = c_0 + \frac{\partial c}{\partial s}\, ds + \frac{\partial c}{\partial B}\, dB + 0\ (ds^2,\ dB^2) \quad ,$$

where $s = -k^2$ and c_o, $\frac{\partial c}{\partial s}$ and $\frac{\partial c}{\partial B}$ are evaluated at some point on the neutral curve. As shown in Lipps (1962), $\frac{\partial c}{\partial s}$ and $\frac{\partial c}{\partial B}$ are given by

$$\frac{\partial c}{\partial s} = -\int_{-Y}^{Y} \varphi^2\, dy \Bigg/ \int_{-Y}^{Y} \left[\frac{(B + \bar{u})\,\lambda^2 - \bar{u}_{yy}}{(\bar{u} - c)^2}\right] \varphi^2\, dy \quad , \qquad (5.1)$$

$$\frac{\partial c}{\partial B} = -\lambda^2 \int_{-Y}^{Y} \frac{\varphi^2}{\bar{u} - c}\, dy \Bigg/ \int_{-Y}^{Y} \left[\frac{(B + \bar{u})\,\lambda^2 - \bar{u}_{yy}}{(\bar{u} - c)^2}\right] \varphi^2\, dy \quad , \qquad (5.2)$$

where $y = \pm Y$ are the latitudinal boundaries at which $\varphi = 0$; (for the evanescent waves, these integrals are essentially independent of Y for $Y \geq 3$).

In (5.1) and (5.2) there are singularities at the critical points where $\bar{u} = c$; Foote and Lin (1950) show that the inviscid solutions on either side of a critical point are joined by taking the path of integration in the complex y-plane around the singularity in the direction consistent with the

limit Im $(c_D) \to 0^+$ for marginally unstable waves, [taking care here to allow for the sign of U_0 in the definition $c = (c_D - U_1)/U_0$]. These singularities give finite (simple pole) imaginary contributions to $\partial c/\partial s$ and $\partial c/\partial B$. This procedure yields correct results only for unstable waves (Im $(c_D) > 0$), so that unstable waves exist only to one side of a neutral curve in the (B,k^2) plane (e.g. Lin, 1955, Ch. 8).

By evaluating $\partial c/\partial s$ and $\partial c/\partial B$ at closely spaced points along individual neutral curves in the (B,k^2) plane, we can build up estimated curves of constant $|c_i|$ that are correct to within $0(ds^2, dB^2)$ close to the neutral curves. (The dimensional growth rate is $k\, c_i\, (U_0/L)$, so if $U_0 < 0$, c_i is negative for unstable waves.) Fig. 10 shows the neutral $|c_i| = 0$ curves for the symmetric evanescent solution [$\varphi = \text{sech}^2 y$ of (3.4a)] and the associated $|c_i| = .025$ curves for unstable waves, on the velocity profile $\bar{u}_D = U_1 + U_0\, \text{sech}^2\, (y/L)$ with $\lambda^2 = 1$, 4 and 10; and also the curves $|c_i| = 0$ and $|c_i| = .0025$ with $\lambda^2 = 100$.

For $\lambda^2 \geq 4$, the phase speeds c_r for any point on the dashed unstable curves is approximately the same ($\pm \leqslant .1$) as for the associated point on the neutral curve with the same value of B [since $0(\partial c_r/\partial s) \sim 0(\partial c_i/\partial s) \ll 0(1)$ for $\lambda^2 \geq 4$]; the phase speeds $c = k^2/6$ for the neutral curves are shown in fig. 3. For values of B outside the ranges of the neutral curves shown, the basic state contains no potential vorticity extrema and so $|c_i| = 0$ for all BTU disturbances by the criterion of Charney and

FIGURE 10. Curves of constant $|c_i| = \mathrm{Im}(c_D)/|U_0|$ in the (B,k^2) plane associated with the symmetric evanescent BTU disturbance (3.4a) on the sech^2 velocity profile, for various values of $\lambda^2 = L^2/L_r^2$. The solid $|c_i| = 0$ curves are the neutral curves shown in fig. 3 in the (B,c) plane. The circles represent estimates of the unstable curves from values of $\partial c_i/\partial s$ on the neutral curves, and the triangles represent estimates from values of $\partial c_i/\partial B$. For values of $B = (\beta_D + L_r^{-2} U_1)/(L_r^{-2} U_0)$ outside the ranges of the neutral curves (e.g., beyond the hatched horizontal boundaries), the flow is barotropically stable.

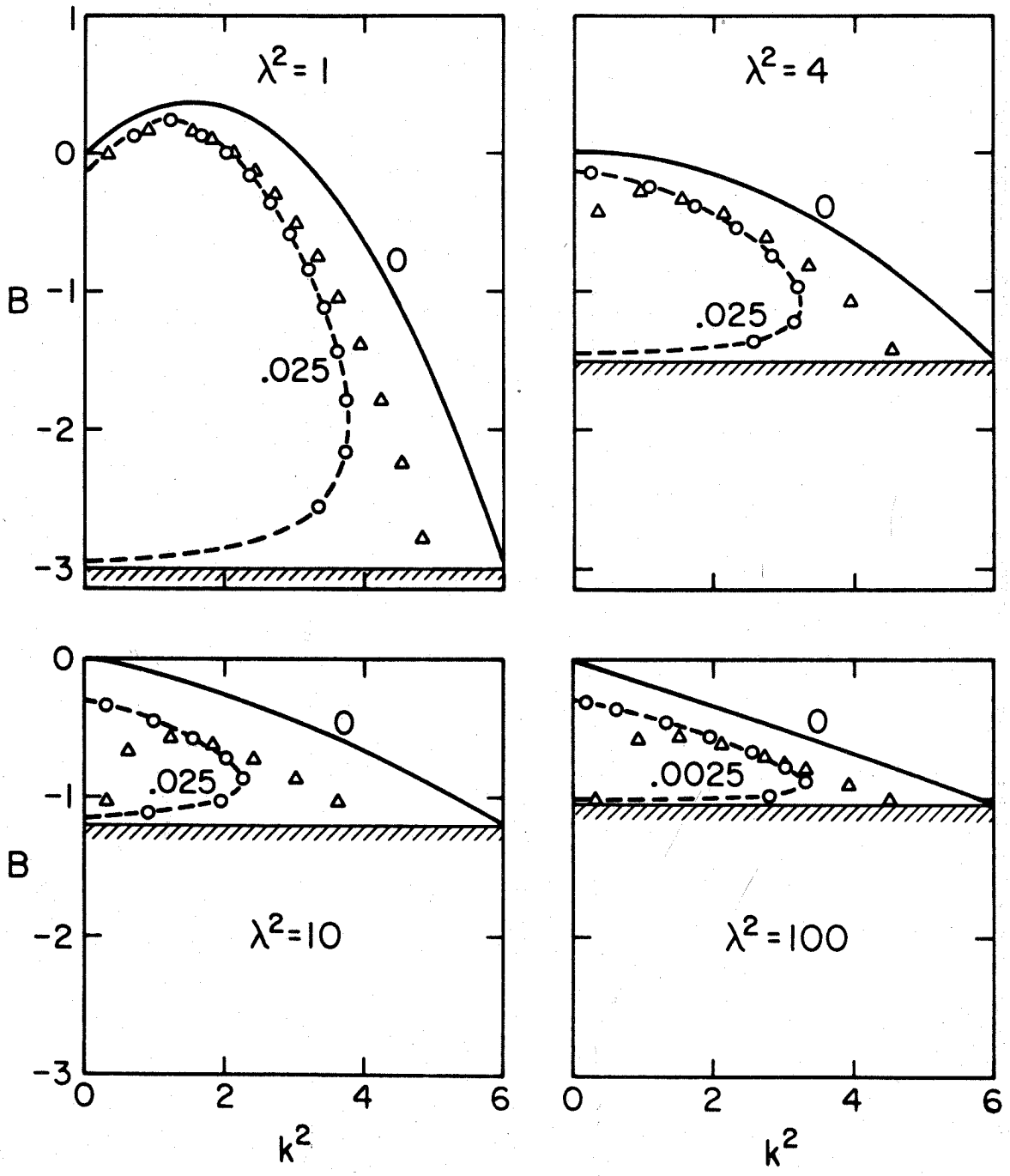

Figure 10

Stern (1962). Consequently as these stable regions are approached in fig. 10, the dashed unstable curves tend to diverge from the neutral curves and the estimates based on $\partial c_i/\partial s$ (circles) tend not to agree with the estimates based on $\partial c_i/\partial B$ (triangles). However the two estimates agree well for intermediate values of B where $|\partial c_i/\partial s|$ and $|\partial c_i/\partial B|$ have their largest values, and extrapolation to large ds and dB would indicate the fastest growth rates for intermediate values of B with $k^2 \sim 2$.

Fig. 11 shows the same set of constant $|c_i|$ curves associated with the antisymmetric evanescent solution [φ = sech y tanh y of (3.4b)] on the sech^2 velocity profile, and fig. 12 shows the same set associated with the evanescent solution (3.8) on the velocity profile $\bar{u}_D = U_1 + U_0 \tanh (y/L)$. For $\lambda^2 = 10$ and 100 in fig. 12, values of $\partial c_i/\partial B$ are approximately half the values that would be consistent with the $\partial c_i/\partial s$ values, and the dashed curves are based completely on $\partial c_i/\partial s$. Apart from this anomaly, the discussion of fig. 10 above applies equally to figs. 11 and 12; in all these cases the estimated growth rates are largest for intermediate values of B (corresponding to values of c_r between ~.3 and ~.7 from figs. 3 and 5) with $k^2 \sim 1$ for fig. 11 and $k^2 \sim .5$ for fig. 12.

For all three types of disturbances in figs. 10 to 12, the maximum growth rates ($\propto k\,|c_i|$) in the (B,k^2) plane are approximately the same for a given value of λ^2, and they decrease as $\lambda^2 = L^2/L_r^2$ increases above ~4. For $\lambda^2 \leqslant 4$ (i.e.,

FIGURE 11. Curves of constant $|c_i| = \mathrm{Im}(c_D)/|U_0|$ (as in fig. 10) associated with the antisymmetric evanescent BTU disturbance (3.4b) on the sech^2 velocity profile. Because $k^2 = 6c - 3 \geq 0$ for the neutral waves, the neutral ($|c_i| = 0$) curves here correspond to the segments of the neutral curves in fig. 3 with $1/2 \leq c \leq 1$.

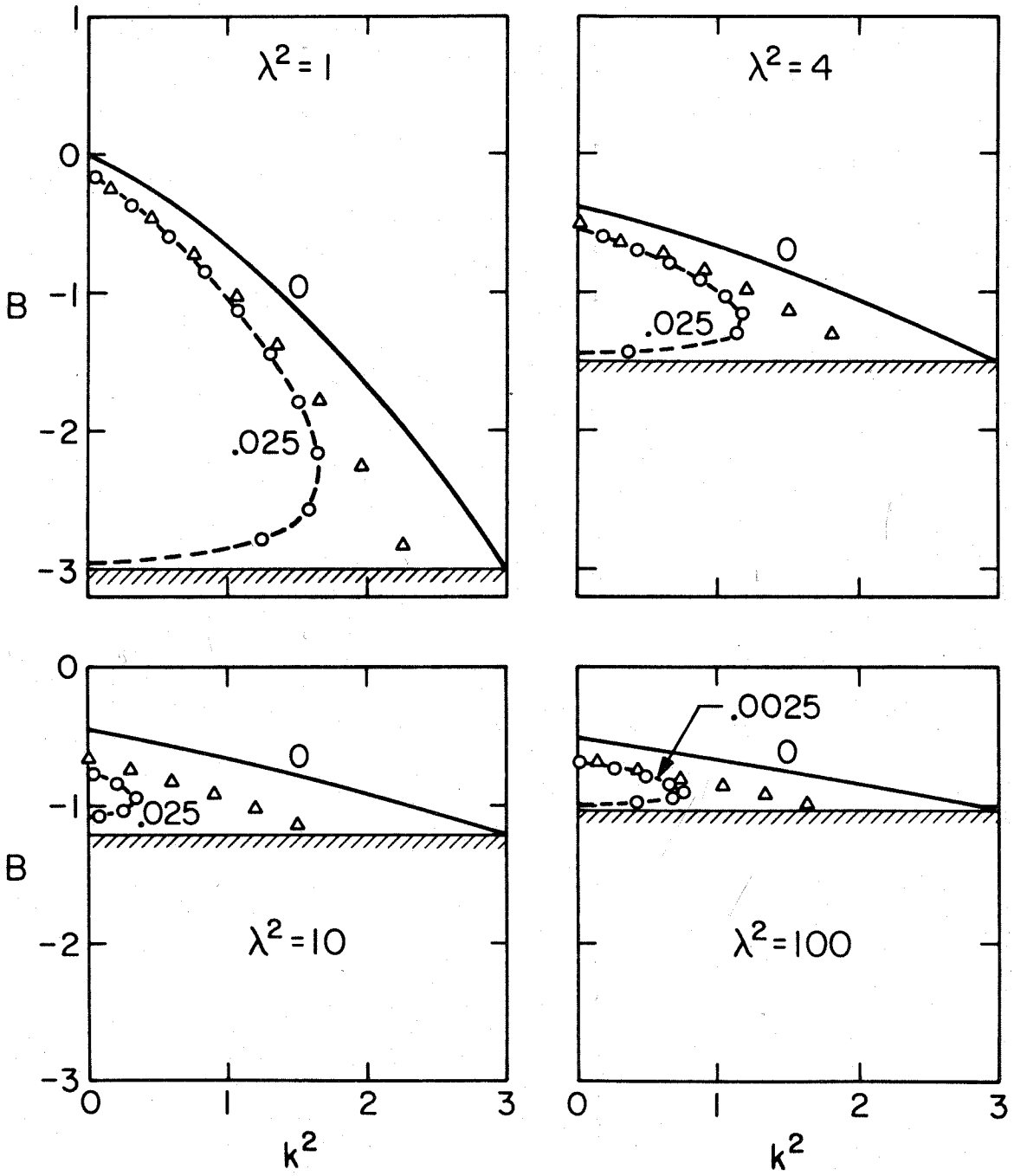

Figure 11

FIGURE 12. Curves of constant $|c_i| = \mathrm{Im}(c_D)/|U_0|$ (as in fig. 10) associated with the evanescent BTU disturbance (3.8) on the tanh velocity profile. Due to the antisymmetry involved in the neutral solutions (see discussion of fig. 5), the dependence of $|c_i|$ on k^2 is independent of the sign of B, allowing $|B|$ to be used as an axis in fig. 12.

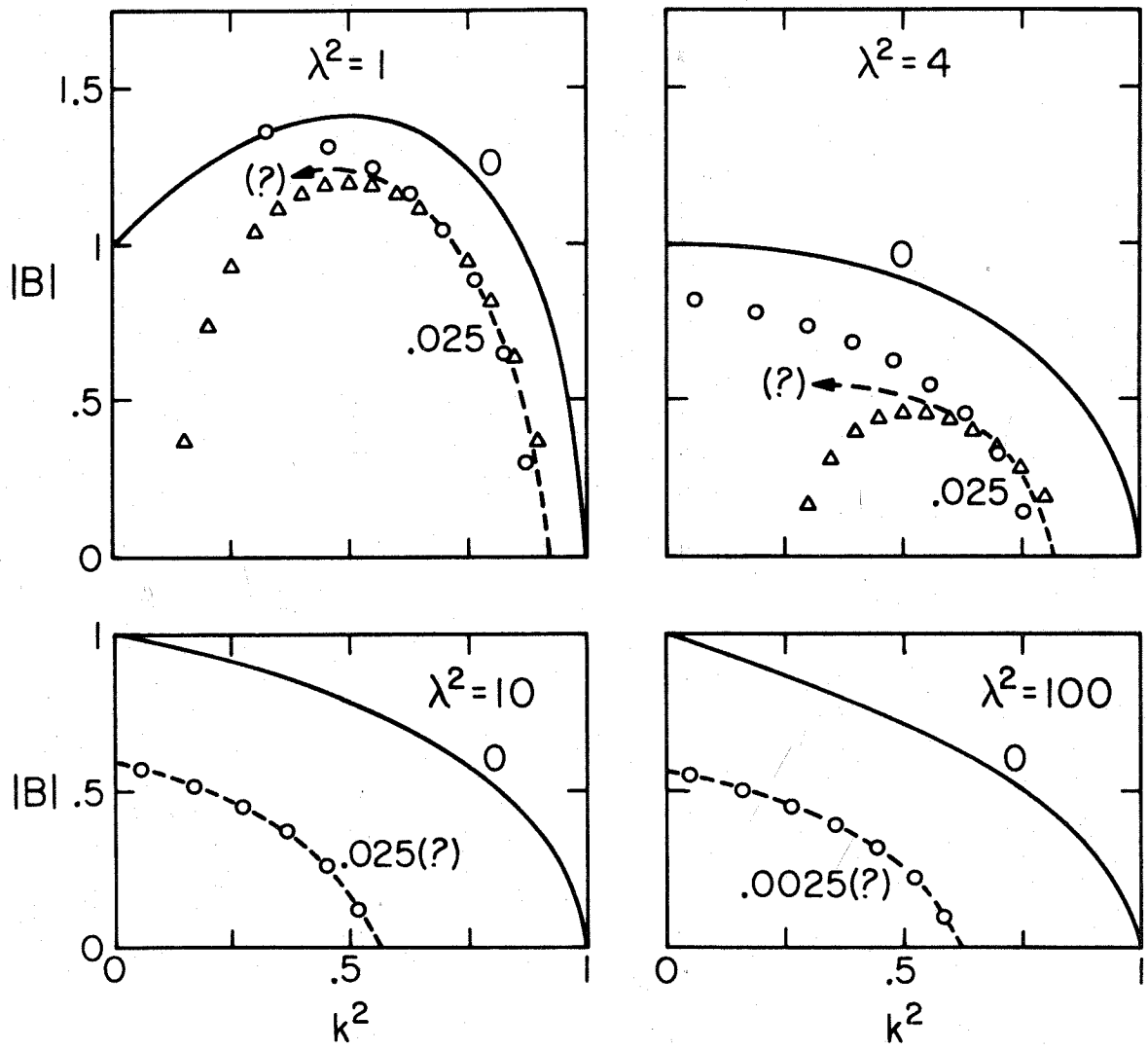

Figure 12

upper layer radius of deformation $L_r \geq 2500$ km) the estimated maximum $k|c_i|$ are $\sim .05$ (corresponding to growth time scales on the order of $\sim(.05)^{-1} L/|U_0| \sim 40$ earth days), and for larger λ^2 the maximum $|c_i|$ decrease roughly as $1/\lambda^2$, at least up to $\lambda^2 \sim 100$ ($L_r \sim 500$ km, growth time scales ~ 400 earth days). This behavior may be a useful diagnostic for the value of L_r on Jupiter from observations of disturbance growth rates (see section 7); it may be explained qualitatively for the two layer model as follows. For larger values of λ^2 (smaller L_r and $\Delta\rho$) the slope of the fluid interface associated with a given velocity profile $\bar{u}_D$ becomes larger, so that any north-south motion in the upper layer would require excessive vertical stretching of fluid columns, and so the growth of disturbances (which depends on north-south advection) is inhibited.

6. BAROTROPIC (BTU) INSTABILITY: NUMERICAL RESULTS

Since the BTU growth rate estimates of section 5 are just linear extrapolations out from the neutral curves, they are not necessarily correct over the whole (B,k^2) plane. In this section we present results of explicit BTU solutions found by numerically integrating the upper layer potential vorticity equation (3.1), yielding exact growth rates and phase speeds as functions of the x-wavenumber k for a few particular basic states.

Numerical results are presented for symmetric disturbances on the 'isolated jet' sech^2 velocity profile with $\lambda^2 = L^2/L_r^2 = 4$ (i.e. $L_r \sim 2500$ km, a reasonable but fairly large value for Jupiter). For evanescent waves, the numerical growth rates below agree well with the corresponding variational estimates, which suggests that the general variational results in section 5 for other evanescent cases and other values of λ^2 are accurate over most of the (B,k^2) plane. These general results have indicated that the maximum growth rates for the other cases (figs. 11 and 12) are comparable to or slightly less than the case (fig. 10) investigated numerically below, and in all cases the growth rates decrease roughly as $1/\lambda^2$ for $\lambda^2 \geq 4$.

Depending on the value of k, the solutions found are either evanescent outside the jet [corresponding to (3.4a)] or are oscillatory outside the jet [corresponding to (3.5a)]. As discussed in section 3.A, we impose rigid wall boundary conditions $\varphi = 0$ at $y/L = \pm Y$; the oscillatory solutions (but not the

evanescent solutions) are strongly affected by the wall locations, and all results below are presented both for Y = 3 (corresponding to walls ~ 15,000 km from the jet center to simulate the possible effect of adjacent belt-zone structure on Jupiter), and for Y = 10 (corresponding to walls ~ 50,000 km from the jet center to represent the finite size of Jupiter).

The method of solution parallels one used by Pedlosky (1964b, sec. 3). Equation (3.1) for $\varphi_1^{(0)} = \varphi(y)$ is integrated numerically for a given k from the jet center at y = 0 (where $\partial\varphi/\partial y$ is set at zero to obtain symmetric solutions) out to the boundary at y = Y. This is done for many values of c covering progressively finer grids in the (c_r, c_i) plane, and the correct eigenvalues for c are the intersections in the (c_r, c_i) plane of the zero lines of $\varphi_r(Y)$ and $\varphi_i(Y)$.

A. Growth Rates vs. x-wavenumber k.

Fig. 13 shows growth rates $\nu_i = \mathrm{Im}\,[k_D\, c_D/(L^{-1}|U_0|)]$ found numerically for symmetric disturbances on the velocity profile $\bar{u}_D = U_1 + U_0\,\mathrm{sech}^2\,(y/L)$, for $\lambda^2 = 4$ and three values of $B = (\beta_D + L_r^{-2}\,U_1)/(L_r^{-2}\,U_0)$ representative of the unstable range of B in the $\lambda^2 = 4$ graph of fig. 10. The phase speeds c_r are found to be nearly independent of k ($\pm \sim .05$) for each graph of fig. 13, and are approximately equal to the basic state velocity at the potential vorticity extrema shown in fig. 3.

By the similarity of the latitudinal forms of $\varphi\,(y)$, most numerical solutions are clearly related to a particular neutral wave type. The segments of the k-axis with numerical solutions corresponding to a particular neutral wave type are indicated in each graph of fig. 13. The symbol 0 indicates the evanescent type (3.4a), and 1, 2,...N,... indicate the oscillatory types (3.5a) with N half-wavelengths between the central structure and each wall [e.g., figs. 14(b) to 16(b)]. The vertical dividing lines are drawn exactly at the wavenumber k_N of the various neutral waves; in each graph the $k_0 = (6c)^{1/2}$ of the neutral evanescent wave is greater than all of the oscillatory $k_N = (6c - 4 - \ell_N^{\,2})^{1/2}$.

FIGURE 13. Non-dimensional growth rates $\nu_i = \mathrm{Im}[k_D\, c_D/(L^{-1}|U_0|)]$ as functions of the x-wavenumber $k = k_D L$ for symmetric disturbances on velocity profile $\bar{u}_D = U_1 + U_0\, \mathrm{sech}^2\,(y/L)$, with $\lambda^2 = L^2/L_r^2 = 4$ and $B = (\beta_D + L_r^{-2}\, U_1)/(L_r^{-2}\, U_0) = -1.4$, -1.0 and -0.5. Results are shown for the two different locations $y/L = \pm Y$ of the rigid wall boundaries, $Y = 3$ and $Y = 10$. Solid curves are for exact numerical solutions and dashed curves are variational estimates from the neutral waves using (5.1). For $B = -1.4$, the phase speeds c_r are $.97 \pm .02$ for all k shown; for $B = -1.0$, $c_r = .83 \pm .03$; for $B = -0.5$, $c_r = .53 \pm .05$.

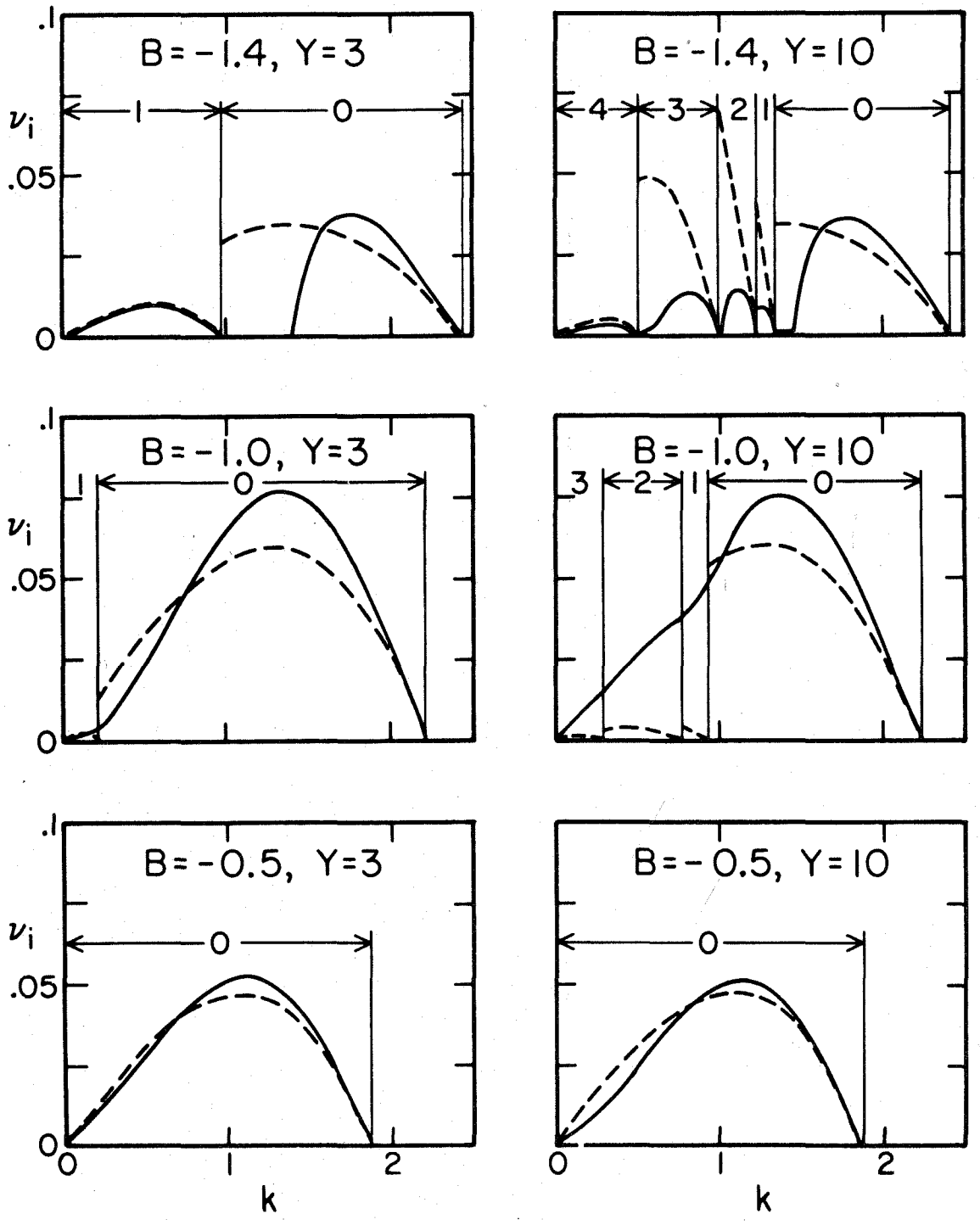

Figure 13

Unstable solutions related to a particular neutral wave with wavenumber k_N are found only for $k < k_N$, consistent with the variational estimates of section 5. However for a given k we generally find just one unstable numerical solution, related to the neutral solution type with wavenumber k_N (>k) closest to k. As k decreases through the next lowest k_{N+1} value of the next neutral wave type, the form of the unstable numerical solution changes rapidly to resemble the new neutral wave type N + 1, with correspondingly rapid changes in the growth rates ν_i in fig. 13. The dashed curves in fig. 13 show the variational estimates extrapolated using (5.1) from the neutral solution appropriate for each k-axis segment. These estimates agree well with the numerical values for evanescent solutions, but they often differ considerably for the smaller k with oscillatory solutions. Perhaps this discrepancy is related to the fact that for a given (small) k, the variational method predicts several unstable solutions corresponding to the several neutral solution-types with $k_N > k$, and does not anticipate the vanishing of all but one of these in the numerical solutions as described above.

Very occasionally for values of k in the transition regions $k \sim k_N$ between two types of unstable solutions, two similar unstable solutions with different c-eigenvalues were found for the same k. One of these solutions always had a comparatively small growth rate ($\nu_i \leqslant .01$) and was not included in fig. 13. For each basic state in fig. 13 and for several values of k, the entire region of the (c_r, c_i) plane in which unstable eigenvalues are possible according to the constraints (2.16), (2.19) and (2.20) was searched for symmetric

solutions. No other solutions were found except those in fig. 13 and those mentioned above; however the simple numerical method used (described above) did not permit the searches to be completely exhaustive within reasonable computation times in the subregions where $|c_r|$ and $|c_i| \ll 1$.

Because $k^2 = 6c - 4 - \ell^2 \geq 0$ for the neutral oscillatory waves, c must be greater than 2/3 for these waves to exist, which for $\lambda^2 = 4$ requires $B < -2/3$ from (3.2). Fig. 13 shows this criterion still holds approximately for unstable waves, since oscillatory solutions are only found for B = -1 and -1.4. For a given value of B, the oscillatory waves have significantly smaller growth rates than the evanescent waves, possibly because the former have significant amplitudes over the whole latitudinal range and must use some of the kinetic energy extracted from the shear $(\bar{u}_D)_y$ in the central jet to amplify the disturbance in the outer regions. However, the oscillatory growth rates decrease only slightly as the distance to the boundaries is increased from 3 to 10, and not at a rate comparable to $\sim Y^{-1}$ as might be expected from the above effect. Perhaps this effect is cancelled by more efficient transport of energy to the outer regions for larger values of Y.

The maximum growth rates in fig. 13 for symmetric disturbances on the sech^2 velocity profile are $\nu_i \sim .07$, and occur for $k \sim 1.3$ on basic states with intermediate values of B, i.e., $B \sim -1$ and $c_r \sim 0.8$ (consistent with the variational estimates in fig. 10). This implies

growth time scales of $\sim (.07)^{-1}\ L/|U_0| \sim 30$ earth days; as discussed above the general variational results in section 5 indicate that these maximum growth rates are typical of or slightly greater than those for other types of BTU disturbances and velocity profiles.

B. Latitudinal Forms.

Three examples of the explicit numerical solutions found above for fig. 13 are shown in figs. 14 to 16. Fig. 14(b) shows the real and imaginary parts of $\varphi(y)$ for the symmetric evanescent solution on the sech^2 velocity profile with $\lambda^2 = 4$, $B = -1.0$ and $k = 1.3$; this solution has one of the largest growth rates ($\nu_i = .07$) in fig. 13. Figs. 15(b) and 16(b) show $\varphi(y)$ for two oscillatory solutions with $N = 1$ ($k = .09$) and $N = 2$ ($k = 0.4$) respectively, on the same basic state as fig. 14 with latitudinal walls at $Y = \pm 10$; these have smaller growth rates than the evanescent solution (see fig. 13 for $B = -1$ and $Y = 10$). The streamline patterns in the (x,y) plane implied by these solutions are discussed in section 7.

The real parts φ_r of the solutions in figs. 14 to 16 are similar to the corresponding neutral solutions [cf. fig. 2(b) and 2(d)]. The evanescent $\varphi_r \approx \text{sech}^2 (y/L)$, but the central 'peaks' around $y \sim 0$ of the oscillatory φ_r in figs. 15 and 16 are larger than those of the neutral solutions. Also, the oscillatory φ_r appear slightly exponential in the outer regions, whereas the corresponding neutral solutions must be entirely sinusoidal from (3.5a).

Figs. 14(c) to 16(c) show lines of constant $k\,x + \arg[\varphi(y)]$ in the horizontal (x,y) plane. These lines define the tracks of the ridges, troughs and zero-lines of the stream function

FIGURE 14. Latitudinal forms of symmetric evanescent unstable BTU solution found numerically for velocity profile $\bar{u}_D = U_1 = U_0 \text{ sech}^2 (y/L)$ with $\lambda^2 = L^2/L_r^2 = 4$ and $B = (\beta_D + L_r^{-2} U_1)/(L_r^{-2} U_0) = -1.0$. The disturbance parameters are $k = k_D L = 1.3$, $c_r = \text{Re}[(c_D - U_1)/U_0] = .81$, $\nu_i = \text{Im}[k_D c_D/(L^{-1}|U_0|)] = .075$.

(a): Velocity profile $\bar{u}_D$ vs. (poleward) latitudinal coordinate y/L, for retrograde jet ($U_0 < 0$). Dashed line shows disturbance phase speed c_r relative to the jet.

(b): Solid curve is $\varphi_r = \text{Re}[\varphi_1^{(0)}]$ vs. y/L; dashed curve is $\varphi_i = \text{Im}[\varphi_1^{(0)}]$ vs. y/L.

(c): Line of constant kx + arg (φ) in the horizontal (x,y) plane. Note difference between x and y scales.

(d): y-dependence of the latitudinal flux of zonal momentum $\overline{u_1' v_1'}$, scaled relative to $|\varphi_1^{(0)}(0)/L|^2$.

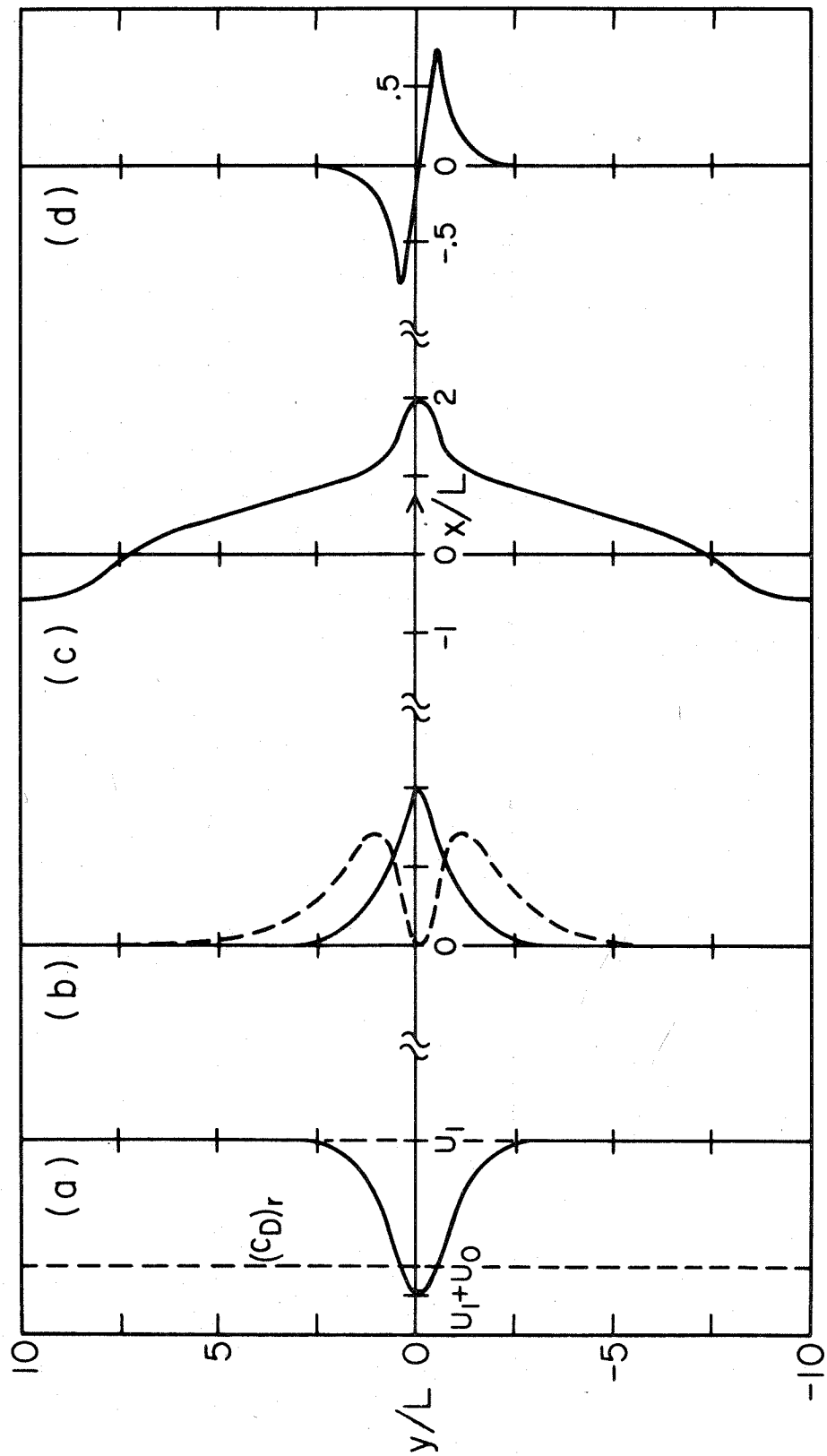

Figure 14

FIGURE 15. Latitudinal forms of symmetric oscillatory (N = 1) unstable BTU solution for the sech^2 velocity profile, with rigid wall boundaries at y/L = ± 10. Parameters are as defined for fig. 14, except here k = 0.9, c_r = .82, ν_i = .047.

(a): $\bar{u}_D$ vs. y/L.

(b): Solid curve is φ_r vs. y/L; dashed curve is φ_i vs. y/L.

(c): Line of constant kx + arg (φ) in the horizontal (x,y) plane. Note difference between x and y scales.

(d): y-dependence of $\overline{u_1' v_1'}$.

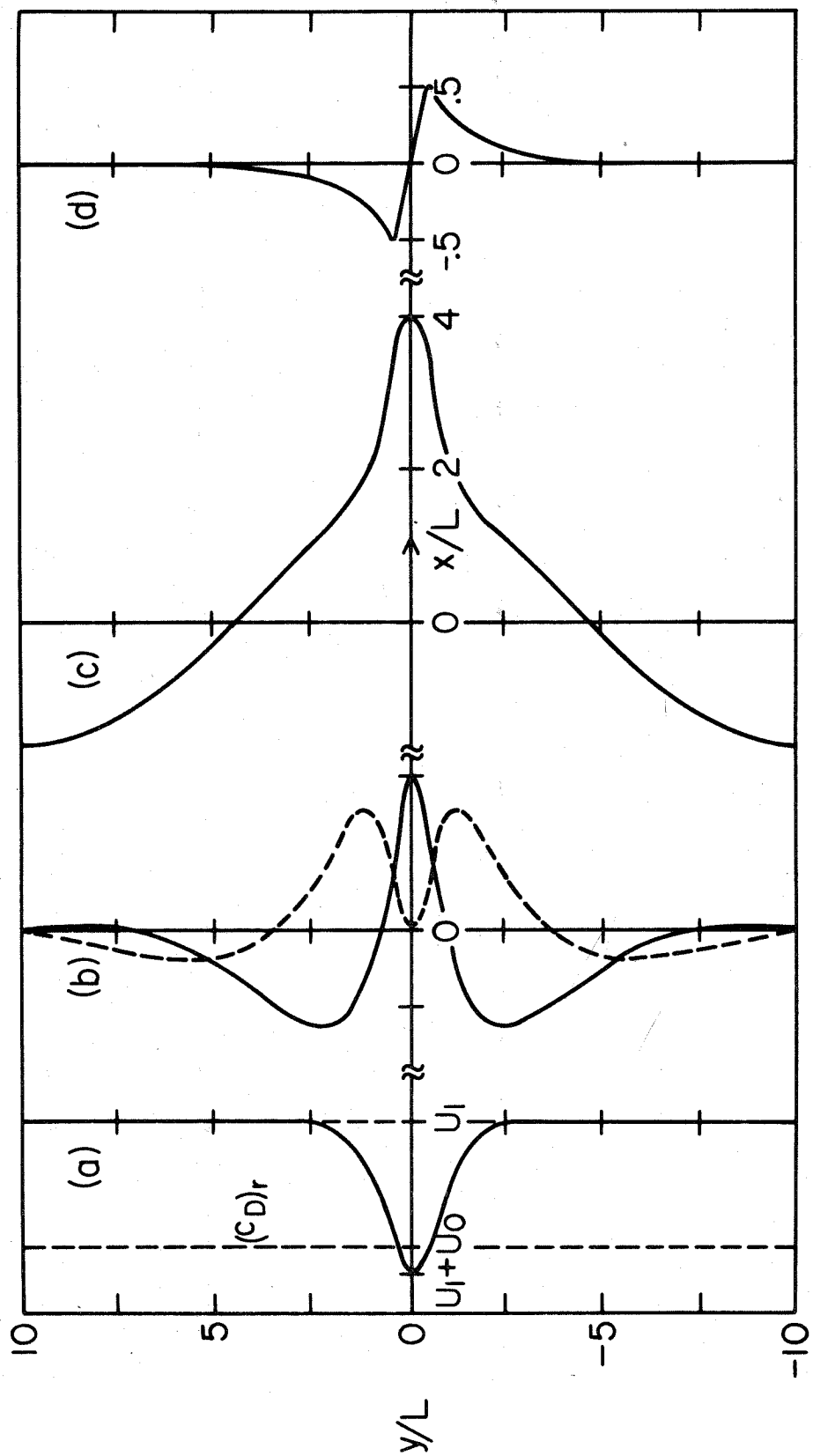

Figure 15

FIGURE 16. Latitudinal forms of symmetric oscillatory (N = 2) unstable BTU solution for the sech^2 velocity profile, with rigid wall boundaries at y/L = ± 10. Parameters are as defined for fig. 14, except here k = 0.6, c_r = .81, ν_i = .032.

(a): $\bar{u}_D$ vs. y/L.

(b): Solid curve is φ_r vs. y/L; dashed curve is φ_i vs. y/L.

(c): Line of constant kx + arg (φ) in the horizontal (x,y) plane.

(d): y-dependence of $\overline{u_1' v_1'}$.

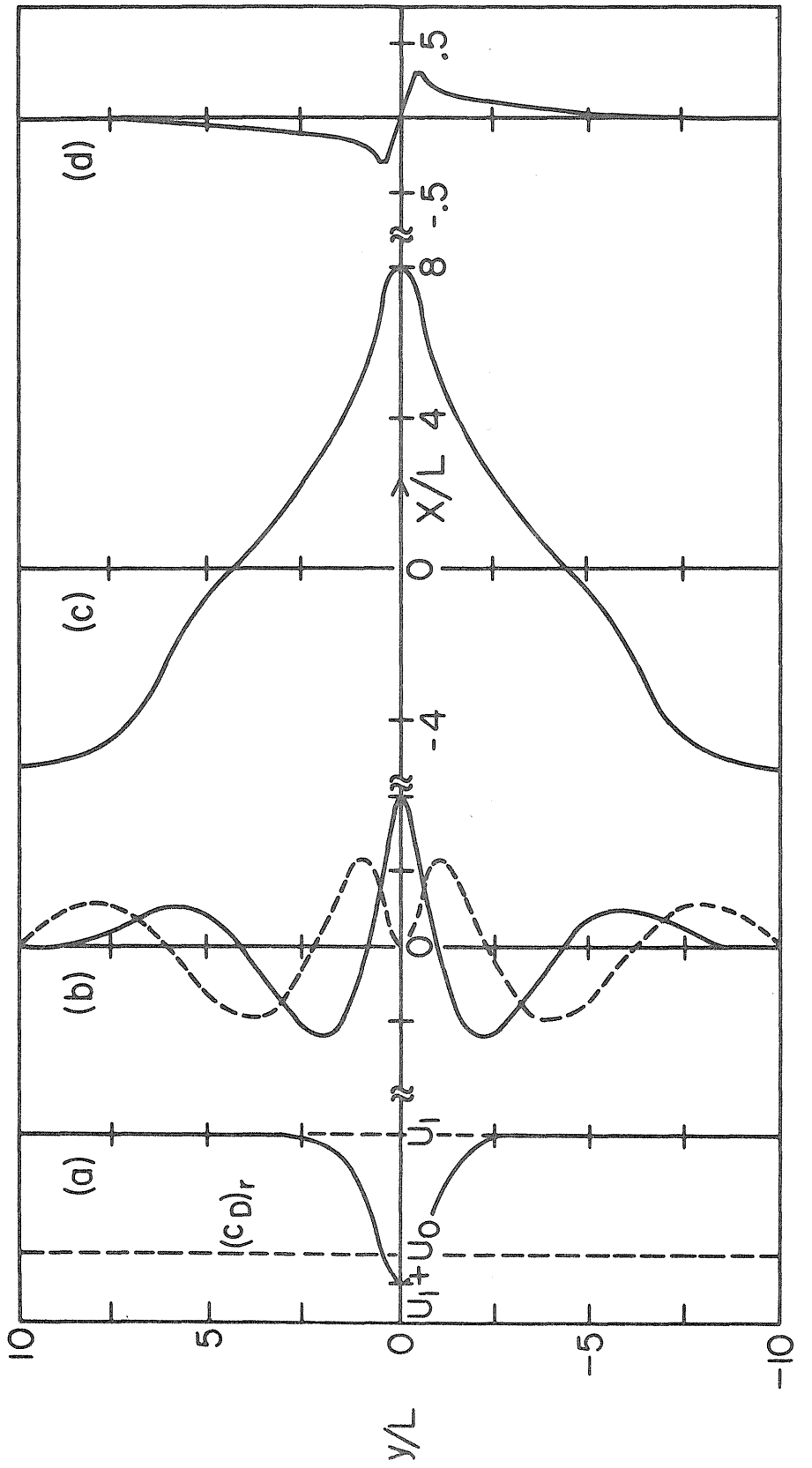

Figure 16

$\psi = \mathrm{Re}\left\{\varphi(y)\ \exp[ik\ (x - ct)]\right\}$ at any one instant of time t, and indicate the skew of the streamline patterns in the (x,y) plane (cf. section 7). (For neutral waves, $\arg[\varphi(y)]$ is independent of y so their ψ-ridges, etc., would run exactly north-south.) The amount of east-west skew is least for the fast-growing evanescent wave in fig. 14(c), and increases as the y-wavenumber of the oscillatory waves increases.

This skewing of the streamfunction pattern is associated with the latitudinal flux of zonal momentum $\overline{u_1' v_1'}$, which appears in the right hand sides of the kinetic energy equations (2.25) and (2.26) and is essential for the barotropic instability of the wave. The y-dependences of $\overline{u_1' v_1'}$ are shown in figs. 14(d) to 16(d); the divergences $(\overline{u_1' v_1'})_y$ of these fluxes are correlated with $\bar{u}_D$ so as to amplify the waves and to take kinetic energy out of the retrograde center of the jet [cf. (2.25) and (2.26)]. The fast-growing evanescent wave has relatively large $\overline{u_1' v_1'}$ concentrated near the jet center, compared to the oscillatory $\overline{u_1' v_1'}$ which have tails extending into the outer regions to transport kinetic energy to the sinusoidal waves there.

C. Secondary Meridional Circulation.

As discussed in section 1.C(i) and 2.F, the eddy transports of momentum and energy due to many local disturbances over time scales of several years may be important for the long-term balances maintaining the zonal mean flow system. The only potentially order 1 eddy fluxes appearing in (2.25) to (2.30) that are due directly to the growing BTU disturbances are the $\overline{u_1' v_1'}$ term, which converts mean to eddy kinetic energy in the upper layer, and the $\overline{p_1' w_1'}$ term which converts some of this eddy kinetic energy to eddy available potential energy of the sloping interface. All other eddy terms in these equations depend on the $0(\delta)$ interactions with the lower layer and so are insignificant by comparison.

As mentioned at the end of section 4.A, net diabatic heating due to planetary fluxes would appear as a forcing term on the right hand side of the zonal mean a.p.e. equation (2.27). There are no 0(1) eddy fluxes in (2.27) for BTU disturbances, so we cannot compare eddy to planetary fluxes as in section 4.A. However, (2.25) shows that for the zonal mean flow to remain constant in time, there must be a (non-geostrophic) mean meridional circulation causing a $\overline{p_1}\ \overline{w_1}$ correlation to balance the slowing of the mean jet by the $\overline{u_1' v_1'}$ eddy term; the $\overline{p_1}\ \overline{w_1}$ term 'pumps' the upper layer mean flow by using mean a.p.e. of the sloping interface, and so appears in (2.27). Below we compute the strength of the meridional circulation implied by a given amplitude

of BTU disturbances, and then compare the $\overline{p_1}\ \overline{w_1}$ term with a typical diabatic heating in (2.27).

To describe these long term balances of the zonal flow system it is more convenient to use the zonal mean dynamical equations rather than the energy equations (Phillips, 1954; Holton, 1972, Ch. 11.4). The analogous equation to (11.33) of Holton, for the zonal mean vorticity of the upper layer of the present two-layer model (with ψ_2 neglected), is (using dimension notation defined in section 2.A)

$$\left(\frac{\partial}{\partial t} + d\right) \bar{\psi}_{1_{yy}} = (\overline{u_1' v_1'})_{yy} - \frac{f_o}{H_1} \bar{w}_I \quad . \tag{6.1}$$

Here the overbar denotes zonal mean, and w_I is the vertical velocity (upwards) of fluid particles at the interface between the two layers. The linear drag term d is a crude representation of internal dissipation by small scale processes. The zonal mean upper layer equation analogous to the thermodynamic energy equation (11.34) of Holton (again with ψ_2 neglected) is

$$\left(\frac{\partial}{\partial t} + d\right) \bar{\psi}_1 = - \frac{f_o L_r^2}{H_1} \bar{w}_I - \bar{R} \quad . \tag{6.2}$$

Here R is a forcing term representing net diabatic heating, and d represents thermal damping by small scale processes with the same time constant as the linear drag in (6.1) for simplicity. (6.1) and (6.2) follow, for instance, from equations (2.25)

of Pedlosky (1964a).

Eliminating $\bar{\psi}_1$ between (6.1) and (6.2), we obtain an equation for $\bar{w}_I$ analogous to (11.37) of Holton:

$$\left(\frac{\partial^2}{\partial y^2} - \frac{1}{L_r^2}\right)\bar{w}_I = \frac{H_1}{f_o L_r^2}\frac{\partial^2}{\partial y^2}\left(-\overline{u_1' v_1'} - \bar{R}\right) , \qquad (6.3)$$

As discussed in Holton (1974, Ch. 11.4), these secondary vertical velocities are necessary to maintain the geostrophic and hydrostatic balances of the zonal flow $\bar{u}_D = -\bar{\psi}_{1_y}$, whether the flow is steady ($\partial \bar{\psi}_1/\partial t = 0$) or not.

By combining (6.3) with the primitive mass continuity equation for the upper layer (integrated over x and z)

$$\frac{\partial \bar{v}_1}{\partial y} - \frac{\bar{w}_I}{H_1} = 0 ,$$

and using rigid wall boundary conditions at which $v_1 = 0$, we could solve for the secondary zonal mean meridional circulation system $\bar{v}_1$, $\bar{w}_I$ in the (y,z) plane of the upper layer, caused by a given eddy flux $\overline{u_1' v_1'}$ and diabatic heating R. However, the latitudinal dependence of R is largely unknown for Jupiter, depending for instance on details of cloud processes and the internal heat flow (Gierasch, Ingersoll and Williams, 1973; Gierasch, 1976; Ingersoll and Porco, 1978).

As in Phillips (1954), we may set $\bar{R} = 0$ in (6.3) and solve for that part of the meridional circulation pattern caused by the

eddy transports of BTU instabilities. We have done this numerically for the $\overline{u_1' v_1'}$ distribution due to the fast-growing evanescent disturbances on the retrograde sech^2 jet presented in fig. 14, and the resulting meridional circulation is shown in fig. 17. By continuity in the lower layer, the streamline cells must be closed by a deep circulation below the fluid interface. There is an 'indirect' cell centered on the retrograde jet, with rising motion poleward of the jet center ($0 < y \leq 1$), equatorward motion in the upper layer through $y = 0$, and sinking motion equatorward of the jet center ($-1 \leq y < 0$). For basic state parameters $U_0 = -30$ m/s, $|U_0/f_0 L| = H_1/L = .03$, we find that the meridional circulation term $\bar{p}_1 \bar{w}_1$ in (2.27) would be comparable to a typical diabatic heating term $\sim 10^3$ ergs/cm^2/sec (e.g., due to latitudinal variations of I.R. emission; see end of section 4.A) if the BTU disturbance velocities u_1' and v_1' were ~ 1 m/s, implying velocities of the meridional circulation $\bar{v}_1 \sim .5$ cm/s and $\bar{w}_1 \sim .03$ cm/s (cf. Gierasch, 1976, table III). Although the actual meridional circulation pattern may be different from fig. 17 due to the diabatic heating R, the magnitudes of $\bar{v}_1$ and $\bar{w}_1$ above are reasonable estimates for the actual strengths if the $\overline{u_1' v_1'}$ eddy flux is actually significant in the long term balance of the zonal flow.

FIGURE 17. Secondary meridional circulation caused by the $\overline{u_1' v_1'}$ eddy flux [shown in fig. 14 (d)] due to unstable symmetric evanescent BTU disturbances with k = 1.3, on the retrograde ($U_0 < 0$) jet $\bar{u}_D = U_1 + U_0 \operatorname{sech}^2 (y/L)$ with B = 1.0 and $\lambda^2 = 4$.

(a): Zonal mean poleward velocity $\bar{v}_1$ in the upper layer, scaled by $|U_0|\ |U_0/f_0 L|\ |U'/U_0|^2\ \lambda^2$ where U' is a typical disturbance velocity in the upper layer.

(b): Zonal mean vertical velocity (upwards) at the interface $\overline{w_I}$, scaled by $|U_0|\ |U_0/f_0\ L|\ |U'/U_0|^2\ \lambda^2 (H_1/L)$.

(c): Streamlines of the meridional circulation $(\bar{v}_1, \bar{w}_1)$ in the (y,Z) plane. The vertical scale for the lower layer is compressed to show the lower layer 'return' flow.

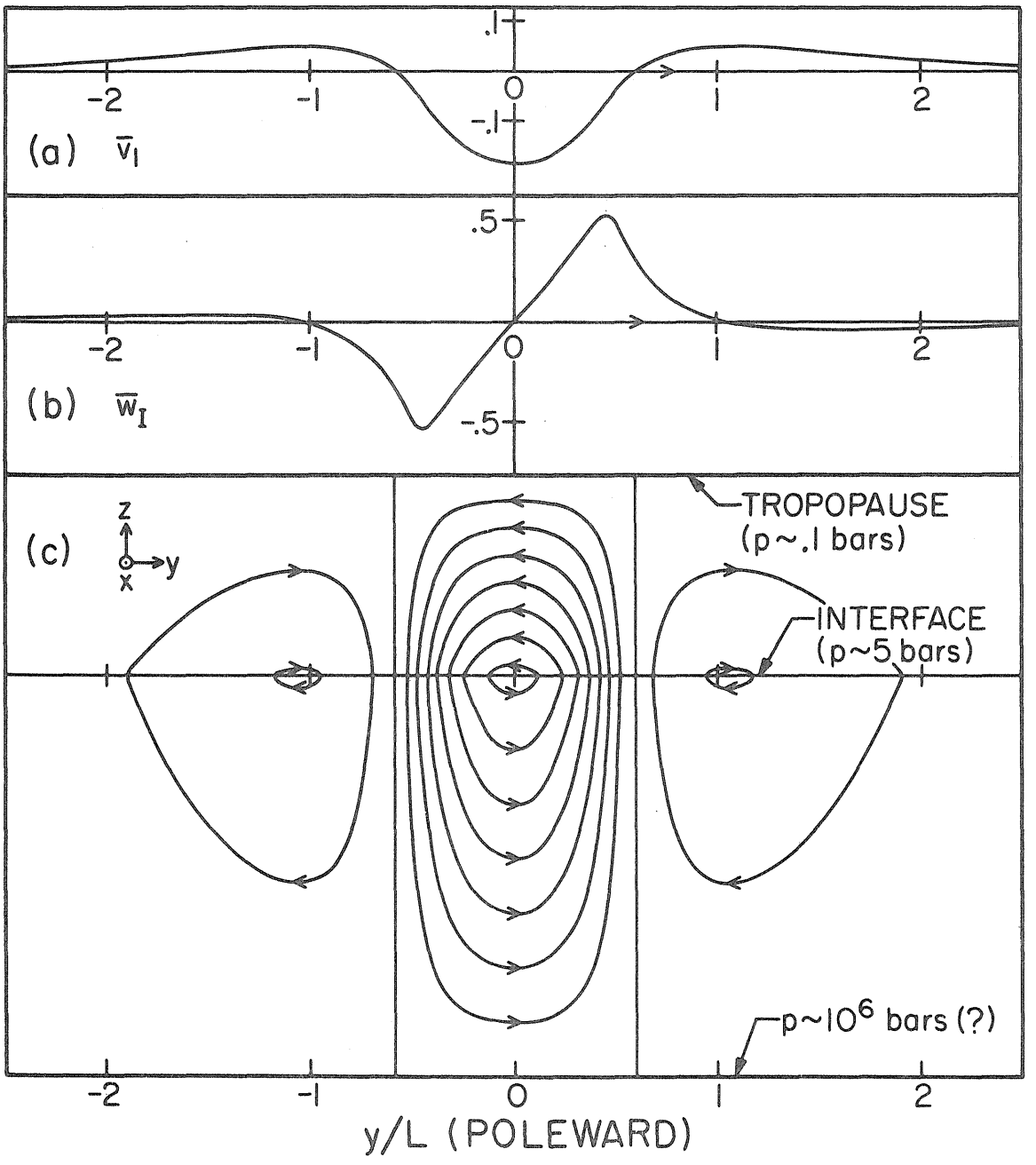
.1
-.1
0
-2
-1
1
2
(a) $\bar{v}_I$
.5
-.5
(b) $\bar{w}_I$
(c)
z
y
x
TROPOPAUSE
(p~.1 bars)
INTERFACE
(p~5 bars)
p~10^6 bars (?)
y/L (POLEWARD)

Figure 17

7. SUMMARY: POSSIBLE OBSERVATIONAL TESTS

In the preceding sections theoretical results have been presented (in varying degrees of generality) for linearized disturbances on two types of upper layer velocity profiles in the two-layer model. By comparing these model predictions with data of Jovian disturbances in Voyager images, we may hope to test whether the concept of an upper 'weather' layer above $p \sim 5$ bars is correct for Jupiter's zonal jet system. However, the general theoretical format of most model results above is not the most suitable for such comparisons. In this section several examples of these results, that may be particularly diagnostic of the validity of the model for Jupiter, are presented in forms designed for easier comparisons with anticipated Voyager data.

A. Effect of Deep Lower Layer.

The basic effect of the deep quiescent lower layer below $p \sim 5$ bars was shown by the δ-expansions of section 2. For values of δ (the ratio of the mean thickness of the upper layer to that of the lower layer) much less than unity, the only types of disturbances with (non-dimensional) growth rates potentially of order one are essentially free divergent barotropic disturbances confined almost entirely to the upper layer (BTU modes). If the observed Jovian disturbances are indeed BTU modes, then since they have only insignificant [$0(\delta)$] interactions with the lower layer, there would be no practical way of determining the appropriate Jovian value of δ from their observations, beyond confirming that $\delta \ll 1$.

The results of section 5 and 6 show that the fastest growing BTU disturbances, on the sech^2 and tanh upper layer velocity profiles at least, have growth rates on the order of ~30 earth days and x and y-scales comparable to the latitudinal scale of the zonal jets, ~5000 km. These quantities are roughly consistent with present observations of many local Jovian disturbances (section 1.A), although more detailed data are necessary to positively identify the observed disturbances as the predicted BTU modes (see below).

B. Phase Speeds: Effect of L_r.

It was shown in section 2.C that for any neutrally stable BTU modes to exist with phase speed c_r within the range of the upper layer zonal flow $\bar{u}(y)$, the basic state upper layer potential vorticity gradient b(y) must vanish at some latitude and c_r must equal the value of $\bar{u}$ at that latitude. [The same criterion holds for baroclinic solutions (BC modes, section 2.E).] The numerical solutions for the sech^2 velocity profile in section 6 show that the same criterion still holds approximately (to within $\pm \leqslant .05$ in the non-dimensional phase speed) for unstable BTU disturbances; also, no unstable solutions were found with c_r outside the range of $\bar{u}(y)$. If c_r of Jovian disturbances and b(y) of the Jovian basic state were measurable from Voyager images, the phase speed criterion above would provide a stringent observational test of the validity of the model for Jupiter. However, the (dimensional) potential vorticity gradient is $\beta_D - (\bar{u}_D)_{yy} + L_r^{-2} \bar{u}_D$, where L_r is the Rossby radius of deformation for the upper layer (see section 2.A). The planetary vorticity gradient β_D is known and $\bar{u}_D(y)$ may be measured from Voyager images, but L_r cannot be measured directly by Voyager since it depends on $\Delta\rho/\rho$, which represents the unknown amount of stable stratification above $p \sim 5$ bars.

However, by assuming the present two layer model is valid

for Jupiter, the above criterion for the phase speeds may provide an indirect rough determination of the upper layer Rossby radius L_r. Fig. 18 shows the dependence of the non-dimensional neutral phase speed $c_r = \text{Re}\,[(c_D - U_1)/U_0]$, determined by the value of $\bar{u}$ at the zeros of b(y), on the non-dimensional basic state parameters $\beta_D L^2/U_0$, U_1/U_0 and $\lambda^2 = L^2/L_r^2$, for the velocity profile $\bar{u}_D = U_1 + U_0\ \text{sech}^2\ (y/L)$. This profile with $U_1/U_0 \leqslant 0$ seems fairly realistic for many of the maxima and minima of $\bar{u}_D(y)$ in the observations to date of Jupiter's zonal flow (Chapman, 1969; Ingersoll and Cuzzi, 1969). Fig. 18 is similar to fig. 3, but the axes in fig. 18 are chosen to separate out the non-observable parameter λ^2 from the observable ones.

For Jupiter, L_r may reasonably lie between ~500 km and ~2500 km (see appendix), which correspond to λ^2 ~100 and $\lambda^2 \sim 4$ respectively for L ~ 5000 km. (For $\lambda^2 \geqslant 100$, the fig. 18 curves would lie very close to the limiting $\lambda^2 = \infty$ curves.) From a given set of observations the parameters $\beta_D L^2/U_0$, U_1/U_0 and c_r can hopefully be measured, so that λ^2 could theoretically be determined from fig. 18. (As mentioned above, all unstable BTU disturbances on a given basic state have phase speeds within ~.05 of the neutral c_r.) However, since the Voyager images can only measure changes in horizontal cloud patterns with time, there may be some ambiguity between changes due to advection by

FIGURE 18. Non-dimensional phase speeds $c = (c_D - U_1)/U_0$ of neutral disturbances on velocity profile $\bar{u}_D = U_1 + U_0 \operatorname{sech}^2 (y/L)$ as functions of the basic state parameter $\beta_D L^2/U_0$, for various values of $\lambda^2 = L^2/L_r^2$ and U_1/U_0.

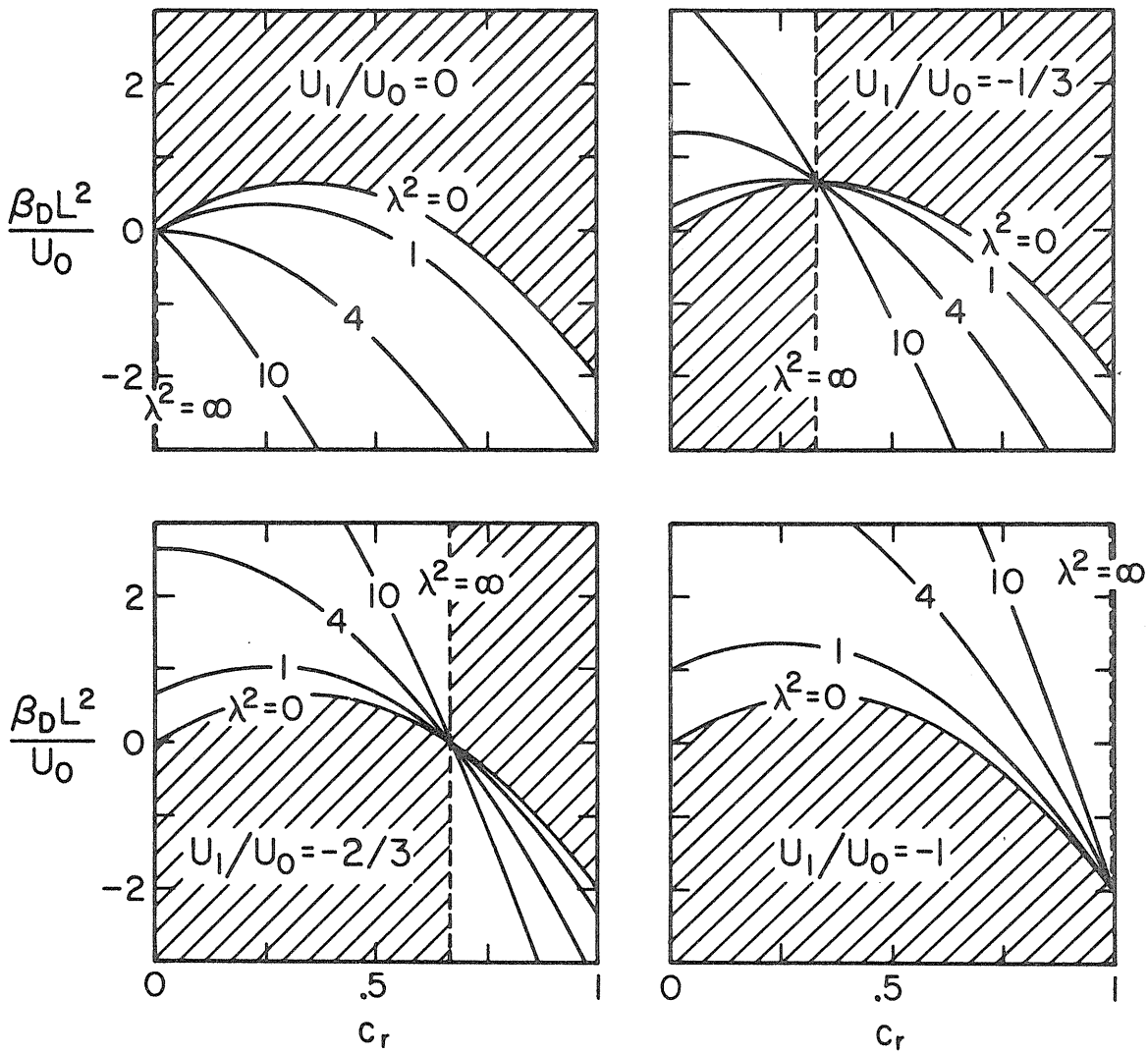
$\frac{\beta_D L^2}{U_0}$
2
0
-2
$U_1/U_0 = 0$
$\lambda^2 = 0$
1
4
10
$\lambda^2 = \infty$
$U_1/U_0 = -1/3$
$U_1/U_0 = -2/3$
$U_1/U_0 = -1$
0
.5
1
c_r

Figure 18

$\bar{u}$ and due to wave motions c_r. Unless this can be resolved and both $\bar{u}$ and c_r can be measured surprisingly accurately, this method may only yield a rough estimate for λ^2, since λ^2 is sensitive to small changes in the measurable parameters in many regions of fig. 18.

As an example, if the dimensional phase speeds $(c_D)_r$ are consistently observed to be approximately zero in system III (i.e., $c_r \approx 0$ which corresponds to the $\lambda^2 = \infty$ dashed lines in fig. 18), this would indicate a large value of λ^2 ($\lambda^2 \geq 10$, so that $L_r \leq 1500$ km). Conversely, if the observations consistently fall in the shaded (no solution) regions of fig. 18, this would indicate the whole model is incorrect for Jupiter; [for instance, if $\beta_D L^2/U_0 \geq 1$ and $U_1/U_0 \approx 0$, i.e., for weak prograde jets with zero (or positive) ambient velocity U_1, theoretical BTU solutions are impossible for all values of λ^2]. The relationships shown in fig. 18 are discussed qualitatively in section 3.A (fig. 3).

C. Growth Rates: Effect of L_r.

The Voyager images should be able to follow individual large-scale disturbances continuously for several months, allowing measurements of any e-folding growth times that are comparable to or less than this time scale. The maximum growth rates of BTU disturbances on both sech^2 and tanh velocity profiles in the two-layer model depend strongly on the order of magnitude of λ^2, so that growth rate measurements may yield an approximate but firm estimate of L_r; this should be consistent with estimates using phase speed measurements as described above.

The solid curves in fig. 19 are contours of non-dimensional growth rates $\nu_i = \text{Im}\,[k_D\, c_D/(L^{-1}|U_0|)]$ in the (B,k^2) plane for the (fast growing) symmetric evanescent disturbances [corresponding to (3.4a)] on the velocity profile $\bar{u}_D = U_1 + U_0\, \text{sech}^2 (y/L)$. The basic state parameter B is $(\beta_D + L_r^{-2}\, U_1)/(L_r^{-2}\, U_0)$, and k is the disturbance x-wavenumber $k_D L$. The non-dimensional phase speeds $c_r = \text{Re}\,[(c_D - U_1)/U_0]$ are also shown by the dashed lines in fig. 19. Both ν_i and c_r in fig. 19 are variational estimates from extrapolating (5.1) out from the neutral curves, as in fig. 10. The numerical solutions in section 6 confirmed that the variational estimates are accurate over most of the (B,k^2) plane, except in regions where oscillatory solutions are possible; however, the oscillatory growth rates of these regions are significantly smaller than the evanescent growth rates (see fig. 13). These

FIGURE 19. Contours of growth rates and phase speeds in the (B,k^2) plane, from variational estimates using (5.1), for symmetric evanescent solutions on the velocity profile $\bar{u}_D = U_1 + U_0 \operatorname{sech}^2 (y/L)$. The basic state parameter B is $(\beta_D + L_r^{-2} U_1)/(L_r^{-2} U_0)$, and k is the disturbance x-wavenumber $k_D L$. Solid curves show non-dimensional growth rates $\nu_i = \mathrm{Im}[k_D c_D/(L^{-1}|U_0|)]$, and dashed lines show non-dimensional phase speeds $c_r = \mathrm{Re}[(c_D - U_1)/U_0]$. Regions where the variational estimates are not expected to be accurate (see text) are shaded.

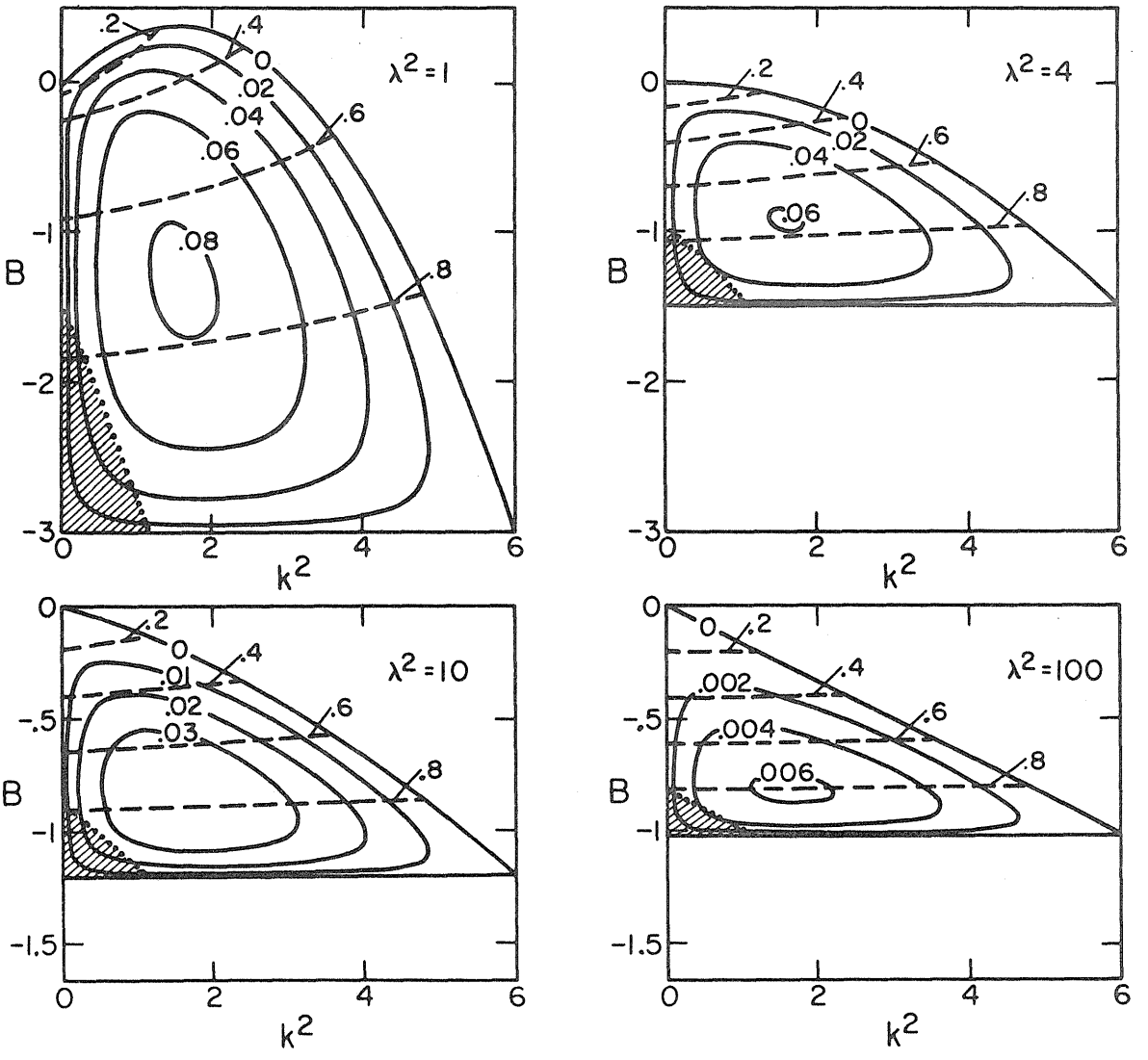

Figure 19

oscillatory regions (for rigid walls at $y/L = \pm 3$) are shaded in fig. 19.

For $\lambda^2 \leqslant 4$, the maximum ν_i in the (B,k^2) plane are fairly constant at $\sim.06$, corresponding to e-folding growth times of $\sim$30 earth days. For $\lambda^2 \geqslant 4$ ($L_r \leqslant 2500$ km) the maximum ν_i decrease at roughly the same rate as λ^{-2}, so that for $\lambda^2 = 10$ ($L_r \sim 1500$ km) the fastest growth times are $\sim$60 earth days, and for $\lambda^2 = 100$ ($L_r \sim 500$ km) the fastest growth times are $\sim$300 days. The phase speeds c_r and x-wavelengths k of these fastest growing waves are fairly independent of the value of λ^2; they are $c_r \sim 0.6$ [i.e., $(c_D)_r \sim U_1 + .6U_0$] and $k \sim 1.3$ ($k_D \sim 6500$ km).

The actual value of the basic state parameter B for a particular Jovian jet may not be the value that gives the maximum BTU growth rates in the (B,k^2) plane. Also, B involves L_r as well as β_D, U_0 and U_1, so that without knowing L_r we do not know B for a particular jet <u>a priori</u>. However, the variety of zonal jets on Jupiter is (hopefully) sufficiently rich that the maximum growth rates are realized for at least some of the jets; as mentioned above, disturbances on these jets should then have $c_r \sim 0.6$ and $k \sim 1.3$.

D. Disturbance Morphology.

In addition to the relationships described above between various parameters of BTU disturbances and the basic states, the two layer model predicts specific upper layer streamline patterns of disturbance velocities in the horizontal (x,y) plane. Equivalent patterns in the vertical (x,z) plane of linear quasi-geostrophic models correctly predict several observed features of baroclinic instabilities in the earth's jet streams; (for instance, the westward tilt of the wave pattern with height; e.g., Charney (1947), Holton (1972) Ch. 7 and 8).

As an example for the present BTU modes, fig. 20(a) shows streamlines of the perturbation velocity field (u_1', v_1') for the fast growing evanescent disturbance with $k = 1.3$ on the sech^2 velocity profile with $B = -1.0$ and $\lambda^2 = 4$ (shown in fig. 14). As discussed for figs. 14 to 16, the wave patterns of unstable BTU waves are skewed to the west at latitudes away from the jet center of retrograde jets; this skew is required for u_1' and v_1' to be correlated so as to remove retrograde momentum $-\rho_1 u_1$ from the central region of the jet and to amplify the disturbance (sections 2.F and 6.B).

In Pioneer images it seems that many features of the disturbances embedded in the zonal jets are visible primarily because of the contrast between the white ammonia clouds (at $p \sim .7$ bars) and the brown/blue lower levels (Gehrels, 1976).

If the cloud features are actively generated by the disturbances, e.g., by vertical velocity $w_1' \propto - \partial \psi_1'/\partial t$, one would expect to see patterns resembling fig. 20(a) moving through the fluid in the east-west direction at the phase velocity $(c_D)_r$. However, if the clouds are pre-existing passive tracers of the horizontal velocities, the measured velocity field at any instant would include the basic state velocity $\bar{u}_D$. Fig. 20(b) shows the streamline pattern of the combined velocity field $(u_1', v_1') + \bar{u}_D$ for the same disturbance as fig. 20(a) and the sech^2 velocity profile $\bar{u}_D$, as measured in a frame moving with x-velocity $U_1 + .5\ U_0$ (i.e., in system III for profiles with $U_1/U_0 = -.5$).

Since the whole pattern of velocities in fig. 20(b) is moving through the fluid with phase speed $(c_D)_r$, a passive area of clouds after a while may be advected into a pattern quite different from that of the instantaneous velocity field. Fig. 21 shows the development in time of a line of fluid particles, initially aligned east-west at the jet center, whose positions at subsequent times (in units of $\tau = L/|U_0|$) have been computed numerically using the velocity field of fig. 20(b). The resulting 'curly' morphology is reminiscent of many mid-latitude disturbances in Pioneer images.

Depending on the type of analysis of Voyager data and the interactions between the disturbances and the cloud layers,

FIGURE 20. Geostrophic streamline patterns in the (x,y) plane.

(a): Disturbance streamlines [i.e., equally spaced contours of the streamfunction $Re(\psi_1)$] showing the instantaneous velocity field (u_1', v_1') in the horizontal (x,y) plane, for the symmetric evanescent unstable BTU disturbance with k = 1.3 on the $sech^2$ velocity profile with B = -1.0 and $\lambda^2 = 4$ (shown in fig. 14). This pattern would travel in the east-west direction with the dimensional phase velocity $(c_D)_r$ (relative to the quiescent lower fluid rest frame, i.e., system III).

(b): Streamlines for the same disturbance as in (a), but with the basic state velocity profile $\bar{u}_D = U_1 + U_0\ sech^2\ (y/L)$ superimposed using $|\varphi_1^{(0)}\ (0)|/L = 0.3|U_0|$, as seen from a frame moving in the east-west direction with velocity $U_1 + .5U_0$ (i.e., system III frame for profiles with $U_1/U_0 = -0.5$).

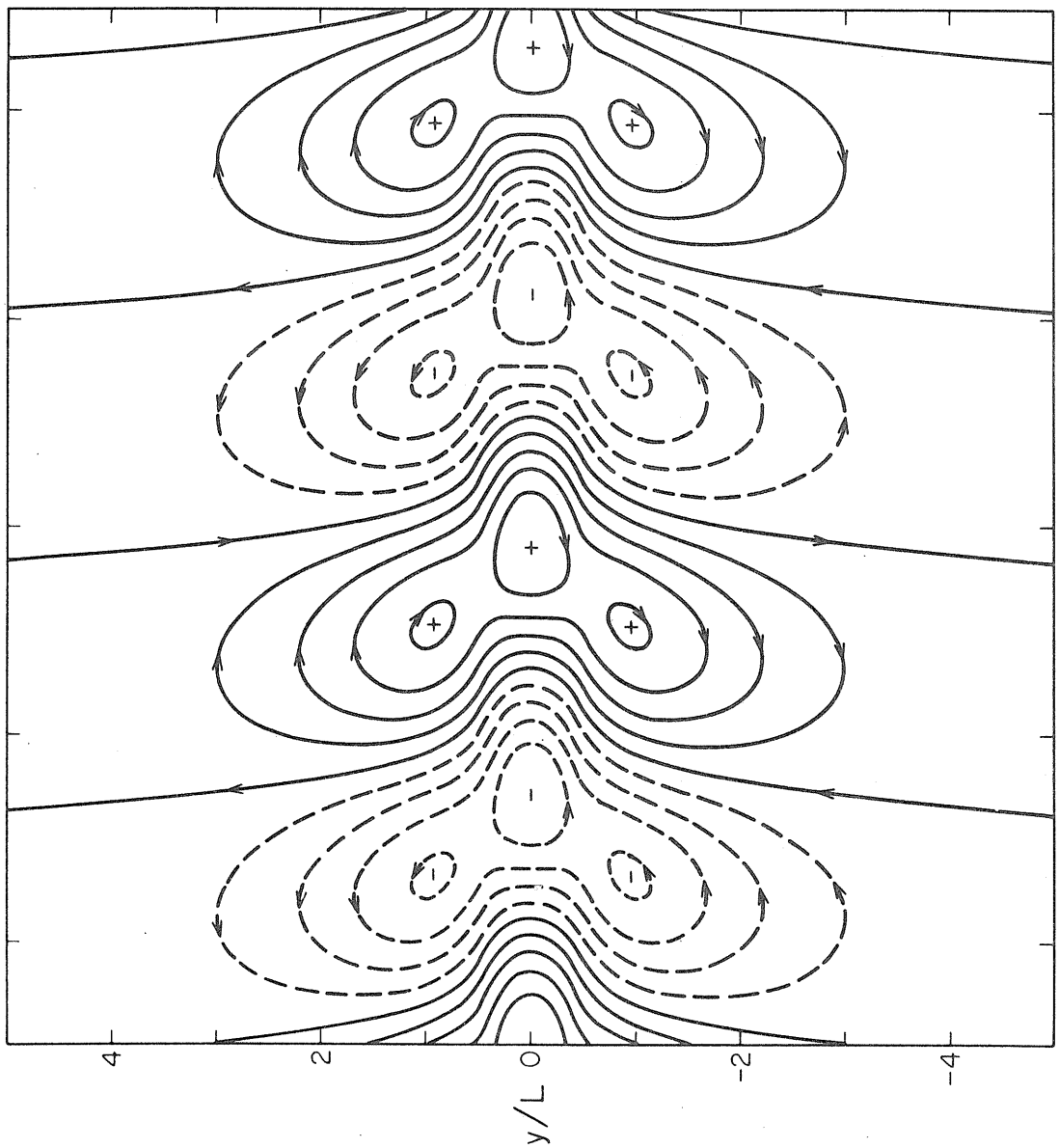

Figure 20(a)

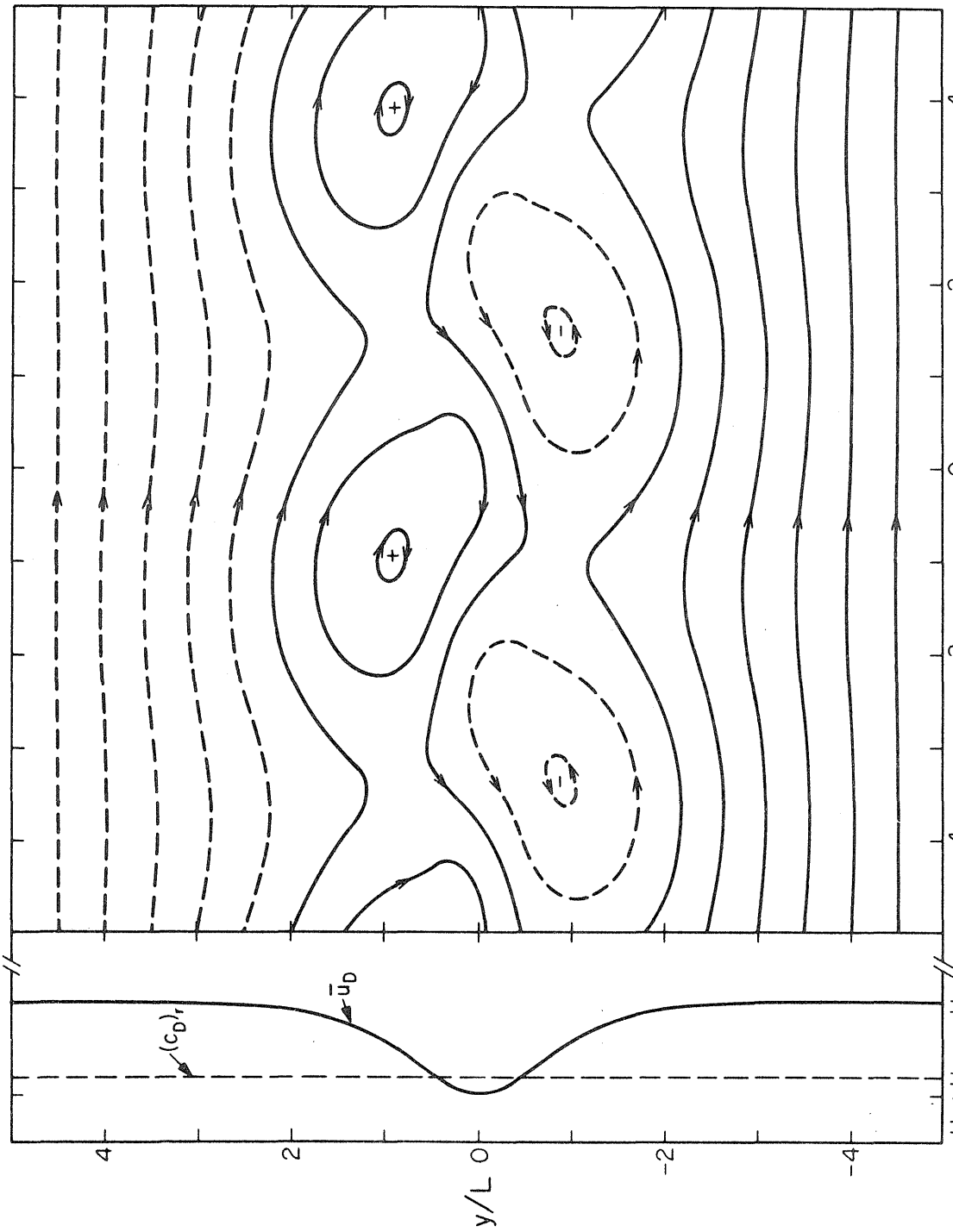

Figure 20(b)

FIGURE 21. Advection of a line of fluid particles in the horizontal (x,y) plane by the velocity fields of fig. 20, i.e., by the basic state sech^2 velocity profile and the BTU disturbance of fig. 14. Units of time τ are $L/|U_0| \sim 2$ earth days, and the initial amplitude of the disturbance was chosen so that $|\varphi_1^{(0)}(0)|/L = 0.2|U_0|$ at $t/\tau = 0$. For $t/\tau \gg 1$ the neglected non-linear advective terms and/or higher order non-geostrophic terms would probably significantly alter the pattern shown. Stretching and compression in the direction of the line of particles are implied in fig. 21 as the spacing between the marker dots changes from the initial uniform spacing.

Thanks are due to Daniel Wenkert of the Division of Geological and Planetary Sciences, C.I.T., for programming the numerical computations required for fig. 21.

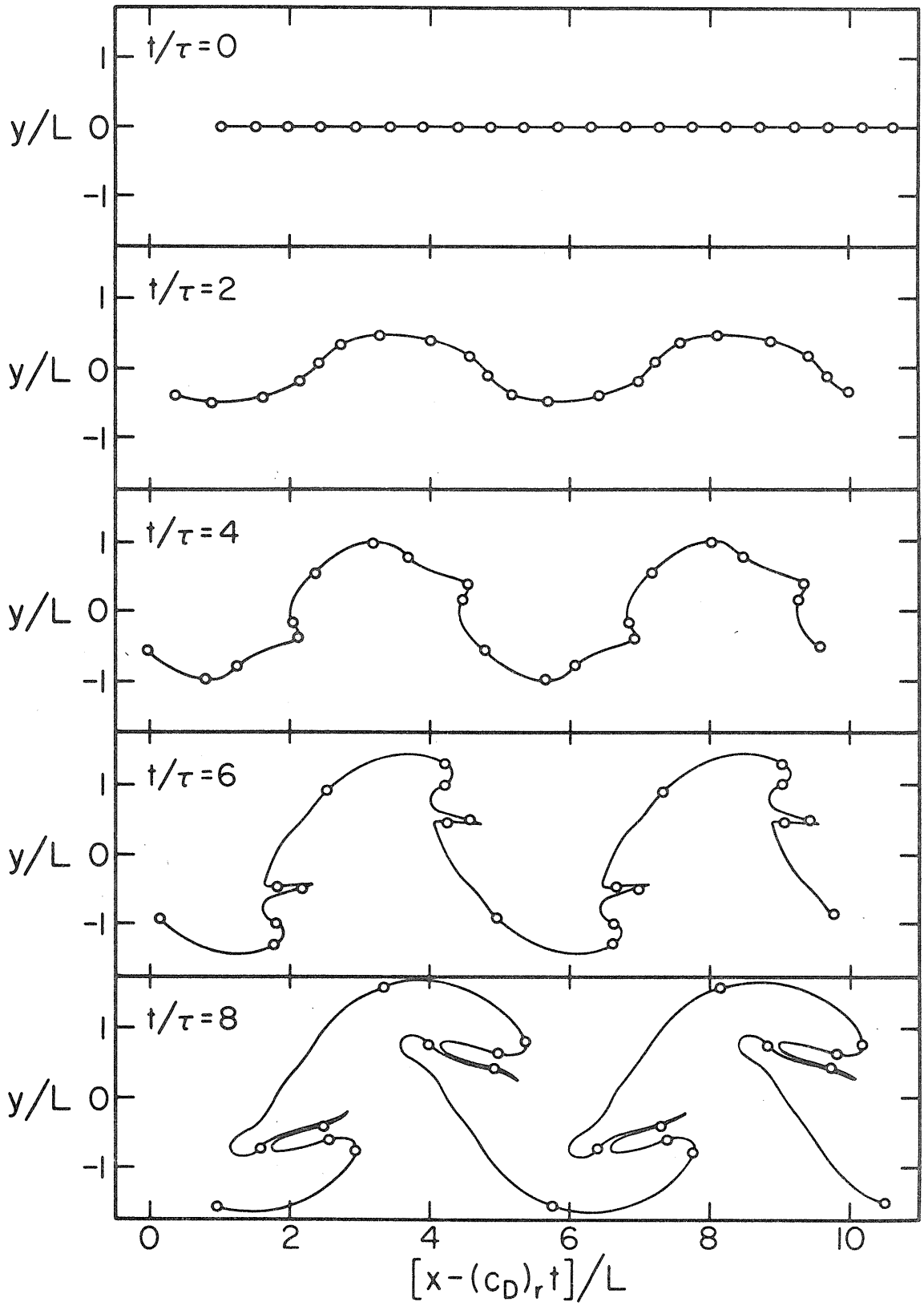

Figure 21

the data may reflect features of any of the patterns in figs. 20(a) , 20(b) or 21. These patterns are for a symmetric evanescent BTU solution; if any observed patterns correspond to oscillatory solutions (cf. figs. 2, 15, 16), they could provide information on the effective locations of the latitudinal boundaries of the disturbances (see section 3.A). If the observed 'skew' in the disturbance streamline patterns [cf. fig. 20(a)] is actually to the east away from the center of retrograde jets, (so that the $\overline{u_1' v_1'}$ eddy transport is amplifying the mean jet), this would be indicative of baroclinic instabilities rather than barotropic instabilities (e.g., Pedlosky, 1964b; Stone, 1969). Since baroclinic growth rates are proportional to $\delta^{-1/2}$ in the two layer model (section 4), this would imply an effective magnitude of δ somehow much larger than the value $\sim 10^{-6}$ suggested above. (A value of $\delta \sim 0(1)$ could possibly be caused by more complex vertical dynamics at intermediate levels around $p \sim 5$ bars than considered above; however such an effect would be outside the scope of terrestrial meteorology.)

For brevity in sections 5 to 7 above, we have presented results only for a few illustrative examples, concentrating mostly on the symmetric evanescent BTU disturbances on the sech^2 velocity profile. This type of disturbance was chosen for its large theoretical growth rates, and the presentations attempt

to show the extent of what can be learned about Jupiter's vertical meteorological structure by comparisons with the observed disturbances. However, there are many other cases contained in the two-layer model that are treated above; antisymmetric and oscillatory BTU disturbances, tanh velocity profile, and baroclinic disturbances. Rather than present all these results in full generality, it should be more efficient to wait at least for some initial Voyager data and then to analyze in detail the theoretical case above that resembles the observed disturbances most closely. There's just so many angles you can possibly see, got to figure on those and let the other ones be (Hunter, 1975).

REFERENCES

Abramowitz, M., and Stegun, I.A. (1965). Handbook of Mathematical Functions. Dover Publ., New York, 1046 pp.

Barcilon, A., and Gierasch, P.J. (1970). A moist Hadley cell model for Jupiter's cloud bands. J. Atmos. Sci. 27, 550-560.

Busse, F.H. (1976). A simple model of convection in the Jovian atmosphere. Icarus 29, 255-260.

Busse, F.H., and Carrigan, C.R. (1976). Laboratory simulation of thermal convection in rotating planets and stars. Science 191, 81-83.

Chapman, C.R. (1969). Jupiter's zonal winds: variation with latitude. J. Atmos. Sci. 26, 986-990.

Charney, J.G. (1947). The dynamics of long waves in a baroclinic westerly current. J. Meteor. 4, 135-163.

Charney, J.G., and Stern, M.E. (1962). On the stability of internal baroclinic jets in a rotating atmosphere. J. Atmos. Sci. 19, 159-172.

Eady, E.T. (1949). Long waves and cyclone waves. Tellus 1, 33-52.

Foote, J.R., and Lin, C.C. (1950). Some recent investigations in the theory of hydrodynamic stability. Quart. Appl. Math. 8, 265-280.

Gehrels, T. (1976). The results of the imaging photopolarimeter on Pioneers 10 and 11. In Jupiter, (T. Gehrels, Ed.), Univ. of Arizona Press, Tucson, pp. 531-563.

Gierasch, P.J. (1976). Jovian meteorology: large-scale moist convection. Icarus 29, 445-454.

Gierasch, P.J., Ingersoll, A.P., and Williams, R.T. (1973). Radiative instability of a cloudy planetary atmosphere. Icarus 19, 473-481.

Gill, A.E., Green, J.S.A., and Simmons, A.J. (1974). Energy partition in the large-scale ocean circulation and the production of mid-ocean eddies. Deep-Sea Res. 21, 499-528.

Hess, S.L., and Panofsky, H.A. (1951). The atmospheres of the other planets. In Compendium of Meteorology, Am. Met. Soc., Boston, pp. 391-400.

Holton, J.R. (1972). An Introduction to Dynamic Meteorology. Academic Press, New York and London, 319 pp.

Hunter, R. (1975). Tiger Rose, Ice Nine Publ. Co., San Rafael, CA.

Ingersoll, A.P. (1976). The atmosphere of Jupiter. Space Sci. Rev. 18, 603-639.

Ingersoll, A.P., and Cuzzi, J.N. (1969). Dynamics of Jupiter's cloud bands. J. Atmos. Sci. 26, 981-985.

Ingersoll, A.P., and Porco, C.C. (1978). Solar heating and internal heat flow on Jupiter. Icarus 35, 27-43.

Kuo, H.L. (1949). Dynamic instability of two-dimensional nondivergent flow in a barotropic atmosphere. J. Meteor. 6, 105-122.

Lin , C.C. (1955). The Theory of Hydrodynamic Stability. Cambridge University Press, 155 pp.

Lipps, F.B. (1962). The barotropic stability of the mean winds in the atmosphere. J. Fluid Mech. 12, 397-407.

Lipps, F.B. (1963). Stability of jets in a divergent barotropic fluid. J. Atmos. Sci. 20, 120-129.

Lipps, F.B. (1965). The stability of an asymmetric zonal current in the atmosphere. J. Fluid Mech. 21, 225-239.

Maxworthy, T., and Redekopp, L.G. (1976). A solitary wave theory of the Great Red Spot and other observed features in the Jovian atmosphere. Icarus 29, 261-271.

Pedlosky, J. (1964). The stability of currents in the atmosphere and the ocean: part 1. J. Atmos. Sci. 21, 201-219.

Pedlosky, J. (1964). The stability of currents in the atmosphere and the ocean: part II. J. Atmos. Sci. 21, 342-353.

Peek, B.M. (1958). The Planet Jupiter. Faber and Faber, London, 283 pp.

Phillips, N.A. (1951) A simple three-dimensional model for the study of large-scale extra tropical flow patterns. J. Meteor. 8, 381-394.

Phillips, N.A. (1954). Energy transformations and meridional circulations associated with simple baroclinic waves in a two-level, quasi-geostrophic model. Tellus 6, 273-286.

Stevenson, D.J. and Salpeter, E.E. (1976). Interior models of Jupiter. In Jupiter, (T. Gehrels, Ed.), Univ. of Arizona Press, Tucson, pp. 85-112.

Stevenson, D.J., and Salpeter, E.E. (1977). The phase diagram and transport properties for hydrogen-helium fluid planets. Astron. J. Suppl. 35, 221-237.

Stone, P.M. (1966). On non-geostrophic baroclinic stability. J. Atmos. Sci. 23, 390-400.

Stone, P.H. (1967). An application of baroclinic stability theory to the dynamics of the Jovian atmosphere. J. Atmos. Sci. 24, 642-652.

Stone, P.H. (1969). The meridional structure of baroclinic waves. J. Atmos. Sci. 26, 376-389.

Stone, P.H. (1970). On non-geostrophic baroclinic stability: part II. J. Atmos. Sci. 27, 721-726.

Stone, P.H. (1972). A simplified radiative-dynamical model for the static stability of rotating atmospheres. J. Atmos. Sci. 29, 405-418.

Stone, P.H. (1976). The meteorology of the Jovian atmosphere. In Jupiter, (T. Gehrels, Ed.), Univ. of Arizona Press, Tucson, pp. 586-618.

Weidenschilling, S.J., and Lewis, J.S. (1973). Atmospheric and cloud structures of the Jovian planets. Icarus 20, 465-476.

Williams, G.P. (1978). Planetary circulations: 1. Barotropic representation of Jovian and terrestrial turbulence. J. Atmos. Sci. 35, 1399-1426.

Williams, G.P., and Robinson, J.B. (1973). Dynamics of a convectively unstable atmosphere: Jupiter? J. Atmos. Sci. 30, 648-717.

APPENDIX

In this appendix, baroclinic instabilities are investigated on $\bar{u}$ = constant velocity profiles using a model with continuous vertical stratification; this models the vertical structure of the basic state and baroclinic disturbances more realistically than the constant density model of the main text, but latitudinal variations of the basic state are neglected.

The appendix as it appears here has been submitted for publication to ICARUS under the title:

'BAROCLINIC INSTABILITIES IN JUPITER'S ZONAL FLOW'

by P.J. Gierasch*, A.P. Ingersoll† and D. Pollard†.

*Cornell University, Ithaca, New York

†California Institute of Technology, Pasadena, California

(The hydrostatic model in sections 2 and 3 of the appendix was originated by the first two authors, and the non-hydrostatic model in section 4 was originated by the third author.)

ABSTRACT

The baroclinic stability of Jupiter's zonal flow is investigated using a model consisting of two continuously stratified fluid layers. The upper layer, containing a zonal shear flow and representing the Jovian cloudy regions above $p \sim 5$ bars, is the same as Eady's (1949) model for the Earth. The lower layer has a relatively large but finite depth with a quiescent basic state, representing the deep Jovian fluid bulk below $p \sim 5$ bars. Due to the presence of the lower layer, the linearized non-dimensional growth rates are drastically reduced from the O(1) growth rates of the original Eady model. Only very long wavelengths relative to the upper fluid's radius of deformation L_1 are unstable. Eddy transports of heat are also reduced relative to estimates based on scaling arguments alone. Since the hydrostatic approximation for the lower layer perturbation breaks down at great depths, a second model is presented in which energy propagates downward in an infinitely deep lower fluid obeying the full linearized fluid equations. In this model, the growth rates are again very small, but now all wavelengths are unstable with maximum growth rates occurring for wavelengths O(1) relative to L_1. These results are consistent with the observed longevity and spatial regularity of Jupiter's zonal jets, and illustrate the importance for the upper layer meteorology of the interface boundary condition with the lower fluid, which is radically different from the rigid lower boundary of the Earth's troposphere.

1. INTRODUCTION

Observations (e.g., Peek, 1958) of Jupiter's atmosphere reveal a zonal flow varying latitudinally on a quarter-wavelength scale of $\sim$5000 km. The overall pattern is highly axisymmetric, with particular jets and their associated cloud bands varying on a time scale of several years. The observations refer to a layer about 100 km thick (pressures 0.1 to 5 bars) where three major cloud layers are supposed to form (Weidenschilling and Lewis, 1973; Ingersoll, 1976). The atmosphere below is thought to be adiabatic to depths greater than 10^4 km (e.g. Hubbard and Smoluchowski, 1973; Stevenson and Salpeter, 1976).

Local disturbances are seen embedded in the zonal flow, with horizontal scales of 500-1000 km and lifetimes of months to years. These disturbances do not destroy the basic structure of the zonal jets, but their accumulated eddy transports could possibly be important in balancing the energy sources and sinks of the zonal flow. This is the role of baroclinic instabilities in the earth's jet streams; however, the Jovian jets seem less distorted by instabilities than the Earth's. Below we investigate the forms and behavior of baroclinic instabilities occurring in model Jovian atmospheres, to see what effect the presence of the deep lower region has on the stability of the upper cloudy region.

We do not attempt to model the energy sources causing the zonal jets. The persistence time of particular zonal flow patterns is several years, which is comparable to the thermal time constant of the cloudy upper layers (Gierasch and Goody, 1969), suggesting that the zonal jets are associated with latitudinal temperature differences in the upper layer. Support for this view also comes from the relation

of the horizontal wind field to zones of upwelling inferred from cloud heights (Hess and Panofsky, 1951; Ingersoll and Cuzzi, 1969). Energy sources that have been proposed to account for these temperature differences include latent heat release (Barcilon and Gierasch, 1970), radiative cooling (Gierasch, Ingersoll and Williams, 1970), and equatorial solar heating (Stone, 1967, 1972; Williams, 1975; but see Ingersoll and Porco, 1978).

To investigate baroclinic instabilities, we first use a simple extension of Eady's (1949) quasi-geostrophic model developed for the Earth's atmosphere. The cloudy region of Jupiter's atmosphere is assumed to be baroclinic with finite static stability. The zonal velocity profile is assumed to vanish (relative to the planetary rotation) at the base of this region, and the deep lower region is assumed to be at rest, with static stability near zero. As in the original Eady problem, the static stabilities of the two regions are taken to be constant, and the lateral variations of zonal velocity, coriolis parameter, and potential vorticity all are neglected. These assumptions lead to a particularly simple mathematical problem from which the effect of the deep lower layer on upper-layer baroclinic instability may be investigated. The general success of the Eady model as applied to the Earth's atmosphere makes it a good first choice for Jupiter investigations, especially considering our lack of knowledge of Jupiter's temperature and wind distributions. We also present below a second simple model in which the lower layer perturbation is allowed to be non-hydrostatic, since on Jupiter the disturbance depth scale in the lower layer may be comparable to or greater than the horizontal scale.

In later papers, we will investigate how the present results are modified by latitudinal variations of the basic state and by ageostrophic effects.

In both models below, we find that the deep lower layer inhibits the growth rate of the fastest growing disturbances relative to those of the original Eady problem, and in our modified Eady model the east-west wavenumber of these modes is reduced. The reduction in growth rates is consistent with Gill et al. (1974), who used an incompressible 2-layer model with a deep lower layer to investigate baroclinic instability in the Earth's oceans. These results are at least qualitatively consistent with the persistence of Jupiter's zonal flow patterns. Further, they help identify needed observations and necessary extensions of the theoretical model. Finally, the results illustrate an important difference between Jovian and terrestrial meteorology, namely, the lower boundary condition, which we hope will be seriously considered in future investigations.

2. MODIFIED EADY MODEL FORMULATION

The motion is assumed to be hydrostatic and quasi-geostrophic, with pressure p as a vertical coordinate. The notation and governing equations follow ch. 8 of Holton (1972). x and y are horizontal distance coordinates to east and north, respectively, and t is time. The eastward and northward velocities are u and v, respectively. $\omega = dp/dt$ is the vertical velocity in this coordinate system. The static stability $\sigma = -(1/\rho_s)\, d \ln \theta_s/dp$ is a function of p only, where $\rho_s(p)$ and $\theta_s(p)$ are the horizontal mean density and potential temperature, respectively. The coriolis parameter is $f = 2\,\Omega_s \sin$ (latitude) where Ω_s is the planetary rotation rate. The motion consists of a basic state $u = \bar{u}(p)$ plus a perturbation $u' = -\partial\psi/\partial y$, $v' = \partial\psi/\partial x$, $\omega' = \omega$. Here $\psi(x,y,p,t)$ is the streamfunction of the perturbation, and is proportional to the perturbation height of surfaces p = constant at (x,y,t).

With these approximations, the equations for ψ and ω are the perturbation vorticity equation

$$\left(\frac{\partial}{\partial t} + \bar{u}\frac{\partial}{\partial x}\right)\nabla_h^2\,\psi - f\frac{\partial \omega}{\partial p} = 0 \quad , \tag{1}$$

and the perturbation energy equation

$$\left(\frac{\partial}{\partial t} + \bar{u}\frac{\partial}{\partial x}\right)\frac{\partial \psi}{\partial p} - \frac{\partial \psi}{\partial x}\frac{d\bar{u}}{dp} + \frac{\sigma}{f}\omega = 0 \quad . \tag{2}$$

Here ∇_h^2 is the horizontal laplacian operator, and we have used $df/dy = \partial\bar{u}/\partial y = 0$, as in the original Eady problem. If $\sigma \neq 0$, we can eliminate ω to obtain the perturbation potential vorticity equation

$$\left(\frac{\partial}{\partial t} + \bar{u}\,\frac{\partial}{\partial x}\right)\left[\nabla_h{}^2\,\psi + f^2\,\frac{\partial}{\partial p}\left(\frac{1}{\sigma}\,\frac{\partial \psi}{\partial p}\right)\right] + \frac{\partial \psi}{\partial x}\,\frac{\partial \bar{q}}{\partial y} = 0 \quad , \tag{3}$$

where

$$\frac{\partial \bar{q}}{\partial y} = -\,f^2\,\frac{\partial}{\partial p}\left(\frac{1}{\sigma}\,\frac{\partial \bar{u}}{\partial p}\right) = 0 \quad , \tag{4}$$

is the basic state potential vorticity gradient. Equation (4) is the essential simplifying assumption of the Eady problem. For the upper region, which extends from p_0 down to p_1, we let $\sigma = \sigma_1 =$ constant and $\bar{u} = (p_1 - p)\,u_0/(p_1 - p_0)$. For the lower region, which extends from p_1 down to p_2, let $\sigma = \sigma_2 =$ constant and $\bar{u} = 0$. If $\sigma_2 = 0$, we cannot use (3) for the lower layer. In this case, (2) implies ψ is independent of p in the lower layer, and (1) implies $\frac{\partial \omega}{\partial p} =$ constant. However, it happens that the correct results for $\sigma_2 = 0$ coincide with the limit, as $\sigma_2 \to 0$, of the results in this paper.

The above equations are applied separately within each layer. The tropopause at $p_0 = 0.1$ bars is assumed to act as a rigid lid on which $\omega = 0$. The same condition $\omega = 0$ is imposed at $p = p_2$, as if there were a rigid horizontal surface at depth. This is meant to represent simply some reflection mechanism for the waves deep in the Jovian interior; e.g., from a molecular-metallic hydrogen phase transition at $p \sim 3 \times 10^6$ bars, across which $\frac{\Delta \rho}{\rho} \sim 0.1$ (Stevenson & Salpeter, 1976, 1977), or from non-hydrostatic effects at depth, as in section 4. We also consider the limit as $p_2 \to \infty$ with σ_2 finite.

The boundary conditions imposed at the interface $p \approx p_1$ follow from continuity of pressure, temperature and mass flux through the interface. ψ is continuous because the height of constant pressure surfaces is continuous, and so is

$$\omega - v\left(\frac{\partial p}{\partial y}\right)_1 \quad , \tag{5}$$

which is proportional to mass flux normal to the interface. Here $(\partial p/\partial y)_1$ is the slope, in pressure coordinates, of the interface with respect to latitude. For $\sigma_1 \gg \sigma_2$, this slope is approximately equal to the slope of potential temperature surfaces $(\partial p/\partial y)_\theta$ in the upper fluid, provided temperature is continuous. Thus we have

$$\left(\frac{\partial p}{\partial y}\right)_1 \approx \left(\frac{\partial p}{\partial y}\right)_\theta = -\frac{(\partial\theta/\partial y)_p}{(\partial\theta/\partial p)_y} = \frac{f}{\sigma_1}\frac{d\bar{u}}{dp} \quad . \tag{6}$$

For quasi-geostrophic flow, both the slope (6) and the ratio ω/v in (5) are of order $Ro(p_1 - p_0)/L$, where Ro is the Rossby number u_0/fL, a small parameter. Thus both terms in (5) are of the same magnitude. However, continuity of ψ implies continuity of $v = \partial\psi/\partial x$, so (5) reduces to ω continuous. The boundary conditions are then

$$\left.\begin{array}{lll} \omega = 0 \quad , & p = p_0 & ; \\ \psi \ \& \ \omega \text{ continuous}, & p = p_1 & ; \\ \omega = 0 \quad , & p = p_2 & . \end{array}\right\} \tag{7}$$

The complete solution is a sum of modes of the form $\psi = \varphi(p)\exp[ik_x(x-ct) + ik_y y]$ and $\omega = \Omega(p)\exp[ik_x(x-ct) + ik_y y]$. For such modes, Eq. (3) becomes

$$- (k_x^2 + k_y^2)\ \varphi + f^2 \frac{d}{dp}\left(\frac{1}{\sigma}\ \frac{d\varphi}{dp}\right) = 0 \quad , \tag{8}$$

and Eq. (2) becomes

$$\Omega = - \frac{i k_x f}{\sigma} \left[(\bar{u}-c)\ \frac{d\varphi}{dp} - \varphi\ \frac{d\bar{u}}{dp}\right] \quad . \tag{9}$$

For constant σ, the two independent solutions are $e^{\alpha p}$ and $e^{-\alpha p}$, where $\alpha^2 = (k_x^2+k_y^2)\ \sigma/f^2$. There are four constants of integration, two from the upper fluid and two from the lower fluid, and four conditions (7) to be applied at the boundaries $p = p_0, p_1, p_2$. As in the original Eady problem, the complex phase speed c is determined by the boundary conditions. In dimensionless form, the equation for c is

$$\left[\nu^2 + \nu\ (\tanh k - k)\right] + \epsilon \left[\nu^2 \tanh k - \nu k \tanh k + (k - \tanh k)\right] = 0 \quad . \tag{10}$$

Here $k = \alpha_1 \Delta p_1 = L_1(k_x^2+k_y^2)^{\frac{1}{2}}$ is the total horizontal wavenumber $(k_x^2+k_y^2)^{\frac{1}{2}}$ scaled by the upper fluid's radius of deformation $L_1 = \sigma_1^{\frac{1}{2}} \Delta p_1/f$, with $\Delta p_1 = p_1 - p_0$. The eigenvalue ν is kc/u_0, whence the disturbance growth rate $k_x c_i = \nu_i (u_0/L_1)[k_x/(k_x^2+k_y^2)^{\frac{1}{2}}]$ is greatest when $k_y = 0$ and is then equal to $\nu_i u_0/L_1$. Finally, $\epsilon = s/\tanh(k\,s\,d)$, where $s = (\sigma_2/\sigma_1)^{\frac{1}{2}}$ and $d = \Delta p_2/\Delta p_1$, with $\Delta p_2 = p_2 - p_1$. s and d measure the stratification and depth, respectively, of the lower fluid relative to the upper fluid.

Each of the two bracketed terms in (10) is quadratic in ν. As ϵ tends to zero, (10) tends to the first quadratic, which is the dispersion relation for the problem of the single upper layer with lower boundary condition $\varphi = 0$ at $p = p_1$. This basic state is stable, with ν real for all k. As ϵ tends to infinity, (10) tends

to the second quadratic, which is the dispersion relation for the original Eady problem of the single upper layer with lower boundary condition $\omega = 0$ at $p = p_1$. This basic state is unstable, with $\nu_i = 0(1)$ for some $k = 0(1)$.

3. MODEL RESULTS

Figure 1 shows the dimensionless growth rate ν_i as a function of k and $\epsilon = s/\tanh(k_s d)$. For $u_0 = 50$ m/s and $L_1 = 1000$ km, (see section 4), the unit of time is 2×10^4 sec, about 0.2 earth days.

According to (10), the value of ν depends only on ϵ and k. However, the fact that ϵ depends on k presents a slight complication. One generally seeks the most unstable disturbance for a given basic state; i.e., one seeks the disturbance wavenumber k that gives the maximum growth rate ν_i for given values of the basic state parameters s and d. For Jupiter, the lower fluid is both deep ($d \gg 1$) and nearly adiabatic ($s \ll 1$). If $ksd \gg 1$, then $\epsilon \approx s$ and the solid curves in Fig. 1 correspond to given basic states. If $ksd \ll 1$, then $\epsilon \approx (kd)^{-1}$ and the dashed curves correspond to given basic states.

In both cases, the dimensionless growth rates ν_i are of order $\epsilon \ll 1$, implying that the growth time scale of the instability is very long compared to the zonal flow time scale L_1/u_0. Near the region of maximum growth rate, we have both k^3 and ν of order ϵ, whence the solution of (10) is approximately

$$\nu = \nu_r + i\nu_i = \frac{1}{6} k^3 \pm i\sqrt{\frac{1}{3} k^3 \epsilon - \frac{1}{36} k^6} \quad . \tag{11}$$

As $d \to \infty$ we have $\epsilon \to s$, whence the maximum ν_i occurs at wavenumber $k = (6s)^{1/3} = (6\epsilon)^{1/3}$ and is given by $\nu_i = s = \epsilon$. As $s \to 0$ we have $\epsilon \to (kd)^{-1}$, whence the maximum ν_i occurs at wavenumber $k = (4/d)^{1/4} = (4\epsilon)^{1/3}$ and is given by $\nu_i = 2d^{-3/4}/3 = 2^{3/2}\,\epsilon/3$. So the wavelengths of these modes are very long compared to the Rossby radius L_1, and their phase speeds $(\nu_r/k)\,u_0$ are very slow compared to u_0, with $\nu_r/k \sim O(\epsilon^{2/3})$.

FIGURE 1 OF APPENDIX.

Non-dimensional growth rate ν_i as a function of non-dimensional wavenumber k in the modified Eady model. The square root of the stratification s and depth d of the lower fluid relative to that of the upper fluid enter through the parameter $\epsilon = s/\tanh(ksd)$. The case of interest for Jupiter is $s \ll 1$, $d \gg 1$, $\epsilon \ll 1$.

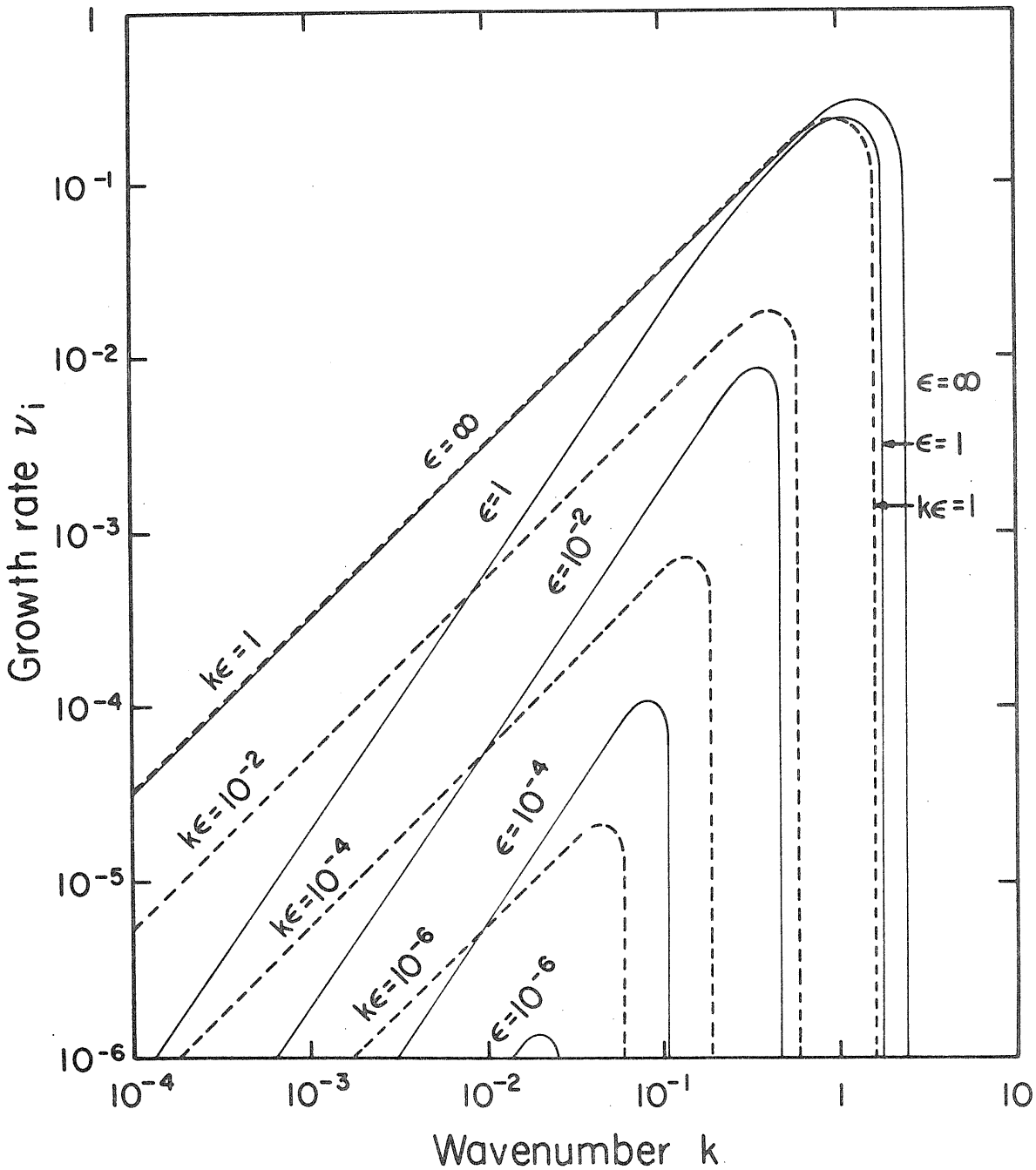

Figure 1 of appendix

Energy relations are derived from (1) and (2) after multiplying by ψ and $\partial\psi/\partial p$ respectively, and integrating with respect to x, y and p over both fluid layers. Surface terms arising from partial integrations in y are assumed to vanish. Denoting averages over the fluid by angular brackets, one obtains

$$\frac{d}{dt}\left\langle \tfrac{1}{2}\left(\frac{\partial\psi}{\partial x}\right)^2 + \tfrac{1}{2}\left(\frac{\partial\psi}{\partial y}\right)^2 \right\rangle = f\left\langle \omega \frac{\partial\psi}{\partial p} \right\rangle \tag{12}$$

$$\frac{d}{dt}\left\langle \frac{f^2}{2\sigma}\left(\frac{\partial\psi}{\partial p}\right)^2 \right\rangle = \left\langle \frac{f^2}{\sigma} \frac{d\bar{u}}{dp} \frac{\partial\psi}{\partial x}\frac{\partial\psi}{\partial p} \right\rangle - f\left\langle \omega \frac{\partial\psi}{\partial p} \right\rangle \tag{13}$$

Eq. (12) gives the rate of change of disturbance kinetic energy; the right side is proportional to the average vertical heat flux upwards. Eq. (13) gives the rate of change of disturbance available potential energy. The first term on the right side is proportional to the horizontal heat flux from the warm side of the zonal jet $\bar{u}$ to the cold side.

For the fastest growing disturbance, the streamfunction ψ is smaller in the lower fluid than in the upper fluid by a factor $O(\epsilon/k) = O(\epsilon^{2/3})$. The bulk of the vertically integrated disturbance energy is available potential energy in the upper fluid. Vertically integrated kinetic energy and available potential energy in the lower fluid are smaller than the upper fluid available potential energy by the same factor $\epsilon^{2/3}$. The complex phase of the disturbance streamfunction does not vary with height in the lower fluid, and varies by only $\epsilon^{2/3}$ in the upper fluid. Consequently, the horizontal heat transport scaled by the disturbance velocity and temperature fluctuations is of order $\epsilon^{2/3}$. Finally, the complex phases of ω

and ψ differ by $\pi/2 + 0(\epsilon^{2/3})$, implying that the vertical heat transport scaled by the disturbance vertical velocity and temperature fluctuation is also of order $\epsilon^{2/3}$. In other words, the fastest growing disturbance is a nearly neutral wave confined largely to the upper fluid with energy conversions and transports of order $\epsilon^{2/3}$ relative to estimates based on scaling arguments alone.

The small factor $\epsilon^{2/3}$ is approximately the square root of the ratio of upper fluid pressure thickness Δp_1 to the pressure thickness of the disturbance in the lower fluid. As shown above, for $s \to 0$ we have $\epsilon^{4/3} \approx k\epsilon \approx 1/d = \Delta p_1/\Delta p_2$. And for $d \to \infty$ we have $\epsilon^{4/3} \approx k\epsilon \approx \alpha_1 \Delta p_1 s = \alpha_2 \Delta p_1$. In the former case the disturbance amplitude is appreciable down to the bottom, whence the relevant pressure thickness in the lower fluid is Δp_2. In the latter case the disturbance amplitude decays as $e^{-\alpha_2 p}$, whence the relevant pressure thickness in the lower fluid is α_2^{-1}.

The growth rates are much smaller than those in the original Eady problem because the upper fluid must now have ψ = zero + $0(\epsilon^{2/3})$ at its lower boundary $p = p_1$. This is imposed by the presence of the deep, hydrostatic, quiescent, nearly adiabatic lower fluid. If ψ were 0(1) at the interface, the pressure and associated geostrophic velocity field would be felt to great depths in the lower fluid, and a propagating disturbance would require, for vorticity conservation in Eq. (1), vertical stretching of the entire lower fluid columns, i.e., prohibitively large vertical

velocity ω at the interface. So, the upper fluid feels a free surface [to within $O(\varepsilon^{2/3})$] as its lower boundary; energy-releasing flow across lines of constant potential temperature (Charney and Stern, 1962) can only take place at $O(\varepsilon^{2/3})$, and so the flow is only unstable at $O(\varepsilon^{2/3})$.

4. NON-HYDROSTATIC LOWER LAYER

The hydrostatic approximation in the quasi-geostrophic model used above requires that, in each layer, the vertical scale of motion is much less than the horizontal scale. Yet for $d \to \infty$ and $s \to 0$, the model predicts that the disturbance extends downwards indefinitely in the lower fluid, so that non-hydrostatic effects would modify the above results to some extent. We have studied only a particularly simple example of non-hydrostatic behavior, with a Boussinesq upper layer, an incompressible lower layer, and a vertical rotation vector. Nevertheless, this example supports our basic conclusions that the deep adiabatic lower fluid inhibits baroclinic instability.

For the upper layer, we use exactly the same quasi-geostrophic model as above, but now p, ω, ψ, and σ refer to a Boussinesq fluid in the region $z_0 \le z \le z_1$, where z is a vertical coordinate increasing downwards. Thus in equations (1) to (9) we replace p by $\rho_s g z$, ω by $\rho_s g w$, ψ by $p'/(f\rho_s)$, σ_1 by $-(\alpha/\rho_s^2 g)\, d\theta/dz$, and Δp_1 by $\rho_s g (z_1 - z_0) = \rho_s g \Delta z_1$. Here ρ_s is the mean density (a constant), w is vertical velocity downwards, p' is perturbation pressure, α is the thermal coefficient of expansion, and θ is potential temperature.

The lower fluid extends downward from $z = z_1$ and is assumed to be incompressible with density ρ_s. The equations in the lower fluid are linearized about a hydrostatic basic state with $\bar{u} = 0$. Thus we have

$$\frac{\partial u}{\partial t} - fv = -\frac{1}{\rho_s}\frac{\partial p'}{\partial x} \quad , \tag{14}$$

$$\frac{\partial v}{\partial t} + fu = -\frac{1}{\rho_s}\frac{\partial p'}{\partial y} \quad , \tag{15}$$

$$\frac{\partial w}{\partial t} = -\frac{1}{\rho_s}\frac{\partial p'}{\partial z} \quad , \tag{16}$$

$$\frac{\partial u}{\partial x} + \frac{\partial v}{\partial y} + \frac{\partial w}{\partial z} = 0 \quad . \tag{17}$$

We want to reduce (14)-(17) to a single equation in one variable. Forming $\frac{\partial}{\partial t}\left[\frac{\partial(14)}{\partial x} + \frac{\partial(15)}{\partial y}\right] + f\left[\frac{\partial(15)}{dx} - \frac{\partial(14)}{dy}\right]$, and using (16) and (17) to eliminate $\partial u/\partial x + \partial v/\partial y$ and p', we get

$$\left(\frac{\partial^2}{\partial t^2} + f^2\right)\frac{\partial^2 w}{\partial z^2} + \frac{\partial^2}{\partial t^2}\nabla_h{}^2 w = 0 \quad . \tag{18}$$

The pressure perturbation obeys

$$\frac{1}{\rho_s}\frac{\partial}{\partial t}\nabla_h{}^2 p' = \left(\frac{\partial^2}{\partial t^2} + f^2\right)\frac{\partial w}{\partial z} \quad . \tag{19}$$

As in section 2, we look at individual solutions of the form $w = W(z)\exp[ik_x(x - ct) + ik_y y]$. Then (18) becomes

$$\frac{d^2 W}{d\hat{z}^2} + R_x{}^2\left(1 - R_x{}^2\nu^2\right)^{-1}\nu^2 W = 0 \tag{20}$$

where $\hat{z} = (k_x{}^2 + k_y{}^2)^{\frac{1}{2}} z$ is a non-dimensional vertical coordinate, ν is kc/u_0, $R_x = (u_0/fL_1)\, k_x(k_x{}^2 + k_y{}^2)^{-\frac{1}{2}}$, and $k = (k_x{}^2 + k_y{}^2)^{\frac{1}{2}} L_1$. The lower boundary condition is a radiation condition on the vertical energy flux, corresponding to a growing disturbance energized by the upper layer. We require that $\overline{p'w}$ be positive and tend to zero as $z \to \infty$, where the overbar means an average over x and y,

and with p' obtained from (19). This follows straightforwardly from the energy equation formed by $u \cdot (14) + v \cdot (15) + w \cdot (16)$.

Solutions of (20) are $W = \exp\left[\pm i R_x (1 - R_x^2 \nu^2)^{-1/2} \nu \hat{z}\right]$. The radiation condition as $\hat{z} \to \infty$ (downwards) requires that we use only the plus sign. Continuity of p' and w at the interface with the upper layer at $\hat{z} = \hat{z}_1$ follow as before from continuity of pressure, temperature and mass flux. Using (19) we then obtain an expression for p'/w at $\hat{z} = \hat{z}_1$ in the lower fluid. This expression constitutes an interface boundary condition for the upper fluid. The eigenvalue c is determined by requiring the upper layer solutions to simultaneously satisfy this interface condition and also $w = 0$ at $z = z_0$. The resulting dimensionless eigenvalue equation for ν is the same as Eq. (10), the equivalent equation in the previous model, but now the small parameter ϵ is given by

$$\epsilon = - i \nu R_x (\Delta z_1 / L_1)(1 - R_x^2 \nu^2)^{\frac{1}{2}} \quad . \tag{21}$$

In the previous model Eq. (10) was simply a quadratic for ν, but now ϵ depends on ν in a complicated way. However, we can still use the fact that ϵ is much less than 1: Defining $\delta = R_x (\Delta z_1 / L_1) \ll 1$, then $\epsilon \sim 0(\delta)$, and we can find a root of the eigenvalue equation close to $\nu = \nu_o$, where $\nu_o = k - \tanh k$ is the non-trivial solution of (10) with ϵ set equal to zero. This is not strictly valid for small values of k, nor does it find all the roots, but a numerical computation of all the roots of the exact eigenvalue equation showed that the only non-spurious (i.e., consistent with

quasi-geostrophic scaling in the upper fluid) unstable root is the one found by the above method, for all values of k.

Correct to lowest order in δ, we find

$$\nu_r \approx k - \tanh k + O(\delta^2),$$
$$\nu_i \approx \delta\ (k - \tanh k)\ \mathrm{sech}^2\ k + E \tag{22}$$

where the error $E = 0\ [\max\ (\delta^2,\ R_x^{\ 2}\ \delta)]$. Maximum growth rates $k_x c_i = \nu_i\ R_x f$ occur for $k_y = 0$, so that the disturbance velocities are entirely in the y direction. The maximum of ν_i occurs at $k = 1.3$ and is given by $(\nu_i)_{max} = 0.11\ Ro\ (\Delta z_1/L_1)$.

In estimating dimensional values from these expressions, the most uncertainty comes from the Jovian upper layer stratification which enters via the Rossby radius L_1. Assuming that the zonal jet system is confined to the cloudy upper layers above $p \sim 5$ bars and that the stratification originates from latent heat release in the water clouds (Gierasch, 1976), then $L_1 \sim 500$ km; a rough upper bound for L_1 corresponding to an isothermal upper layer is ~ 3000 km. Using $L_1 = 1000$ km, $\Delta z_1 = 100$ km, $u_0 = 50\ m\ s^{-1}$, and $f = 3.5 \times 10^{-4}\ sec^{-1}$, we find that

$$(\nu_i)_{max} \sim 1.6 \times 10^{-3} \text{ at } k = 1.3$$

which corresponds to a growth time scale of ~ 0.4 earth years with $k_x^{-1} \sim 750$ km.

5. DISCUSSION

Although both the pure quasi-geostrophic model of sections 2 and 3 (called 'H' below) and the non-hydrostatic lower layer model of section 4 (called 'NH' below) predict drastic reductions in baroclinic growth rates due to the presence of the lower layer, their results differ in some respects. Below we compare the two models and discuss which, if any, is most applicable to Jupiter.

In model H, the small parameter that reduces the growth rates is $\epsilon^{4/3}$, the ratio of the upper fluid pressure thickness Δp_1 to the pressure thickness of the disturbance in the lower fluid. The equivalent small parameter in model NH, from (22), is $\delta = R_x \Delta z_1 / L_1$ which is somewhat analogous in meaning to $\epsilon^{4/3}$, since L_1/R_x is approximately the vertical wavelength in the lower fluid and Δz_1 is the upper fluid thickness.

Referring to fig. 1, we see that the maximum growth rates ν_i in model NH would be comparable to those of model H if, for instance, $\sigma_2 = 0$ and $k\epsilon = d^{-1} = \Delta p_1 / \Delta p_2$ were $\sim 3 \times 10^{-4}$, i.e., if $p_2 \sim 10^4$ bars. However, the wavelength-dependences of ν_i in (10) and (24) are different; in model H with $\sigma_2 = 0$, only long wavelengths $\left[k < (12/d)^{1/4}\right]$ are unstable, but in model NH, the non-hydrostatic effects have destabilized all wavelengths and the maximum growth wave has $k \sim 0(1)$. Consequently, the phase speeds of the most unstable waves in model NH are $0(1)$ relative to u_0, compared to $0(d^{-3/4})$ for the unstable waves of model H. These differences indicate that non-hydrostatic processes not contained in the hydrostatic

model H can significantly affect the phase speeds and wavelength-dependences of baroclinic waves. The fundamental result common to both models is the reduction in growth rates, which depends on the effective pressure thickness of the disturbance in the lower layer.

The pressure level $p_2 \sim 10^4$ bars for the lower boundary of model H suggested by the comparison above with model NH is somewhat misleading. For an adiabatic, perfect gas lower layer in model NH (not shown above), the vertically propagating waves decay much more slowly with depth than for the constant density lower layer of section 4. The corresponding growth rates are then much smaller, and are comparable to model H growth rates with the rigid lower boundary at $p_2 \sim 10^8$ bars. This is well below the metallic-molecular phase transition at $p \sim 3 \times 10^6$ bars, at a depth of $\sim$0.24 relative to Jupiter's radius. So a better model would have a non-hydrostatic lower layer with a rigid lower boundary at $p \sim 3 \times 10^6$ bars. The analysis would take into account the finite size of Jupiter, and would employ a realistic equation of state. However we suggest, on the basis of results shown above, that the growth rates will still be small as long as the lower fluid is deep and nearly adiabatic.

Another possibly serious deficiency is the neglect

of the effects of convection. Convection may introduce a negative static stability within the lower layer, thereby altering the basic states considered above. Also, vigorous convection cells associated with Jupiter's internal heat flow, with scales on the order of one scale height, may seriously dissipate the baroclinic waves. However, in the model lower layers ($p > p_1$), both the horizontal and vertical scales of the unstable baroclinic waves are sufficiently large, compared to one scale height, that the waves may not be seriously affected. Gierasch (1976) has estimated turnover times and eddy diffusivities of Jovian convection cells using mixing-length theory which imply time scales of $\sim$ 100 days for horizontal mixing over $\sim$ 1000 km at $p \sim 10$ bars. To model this effect, we included Rayleigh friction terms in the three momentum equations (14)-(16) of model NH, with a time constant t_c. The analysis goes through as before, and the phase speeds and growth rates are only altered by a multiplicative factor $1 + 0(\nu_r^{-2} L_1^2 u_0^{-2} t_c^{-2})$, which is $\sim 1 + 0(10^{-4})$ for $\nu_r \sim 0(1)$ and $t_c \sim 100$ days. This suggests that the baroclinic waves are hardly affected at all by the convection in the lower layer. In the upper layer ($p_0 < p < p_1$), the vertical scale of the waves is comparable to one scale height; however, we are hypothesizing that mixing-length convection is inhibited in this region by the stable stratification of the basic state, and that the internal heat is transported upwards either by baroclinic instabilities, by a secondary mean flow associated with the zonal jets, or by cumulus-tower convection as in the earth's intertropical convergence zone.

REFERENCES

Abramowitz, M., and Stegun, I.A., Eds. (1965). Handbook of Mathematical Functions. Dover Publ., New York.

Barcilon, A., and Gierasch, P.J. (1970). A moist Hadley cell model for Jupiter's cloud bands. J. Atmos. Sci. 27, 550-560.

Charney, J.G., and Stern, M.E. (1962). On the stability of internal baroclinic jets in a rotating atmosphere. J. Atmos. Sci. 19, 159-172.

Eady, E.T. (1949). Long waves and cyclone waves. Tellus 1, 33-52.

Gierasch, P.J. (1976). Jovian meteorology: large-scale moist convection. Icarus 29, 445-454.

Gierasch, P.J.,and Goody R.M. (1969). Radiative time constants in the atmosphere of Jupiter. J. Atmos. Sci. 26, 979-980.

Gierasch, P.J., Ingersoll, A.P., and Williams, R.T. (1973). Radiative instability of a cloudy planetary atmosphere. Icarus 19, 473-481.

Gill, A.E., Green, J.S.A., and Simmons, A.J. (1974). Energy partition in the large-scale ocean circulation and the production of mid-ocean eddies. Deep-Sea Res. 21, 499-528.

Hess, S.L., and Panofsky, H.A. (1951). The atmospheres of the other planets. In Compendium of Meteorology, pp. 391-400. Am. Met. Soc., Boston.

Holton, J.R. (1972). An Introduction to Dynamic Meteorology, pp. 124-128. Academic Press, New York and London.

Hubbard, W.B., and Smoluchowski, R. (1973). Structure of Jupiter and Saturn. Space Sci. Rev. 14, 599-662.

Ingersoll, A.P. (1976). The atmosphere of Jupiter. Space Sci. Rev. 18, 603-639.

Ingersoll, A.P., and Cuzzi, J.N. (1969). Dynamics of Jupiter's cloud bands. J. Atmos. Sci. 26, 981-985.

Ingersoll, A.P., and Porco, C.C. (1978). Solar heating and internal heat flow on Jupiter. Icarus 35, 27-43.

Peek, B.M. (1958). The Planet Jupiter. Faber and Faber, London.

Stevenson, D.J., and Salpeter, E.E. (1976). Interior models of Jupiter. In Jupiter, (T. Gehrels, Ed.), pp. 85-112. Univ. of Arizona Press, Tucson.

Stevenson, D.J., and Salpeter, E.E. (1977). The phase diagram and transport properties for hydrogen-helium fluid planets. Astron. J. Suppl. 35, 221-237.

Stone, P.H. (1967). An application of baroclinic stability theory to the dynamics of the Jovian atmosphere. J. Atmos. Sci. 24, 642-652.

Stone, P.H. (1972). A simplified radiative-dynamical model for the static stability of rotating atmospheres. J. Atmos. Sci. 29, 405-418.

Weidenschilling, S.J., and Lewis, J.S. (1973). Atmospheric and cloud structures of the Jovian planets. Icarus 20, 465-476.

Williams, G.P. (1975). Jupiter's atmospheric circulation. Nature 257, 778.